

Helsinki University of Technology, Laboratory of Paper Technology
Reports, Series A23
Espoo 2005

SURFACE SIZING WITH STARCH SOLUTIONS AT HIGH SOLIDS CONTENTS

Juha Lipponen

Dissertation for the degree of Doctor of Science in Technology to be presented with due permission of the Department of Forest Products Technology, for public examination and debate in K hall at Helsinki University of Technology (Espoo, Finland) on the 28th of January 2005 at 12 noon.

Helsinki University of Technology
Department of Forest Products Technology
Laboratory of Paper Technology

Teknillinen korkeakoulu
Puunjalostustekniikan osasto
Paperitekniikan laboratorio

Distribution:
Helsinki University of Technology
Department of Forest Products Technology
Laboratory of Paper Technology
P.O. Box 6300
FIN-02015 HUT

2nd edition

ISBN 951-22-7553-8
ISBN 951-22-7491-4
ISSN 1237-6248

Picaset Oy
Helsinki 2005

Preface

This work was carried out during the years 2001–2004 at Metso Paper Järvenpää. I would like to express my sincere gratitude to my employer, Metso Paper, Inc., for making it possible for me to carry out my studies and complete my dissertation within the Metso Academy program. I also extend my thanks to the following companies for their cooperation: Ciba Specialty Chemicals Inc., Raisio, Finland; UPM-Kymmene Kymi Paper Oy, Kuusankoski, Finland and VTT Processes, Jyväskylä, Finland.

I would like to thank Professor Hannu Paulapuro of the Laboratory of Paper Technology at Helsinki University of Technology for his guidance throughout my work.

I extend my warm thanks to Dr. Johan Grön for his encouragement during my research, as well as for his never-ending patience and expertise in commenting on my results and scientific writing.

My superiors during the conduct of this research, Mr. Seppo Luomi and Mr. Timo Valkama, deserve my sincere gratitude. Dr. Markku Karlsson's and Mr. Pauli Kytönen's role in inspiring my work throughout its entire duration was also instrumental.

I would like to warmly thank my co-workers – especially Mr. Stig-Erik Bruun and Mr. Timo Laine – and also Mr. Jouni Astola, Mr. Jussi Jääskeläinen, Mr. Timo Lappalainen, Mr. Juha Pakarinen, Mr. Pekka Pakarinen and Ms. Tiina Solasaari for their essential contribution to the research during the various phases of the work.

Professor Toivo Katila and Mr. Tapani Koivumäki of the Foundation of Technology in Finland deserve my gratitude for the unexpected honor of my nomination for Young Scientist of the Year in 2003 based on the research reported in this dissertation.

To my family I want to express my sincere gratitude for their support during all stages of my education.

And finally, the most important thanks of all, I would not have been able to survive this process without your love and support, my dearest Anne.

Järvenpää, January 2005

Juha Lipponen

Abstract

Surface sizing at high solids contents from 8% to 30% yields up to 75% savings in afterdrying capacity. Decreasing the wetting of the sheet will also increase paper machine efficiency by reducing the number of web breaks. Also, the same afterdrying capacity can be used for both MSP coating and surface sizing at size solids contents of 20%–30%.

Surface sizing solids contents of up to 30% have not been used due to the insufficient stability of starch at elevated solids contents and maintaining the binding power of the starch. Also the ability to maintain the amount of starch at the MSP application at very high solids contents has been lacking. Here, both the chemistry of the starch solutions and the application technology used needed to be developed in order to produce the desired applied starch amount at starch solids contents of up to 30% with desired binding properties. The features of the base paper also needed to be adjusted to fit the features of high solids surface sizing.

The findings of this study prove that it is possible to use a wide variety of starch viscosities and molecular weights even at increased solids contents. Increasing starch solids contents with more stable starches is therefore not restricted to highly degraded starches only with their lower binding power. When the solids content of the starch solution is increased from 8% to 30%, less starch penetrates into the sheet and more starch remains on the paper surface. The concentration of starch on the surface of paper decreases sheet porosity, oil absorption and internal strength, as well as increases its surface strength and bending stiffness. At very high solids contents internal strength behavior also suggests that starch may locally penetrate into the larger sheet pores. This observation is supported by pore size distribution analysis. The base paper for high solids surface sizing can also be optimized by adjusting the press to dryer web draw. Here, the aim could be to minimize the press draw below 2% when internal strength or air permeability are critical.

A method for obtaining more informative starch distribution curves was developed to provide a helpful tool in characterizing the effect of various process parameters on the z -distribution of starch in the sheet. An additional feature of this method is the definition of a dimensionless penetration number Q_{tot} that can be used to quantitatively compare the penetration of surface sizing starch in different paper samples.

A novel interpretation is presented of the role of surface sizing starch with respect to the elastic modulus and bending stiffness properties of the sheet. When increasing the elastic modulus or bending stiffness of the sheet, starch may merely promote shrinkage potential instead, which leads – when shrinkage is not allowed – to increased drying stress that, in turn, leads to an increase in the elastic modulus of the sheet and a further increase in bending stiffness.

Keywords: air permeability, base paper, bending stiffness, copy paper, cross-section, distribution, drying, elastic properties, image analysis, internal bond, iodine, oil absorption, penetration, solids content, staining, starch, starch properties, surface sizing, surface strength
ISBN 951-22-7553-8, ISBN 951-22-7491-4, ISSN 1237-6248

juha.lipponen@metso.com

Table of Contents

Preface	iii
Abstract	iv
Table of Contents	v
List of Abbreviations	viii
1. Introduction	1
2. Objectives and Approach	6
2.1 Objectives.....	6
2.2 Approach.....	7
3. Literature Review	9
3.1 Starch Requirements for High Solids MSP Surface Sizing	9
3.2 Papermaking Conditions Influencing the Solids Content of the Starch Solution	9
3.3 Influence of Starch Amount and Z-Distribution on Paper Properties.....	12
3.4 Determining Various Z-Directional Distributions in a Paper Sheet	14
4. Experimental	17
4.1 Materials.....	17
4.1.1 Starches.....	17
4.1.2 Furnishes and Base Papers	17
4.2 Methods.....	18
4.2.1 Paper Analysis Methods	18
4.2.2 Papermaking Conditions	20
4.2.3 Surface Sizing and Calendering	21
4.2.4 Preparation of Sheets through Starch Impregnation with Different Starch Amounts	22
4.2.5 Starch Penetration Analysis.....	25
5. Surface Sizing with Starch Solutions at High Solids Contents Up to 30%.....	35
5.1 Results.....	35
5.1.1 Rheological Properties of Starch Solutions.....	35
5.1.2 Influence of Starch Solution Solids Content on Film Application, Starch Penetration and the Properties of Paper.....	39
5.1.3 Effect of Increasing the Solids Content on Drying Capacity and Runnability.....	50
5.2 Summary	51
6. Starch Penetration Analysis through Iodine Staining and Image Analysis of Cross- Sections of the Paper Structure	54
6.1 Results.....	54

6.2	Summary	59
7.	Mechanical Properties of Woodfree Paper Sheets at Different Surface Size Starch Amounts	61
7.1	Results	61
7.2	Summary	66
8.	Effect of Basis Weight and Press Draw on Woodfree Paper Properties during High Solids Surface Sizing.....	69
8.1	Results.....	69
8.2	Summary	75
9.	Concluding Remarks	77
	Literature	79

This dissertation is mainly based upon Papers I through V. The dissertation begins with a literature overview on surface sizing and woodfree papermaking technology, where their development to present day is reviewed as a basis for the discussion in the following sections. This literature review on surface sizing and woodfree papermaking in general is followed by a discussion of the possibility of increasing starch solids contents using state-of-the-art Metered Size Press (MSP) technology (*Papers I and II*). A novel tool for gaining a more fundamental understanding of the surface sizing process through the z-directional penetration of starch in a paper sheet is then introduced (*Paper III*). A set of sheet measurements describing the properties of paper as a function of surface size starch amounts is presented (*Paper IV*) as a basis for utilizing the analysis method put forth for the characterization of the sheet structure as a function of local starch content in the z-direction. Possibilities for optimizing the papermaking process with the specific aim of compensating for the related negative effects on final paper properties, e.g. decrease in internal strength, are finally investigated. With respect to the paper making process, basis weight and press to dryer draw are studied in relation to tuning the internal strength properties of the paper sheet (*Paper V*). This dissertation is mainly based upon the following five papers, which can be found as Appendices I through V.

I	Lipponen, J., Grön, J., Bruun, S-E. and Laine, T. Surface Sizing with Starch Solutions at High Solids Contents up to 18%, <i>Journal of Pulp and Paper Science</i> , 30(3) pp. 82 (2004).
II	Lipponen, J., Grön, J., Bruun, S-E. and Laine, T. Surface Sizing with Starch Solutions at Solids Contents up to 30%, <i>Professional Papermaking</i> 1/2003, p. 55 (2003).
III	Lipponen, J., Lappalainen, T, Astola, J. and Grön, J. Novel Method in Quantitative Determination of the Starch Z-Directional Distribution in Cross Sectional Images of Surface Sized Paper Samples. <i>Nordic Pulp and Paper Research Journal</i> 19(3) pp. 300 (2004).

- IV Lipponen, J., Pakarinen, J., Jääskeläinen J. and Grön, J. Mechanical Properties of Woodfree Paper Sheets at Different Surface Size Starch Amounts. Accepted for publication in Paperi ja Puu – Paper and Timber (2004).
- V Lipponen, J., Grön, J. Effect of Press Draw and Basis Weight on Woodfree Paper Properties during High Solids Surface Sizing. Tappi J., 4(1) pp. 15 (2005).

The author has made the following contributions to the above publications I–V:

- I and II Designing the experimental plan, executing the pilot scale study, conducting wet and remaining film measurements during the trial, analyzing the paper measurement results, and writing the paper
- III Outlining the targets of the study and presenting the starch penetration analysis problem to the imaging and image analysis experts. Participating in and commenting on methodology development, analyzing the results and preparing a numerical presentation of the results obtained. Writing the paper (excluding the section explaining the image analysis of the cross-sections).
- IV Outlining the targets of the study and describing the methodological approach of the study, as well as writing the majority of the paper.
- V Designing the experimental plan, executing the pilot scale study, analyzing the paper measurement results, and writing the paper.

List of Abbreviations

η	Viscosity (mPa)
θ	Temperature (°C)
ρ	Starch content (%)
τ_B	Yield stress (mPa)
ϕ_c	Solids content (%)
$\dot{\gamma}$	Shear rate (s ⁻¹)
<i>A</i>	Area
AKD	Alkylketene dimer
BF	Bright field
BR ₁₀₀	Brookfield viscosity at a spindle speed of 100 rpm (mPas)
BSE	Back scattered electron
C2S	Simultaneous coating on both sides
CaCO ₃	Calcium carbonate
CCD	Charge Coupled Device
CD	Cross direction of the paper web
CLSM	Confocal Laser Scanning Microscopy
CRT	Cathode ray tube
CSF	Canadian standard freeness (ml)
CV	Coefficient of variance
<i>d</i>	Ply thickness
DF	Dark field
DP	Degree of polymerization
DS	Degree of substitution
DS-COOH	Degree of substitution of carboxyl groups
DS-NH ₄	Degree of substitution of quaternary ammonium groups
<i>E</i>	Elastic modulus
EDX	Energy-dispersive X-ray spectrometry
ESEM	Environmental scanning electron microscopy
<i>G</i>	Median filtered vector
<i>GR</i>	Grayscale
ICP-AES	Inductively coupled plasma atomic emission spectroscopy
I-KI	Iodine potassium iodine
IR	Infrared
<i>L</i> *	Reference target (lightness)
LMIG	Liquid metal ion gun
LWC	Lightweight coated magazine paper
MD	Machine direction of the paper web
MIR	Multiple Internal Reflectance
MSP	Metered size press

M_w	Average molecular weight
OBA	Optical brightening agent
OsO ₄	Osmium tetroxide
P	Penetration curve
P&J	Pusey & Jones (a hardness measuring unit)
PCC	Precipitated Calcium Carbonate
Q	Penetration number
RGB	Red-Green-Blue
ROI	Region of Interest
S_b	Bending stiffness
SDTA	Short-dwell blade application
SEC	Size exclusion chromatography
SEM	Scanning electron microscopy
SSC	Simulated starch content
T	Threshold value
ToF SIMS	Time of flight secondary ion mass spectroscopy
UCWF	Uncoated woodfree
w	Thickness
WF	Woodfree
z	Thickness-direction coordinate

1. Introduction

Uncoated woodfree grades, such as copier paper, are considered to be among the most technically developed grades as they have to meet very demanding and comprehensive manufacturing specifications. High bulk and stiffness are required to ensure acceptable performance on a sheet-fed press and subsequent folding to reduce the risk of jamming at higher printing speeds. With office papers good sheet stiffness also typically characterizes a premium quality sheet. This is normally related to lower filler content, the use of eucalyptus fiber, and consequently the higher bulk of the sheet. High stiffness demands introduce additional challenges when a reduction in basis weight is required. Low sheet porosity increases process speeds by decreasing the drying time of inks, and therefore reduces setoff. Print-through is also reduced with reduced porosity. Sheet sortability and finishing are, to a large extent, connected with the curling tendency of the sheet and also affect its runnability on a printing press. Dustlessness, toner consumption, cleanliness, maintenance savings, copier/printer durability, and a reduction in the number of defective pages are all related to the operating and maintenance costs of copiers and printers. The multifunctional use of laser printers, ink-jet printers and plain paper faxes in addition to copying is a requirement with higher quality grades. The growth of network printing that also includes copiers will increase the demand for multifunctional office paper sheets (Source: Jaakko Pöyry Consulting).

The development of these properties – while at the same time reducing production costs – presents a challenge in the development of paper properties. Production and growth rates for different paper and board grades are illustrated in *Figure 1*. One can notice in this figure that woodfree grades are among the fastest growing paper grades, which makes them important in terms of their market volume also in the future.

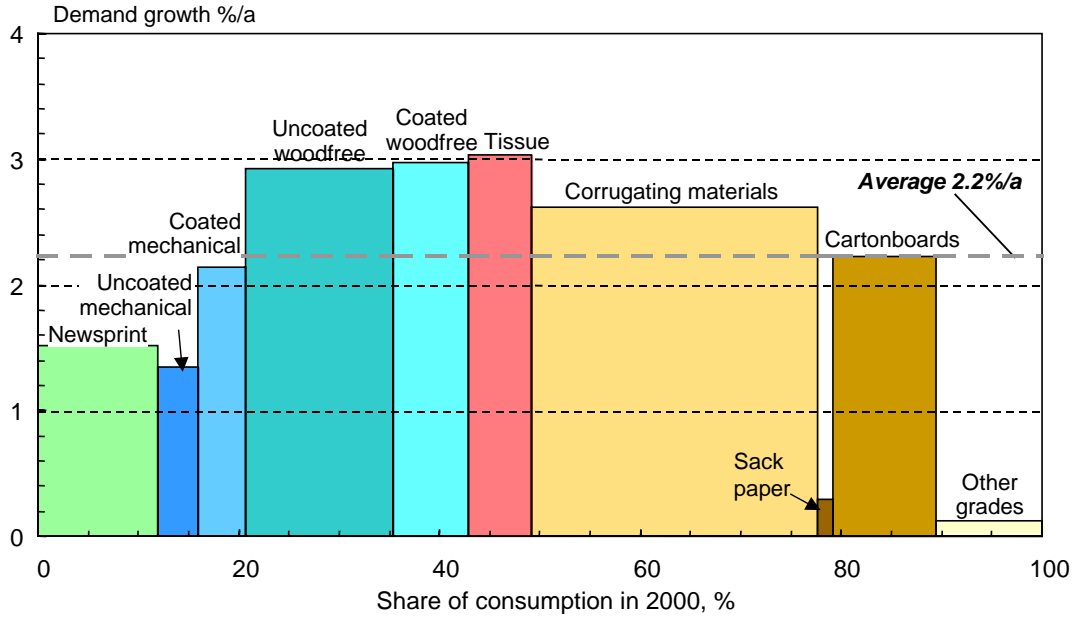


Figure 1. Growth and shares of paper and board grades up to 2015 (Source: Jaakko Pöyry Consulting, 2000)

Within the uncoated woodfree grades, the growth rate of office paper sheets (copying and printing) is expected to exceed 4% annually up to 2013 (Figure 2).

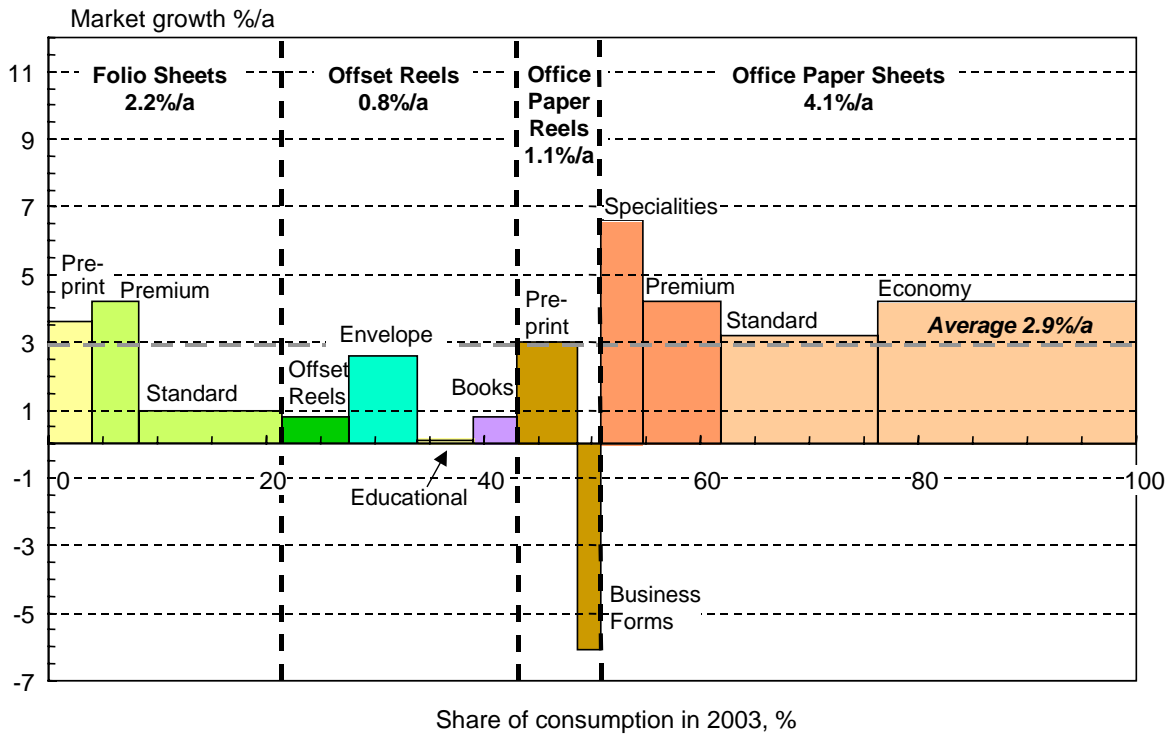


Figure 2. Growth and market shares of uncoated woodfree grades in Europe up to 2013 (Source: Jaakko Pöyry Consulting, 2003).

The variables that determine the quality and efficiency of papermaking can be derived from such basic sciences as chemistry and physics, and such applied sciences as engineering (e.g. mechanical, electrical and automation). In the context of the paper industry, these fields of science are reflected in papermaking technology through the desired paper structure, runnability and papermaking concepts (from stock preparation to roll and ream wrapping processes). These variables contribute to the quality and productivity of papermaking, which eventually defines the boundaries for the profitability of the business itself – from a technological point of view. This approach is illustrated in *Figure 3*. This study attempts to increase the profitability of uncoated woodfree paper production by improving the productivity and quality of the surface sizing process. Here, the objective is to considerably increase starch solution solids contents in surface sizing with the help of a more economical paper machine concept in order to gain related positive effects on the structure of paper, runnability, and drying capacity.

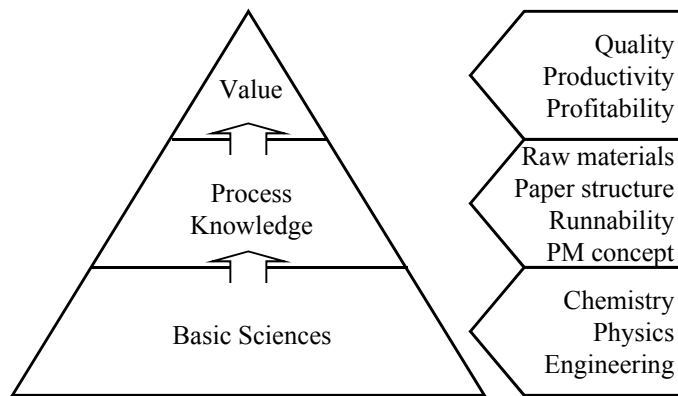


Figure 3. Interaction of papermaking profitability and basic sciences through papermaking process issues.

Surface sizing solids contents of up to 30% have not been used due to the insufficient stability of starch at elevated solids contents and maintaining the binding power of the starch. Also the ability to maintain the amount of starch at the MSP application at very high solids contents has been lacking. Here, both the chemistry of the starch solutions and the application technology used need to be developed in order to produce the desired applied starch amount at starch solids contents of up to 30% with desired binding properties. The features of the base paper also need to be adjusted to fit the features of high solids surface sizing.

The uncoated woodfree paper manufacturing process consists of a sequence of subprocesses, all of which play important roles in the overall process. In these various papermaking processes, water is removed from the fiber network and the paper web is created as fibers bond with each other mainly through hydrogen bonds. In the surface sizing process more water is introduced into the sheet, which breaks up the hydrogen bonds formed in the web. This rewetting is hindering MSP and afterdrying runnability (through

collapsed web strength and tension holding ability as the hydrogen bonds are released) and drying capacity (through increased afterdrying needs). These features are illustrated in *Figure 4*.

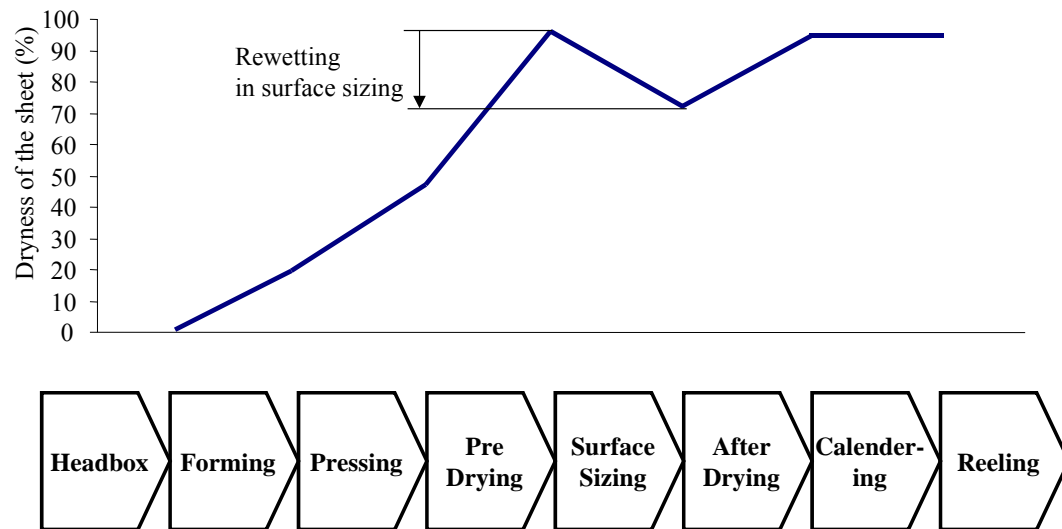


Figure 4. A schematic illustration of the process phases in manufacturing uncoated woodfree paper from the viewpoint of sheet dryness at each process phase.

Surface sizing is an operation in which a sizing agent is applied to the surface of the previously formed web (Hoyland *et al.* 1977). The main role of surface size is to strengthen the surface and bind particles, such as fibers and fillers, to the surface. Starch is also expected to add internal strength to the sheet through liquid penetration in the z-direction (Bergh 1984). There are numerous techniques for applying starch on the paper surface, such as a pond size press, gate roll size press, or a metered size press (MSP). The various technologies used in surface sizing are widely described in literature (Grön and Rantanen 2000). *Figure 5* illustrates the structure of paper with surface sizing (Lipponen *et al.* 2002). There have not been any major technological leaps in WFU surface treatment techniques since the introduction of film transfer size presses in the 1980s. At the same time, some fundamental process innovations have been introduced to the market for the earlier stages of the woodfree paper manufacturing process, such as stratified headboxes, gap forming, closed press sections, next generation drying methods, and improved runnability technology (e.g. Odell and Kinnunen 1998; Juppi and Kaihovirta 2002).



Figure 5. The effect of surface sizing on the structure of paper.

The developments described above represent evolution within MSP surface sizing and other subprocesses, consisting of technological advances in paper machinery, paper structure and papermaking chemistry. However, further development of the paper manufacturing process requires a multiskilled approach to papermaking technology as a whole. Optimization should proceed from local 'micro-optimization' toward production line-wide 'macro-optimization' – taking into account various interdependencies throughout the whole process.

This study is an attempt to identify ways to substantially decrease the investment and production costs involved in uncoated woodfree paper manufacturing by developing more cost-effective paper machine concepts that utilize considerably higher solids contents in surface sizing. This study is conducted by describing and optimizing the structure of paper in trials affecting the z-directional distribution of starch, together with the methods used to characterize related changes. Further process optimization with respect to the base sheet and final paper properties is also a subsequent topic of interest. Here, the final goal of this study is to find opportunities for increasing the profitability of WFU processes by reducing the investment cost of the process equipment, decreasing production costs (e.g. energy consumption) and increasing runnability potential.

2. Objectives and Approach

2.1 Objectives

The objective of this study was to considerably increase the starch solids content used in surface sizing. The intent was to increase the starch solids content without increasing the applied amount of surface sizing starch. This requires the ability to reduce the film amount in the MSP application. Less water would then be applied to the sheet in the MSP process, which would increase drying capacity and reduce steam consumption per paper ton produced. This interdependence is illustrated in *Table I* at two different starch solids content levels (i.e. 10% and 30%) and a constant starch amount.

Table I. Change in steam consumption when increasing starch solids content from 10% to 30% while maintaining the applied starch amount constant.

Starch Amount g/m ²	Starch Solids Content %	Web Dryness After MSP %	Applied Water Amount g/m ²	Steam Consumption (¹) kg/h	Steam Consumption (²) t/y
3	10	73.8	27	12442	74
3	30	91.6	7	3226	19
Difference			20	9216	55

(¹ Speed and width of the machine 1200 m/min and 8 m, 1 kg of steam needed to evaporate 0.8 kg of water

(² Time efficiency 85%

In *Table I*, one can observe that increasing the starch solids content remarkably decreases drying energy consumption. Considering the total drying capacity available on a machine one can also calculate that paper machine drying capacity can be increased by approximately 20% (assumptions: press dryness 45% and predryer moisture 3%) when less water is applied to the sheet at MSP. This would then mean that the production speed of an operating paper machine could be increased by 20% within the existing space (i.e. without moving the reel forward). The size press would, however, have to be moved forward in the process due to changes in drying capacity requirements between the predryer and afterdryer sections. The difference in dryness after MSP is also remarkable. Considering the exponential dependence of web strength on dryness, there is as well an increase in runnability potential with higher surface sizing starch solids contents. Improved runnability is understood here as decreased break frequency and increased sheet stability after MSP and during afterdrying due to reduced wetting and increased sheet wet strength and elasticity.

The optimization of starch properties in terms of solids content, molecular weight and various rheological properties was an essential part of this research. There was a consequent need to maintain the runnability and the film forming capability of the process when applying thinner starch films on roll surfaces. Here, the combination of the

controllable rheological properties of the starch solution with the required binding potential was of great importance to this study.

Improved sheet properties were also one of the major objectives of the study as surface sizing with increased solids contents was studied. Here, starch is to remain more on the surface giving a number of favorable properties to paper, such as increased surface strength and stiffness, as well as decreased porosity. Decreased penetration is also expected to reduce the internal bonding of the sheet. When starch is concentrated on the surface of the sheet, compensating for the reduced internal bond and the resulting requirements on machine running parameters and base paper properties were also of interest in this study.

In order to evaluate the effects of different surface sizing conditions and starch penetrations, a novel method was developed for determining and characterizing the distribution of starch quantitatively. The desired starch penetration level could then be determined based on various paper quality parameters.

The bending stiffness of the paper sheet is expected increase as starch is concentrated on the surface. Given the interdependence of the elastic modulus and bending stiffness, and in more general terms the dependence of bending stiffness on the z-directional distribution of the elastic modulus based on the distribution of starch, the elastic modulus as a function of starch content is of interest in this work. The level of bending stiffness can then be calculated based on the determined elastic modulus distribution.

2.2 Approach

The solids content increase was verified in pilot trials that involved process optimization, including development work on the properties of starch and on related application technology. The film amount was restricted in this study in order to keep the starch amount constant. A wide range of the rheological properties of the starch solutions were determined. Viscosity measurements were performed within a broad range of shear rates and yield stress was measured as an indicator of sheet release properties. The results were presented as a function of starch solids content with two constant starch amounts to evaluate its effect on paper properties.

The internal strength of the sheet was expected to decrease as starch remained on the surface of the sheet. The optimization of the base paper properties was performed by adjusting such paper machine running parameters as press to dryer draw and by decreasing the basis weight of paper, both of which were expected to reduce the internal strength of the base sheet. Compensating for this decrease in the internal strength of the final paper as the starch solids content increased was then attempted.

Starch solids content was expected to have an effect on the z-directional distribution of starch. A novel method for the quantitative characterization of starch penetration was therefore developed. This method was then utilized to evaluate starch distributions in samples sized at different starch solids contents.

The effect of starch content on the sheet's elastic modulus was measured in order to determine the bending stiffness mechanism in terms of different z-directional starch distributions. The z-directional distribution of the elastic modulus determined based on the distribution of starch (measured using the method introduced in this study) can then be used in the numerical modeling of bending stiffness.

3. Literature Review

3.1 Starch Requirements for High Solids MSP Surface Sizing

Starches used for surface sizing are normally both native and modified starches, which are either physically or chemically modified through the introduction of functional groups (Bergh 1997). The main raw materials for starch are standard yellow corn, wheat, potato and waxy corn. Different starch raw material sources give their signature properties to starch solutions through differences in the molecular structures of starches. These differences explain some of the rheological properties of various starches in terms of their relative amylopectin and amylose content, for example (Sirois 1992). There are many modification methods, such as oxidation, thermal modification, and ionization. Remmer and Eklund (1991) report that the viscosity of the starch solution is the most important liquid parameter determining its sorption rate. They also claimed that the degree of cationization of the starch used did not influence its sorption into paper. Felder (1991), on the other hand, uses cationization as an explanation in discussing the differences in strength values (e.g. internal strength) when comparing pilot trial results obtained with cationic and enzymatically converted starch.

Certain properties are required of starch at the MSP metering and transfer stages, such as the ability to remain stable even at high solids contents (Oja *et al.* 1991). The rod metering process is critical since the leveling and overall quality of the film directly influence paper properties. Here, the rheological properties of starch will be crucial in terms of its stability. (Bruun 2000 and Glittenberg 2000)

Paper properties, such as surface and internal strength, that are promoted by surface sizing have been controlled through starch modification to achieve different viscosity levels and the desired starch penetration. This modification has consisted of degrading the starch molecules to different degrees to get the desired rheological properties for the starch solution. Glittenberg and Becker (2002) present results in surface sizing at solids content of even up to 40%. They report excellent starch stability and runnability of the MSP unit using starches degraded down to short molecular lengths. But, if a starch molecule is broken down into too short chains it can turn into sugars with limited film forming capacity and ability to enhance the desired paper properties. Then its functionality as a binder is considerably reduced (McQueary and Thomas 1991).

3.2 Papermaking Conditions Influencing the Solids Content of the Starch Solution

A number of studies have been carried out on surface sizing with the MSP technique, even at high solids contents. However, increased solids contents have restricted the ability to maintain low dry starch amounts, i.e. below 1.5 g/m²/side. This study is aimed at

maintaining constant application of dry starch to paper despite high solids content. This is accomplished by optimizing the application conditions, e.g. roll cover hardness, grooved rod type, and even using smooth rods. Here, a smooth rod diameter was selected based on targeted starch amount. When applying starch solutions at high solids contents, more uniformity is required of the thin starch film. Therefore, the inclination was to use very finely grooved rod profiles and at the highest solids contents even smooth rods, which also extend the roll grinding interval and rod changing cycle.

Küstermann (1990) and Felder (1991) studied surface sizing using a metered size press (MSP) with varied solids contents and aiming for a constant wet film amount, which resulted in varying starch amounts in the paper. However, they do not report in their work on the effects of increased solids contents while maintaining a low and constant applied dry starch amount. They do report effects on tensile strength and plybond strength, for example, as do Brogly and Harvey (1993) in their study in which starch pickup is varied at a constant (7%) solids content. However, varying the starch solution solids content in flooded nip size press, MSP and SDTA applications will affect the penetration of starch (e.g. Bergh and Åkesson 1988).

The solids content of surface size varies typically within a range of 3% to 18% depending on the application technology used. When adjusting the dry pickup at a size press, the starch solids content is typically between 3% and 9% (Klass 1997). Today, the pond size press still adds quality advantages over film transfer technology through more complete starch penetration (Grön and Rantanen 2000). However, there is a clear trend toward the use of film transfer technology (especially MSP) due to several disadvantages with the pond size press (Bergh 1997). Following are some of the drawbacks of pond size press technology:

- a tendency for turbulence in the pond creating flow instabilities and an uneven CD starch distribution at higher speeds (Klass 1992),
- high liquid pickup due to a low solids content to avoid pond instabilities, resulting in wetting and reduced strength properties (Hansson and Klass 1984),
- high demand for drying capacity at the afterdryer section due to high liquid pickup, which often limits production capacity (Hansson and Klass 1984), and
- limited adjustment options for the starch solids content and the applied dry amount due to almost constant liquid pickup determined by the dryness of paper and the level of internal sizing (Dill 1974, Klass 1997).

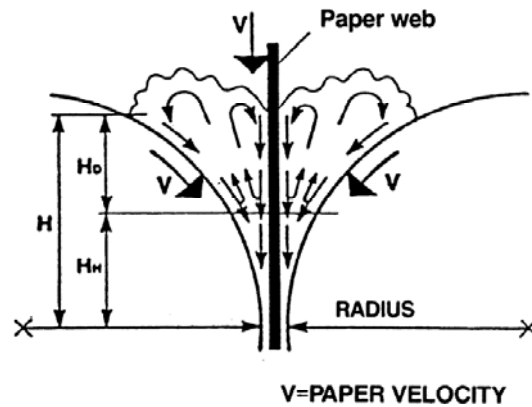


Figure 6. An illustration of the hydrodynamic forces and resulting instabilities in the open pond of the flooded nip size press (Klass 1990).

The metered size press was introduced in the early 1980s to overcome runnability problems related to pond size presses (Bergh 1997). It was then possible to deal with the problems noted above through

- an increased size solids content that reduced afterdrying capacity requirements and the number of breaks,
- a reduced interdependence between starch solids content and pickup, and
- a reduced dependence of size press pickup on internal sizing and base sheet moisture content. (Klass 1997)

Starch solids contents for MSP sizing vary between 5% and 18% at size amounts giving 0.7 g/m² to 4 g/m² (Klass 1997). However, with modern high-speed fine paper and packaging board machines this can lead to an uneconomical process due to high drying capacity demands on a long afterdryer section. In cases where the use of versatile MSP units with both coating and surface sizing capabilities is desirable, drying capacity needs to be over-dimensioned for coating to be able to evaporate the water applied during surface sizing.

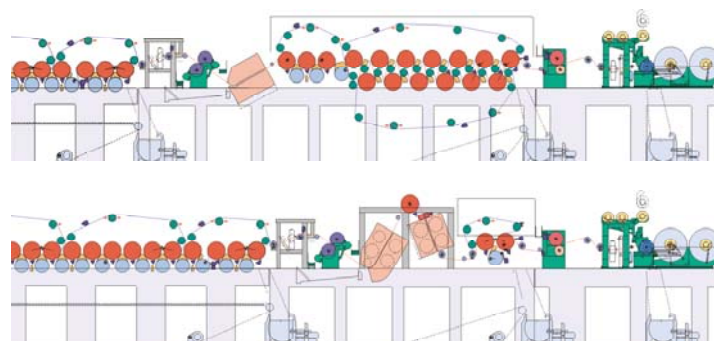


Figure 7. A schematic illustration of required afterdrying capacity in terms of the paper machine layout. The top layout represents the dry end of a modern uncoated woodfree machine with a starch solids content of 10%. In the bottom layout the speed of the line can

be increased by up to 20% – without increasing the length of the machine – by increasing the starch solids content to 20% (Source: Metso Paper, Inc).

Starch remaining on the surface of the sheet will decrease the internal strength of the sheet due to reduced liquid penetration of the starch solution (e.g. Bergh 1984). According to Juppi and Kaihoviirta (2002), the press draw has a significant effect on many mechanical properties, such as internal strength and porosity, of the woodfree base sheet. By reducing the press draw from 3% to 1% the internal strength of the sheet can be increased by up to 30%. This reduction of press draw was made possible by using a focused and intensified negative pressure region on the opposite side of the dryer fabric at the opening wedge of the dryer cylinder. Also, lowering the base sheet's basis weight below 80 g/m² is known to increase Scott bond values due to the decreased probability of potential rupture planes during Scott bond measurement (Kajanto 2000).

3.3 Influence of Starch Amount and Z-Distribution on Paper Properties

The effect of starch on paper properties has been widely studied with respect to wet end starch (e.g. Brown 1969, Laeigh *et al.* 1990, McQueary 1990 and Deters 1990). The emphasis in adding starch (either internal or surface sizing) is to boost such properties as water resistance, grease and solvent resistance and surface strength (Meaker 1984). The main role of surface size is to promote surface properties, i.e. strengthen the surface and to bind such particles as fibers and fillers to the surface. Starch is also expected to add internal strength to the sheet through liquid penetration in the z-direction (Bergh 1984). The main advantage of surface sizing over internal sizing is the excellent retention of the starch solution (Hoyland *et al.* 1977). At the flooded nip size press liquid pickup is mainly determined by the dryness of paper and its level of internal sizing (Dill 1974).

There are several studies in which the interdependence of z-directional strength properties and starch solution solids – explained by differences in starch penetration – is reported. Bergh and Åkesson (1988) report that starch could be retained on the paper surface by increasing starch solids contents up to 15% when using a short dwell (SDTA) application technique. Solids contents of 5%, 10% and 15% were used with about 0.5, 1.0 and 1.5 g/m² dry pickup, respectively.

There are, on the other hand, many studies on different application methods resulting in varied z-directional starch penetration behavior – also at comparable dry starch amounts – and consequently in different internal and surface properties of paper. Hansson and Klass (1984) investigated differences between the Billblade technique and pond size press with respect to starch penetration differences. It was found that blade application produced less starch penetration and increased the surface strength of paper. Tehomaa *et al.* (1992) compared SDTA blade application with MSP application for surface sizing and discovered clear differences in such fine paper properties as smoothness, porosity, stiffness, surface

strength and opacity using a constant dry pickup level. Here, it was found that Bendtsen air permeability decreased with blade application from 600 to 100 ml/min at a dry starch pickup of 2 g/m². In this study the lower starch penetration at an equivalent starch amount resulted in more attractive quality potential for blade application than for MSP. However, the conclusion of the study was in favor of MSP technology due to its better runnability and higher efficiency potential.

Such parameters as the elastic modulus of paper with different surface sizing starch contents could be of interest. However, comprehensive information on this is lacking in existing literature. Information on the elastic modulus (e.g. Setterholm and Kuenzi 1970) of the sheet structure is used in determining the bending stiffness of a sheet. Lekhnistkii (1968) expressed a general bending stiffness theory for an anisotropic thin plate. However, we now present paper as a specific case of this theory as an orthotropic and isotropic thin plate with the Poisson's ratio ν equal to zero in all directions. Then, the bending stiffness S_b of a symmetrical layered structure where the elastic modulus of the surface plies is equal to E_1 and that of the mid-ply to E_2 , while the total sheet thickness equals d and the thickness of the mid-ply equals d_2 , can be expressed as follows (Kajanto 2000):

$$(1) \quad S_b = \frac{E_1 d_1^3}{12} + \frac{E_2 (d^3 - d_1^3)}{12}$$

Based on the definition of bending stiffness given in *Eq. 1*, elastic modulus should increase as a function of starch content in the z-direction, i.e. when concentrating starch on the surface (increasing the starch content of the surface layer). Kartovaara (1989) proposed a profile model for predicting bending stiffness values taking into account the elastic modulus distribution using the change in the elastic modulus near the surfaces based on the roughness profile. Generally, without assuming sheet symmetry or definitive thickness and elastic modulus properties for each ply, bending stiffness can be expressed in more universal terms as (Kajanto 2000)

$$(2) \quad S_b = \int E(z) z^2 dz$$

The z-directional elastic modulus distribution (i.e. $E(z)$) can be used when determining the bending stiffness of a sheet. This would require studying factors governing the elastic modulus of paper structure. Here, the effect of starch content on elastic modulus is of interest. A quantitative approach to looking into the behavior of bending stiffness S_b would then be possible when determining the z-directional starch distribution of a sheet. This approach is illustrated in detail in *Figure 8*.

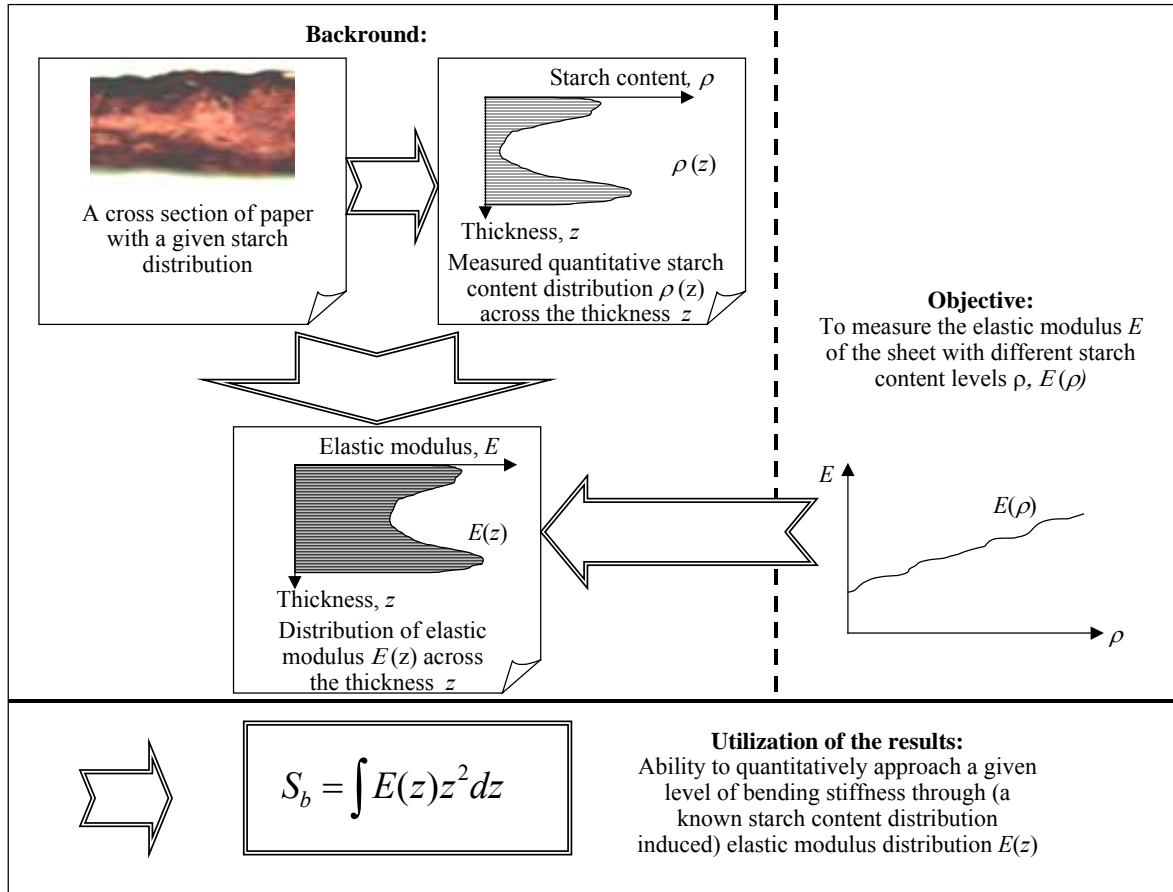


Figure 8. Illustration of the background of determining the elastic modulus E as a function of starch content ρ , $E(\rho)$.

3.4 Determining Various Z-Directional Distributions in a Paper Sheet

Starch penetration and the consequent z -distribution of starch in the sheet are often discussed when different surface sizing methods or process variables, such as solids contents or viscosity levels, are evaluated against the properties of paper (e.g. Hoyland *et al.* 1977; Wight 1988; Sollinger 1988; Küstermann 1990; Ryder 1997). These conclusions are frequently supported by qualitative evaluations of cross-sectional images describing the starch penetration (e.g. Fineman and Hoč 1978; Bergh 1984; Hansson and Klass 1984; Rantanen and Westergård 1987; Bergh and Åkesson 1988; Tehomaa *et al.* 1992; Kimpimäki and Rennes 2000; Lipponen *et. al* 2002). Here, paper properties are assumed to reflect the penetration behavior of starch. Marton (1974) studied ash and starch z -distributions through tape pull layer separation and analyzed the resulting samples. Cross-sectional images are commonly used to support the conclusions made based on differences in starch penetration. Cross-sectional images with iodine staining are prepared by dipping paper samples in a solution of iodine potassium iodine (I-KI), whereby the starch in the sheet structure is dyed dark. An image is then acquired from the cross-section with a light microscope. This method is fast and inexpensive compared to the microtome preparation

procedure, for example. However, the process stages of the iodine staining penetration evaluation method are not standardized and the cross-sectional images are analyzed only visually. Further, a single cross-section – usually cut less than a millimeter in length – leaves the observation vulnerable to local variations in starch penetration caused by the properties of the base sheet, such as flocculation. This would then introduce a great deal of uncertainty into this type of evaluation of starch penetration. Iodine staining is also a well-known method for the determination of starch on the paper surface. Zsoldos and Sebess (1975) presented a new method for the determination of starch on the paper surface. In their method, the starch iodine reaction is performed in two stages: the water amount required for the reaction is achieved through water vapor condensation on the paper surface, and the required amount of iodine is sublimated from solid crystalline iodine.

Microtomic cross-sections are often used in illustrating paper structure in the *z*-direction. Preparing the microtomic cross-sections requires embedding the specimen in epoxy resin and curing it for a considerable period of time. The resulting blocks are then ground and polished. The final cross-sections are thereafter cut into thin slides for light microscope viewing, or further prepared for SEM analysis (e.g. Peterson and Williams 1992). Bailey and Bown (1990) use cross-sectional images for the qualitative evaluation of filler and coating color distributions in the paper sheet. SEM images are also used as a basis for the *z*-directional structural characterization of paper through image analysis of the cross-sections (Allem 1998, Grön and Ahlroos 1998, Allem and Uesaka 1999, Dickson 2000, Chinga and Helle 2002). However, in the examination of highly variable structures such as paper, small scale samples obtained with microtomic sectioning fail to fully represent significant structural features of the sheet. Williams and Drummond (1994) described an improved method for preparing large microtomic cross-sections for SEM analysis, presenting a polishing method conventionally used for the preparation of polished metallographic sections. With the method presented, samples of 200 mm total width could be prepared in less than 2 hours. However, the curing of resin still requires up to two days. In examining the cross-sections obtained through SEM, for example, grayscale segmentation based on thresholding grayscale histograms of digital images is a common approach. Manual thresholding, however, will vary between operators and even with one person over time. To avoid any subjective dependence in the thresholding of grayscale images on personal factors (e.g. Barratte *et al.* 1997), automated procedures are important to improve repeatability and to reduce subjectivity, as well as arduous work.

The ToF-SIMS (Time of Flight Secondary Ion Mass Spectroscopy) technique is used to analyze solid samples. This technique combines high surface sensitivity with low detection limits and high mass resolution. With the ToF-SIMS technique, it is possible to make distribution maps of ions with good spatial resolution. This technique is used, for instance, in probing the chemistry of surfaces (Kulick and Brinen 1998), in detecting desizing agents (Brinen and Kulick 1995), in analyzing AKD (Zimmerman *et al.* 1995), in detecting trace elements in wood (Bailey and Reeve 1994), and in analyzing printed papers (Preston *et*

al. 2000). This method is presented in a schematic illustration of the arrangement used in Figure 9.

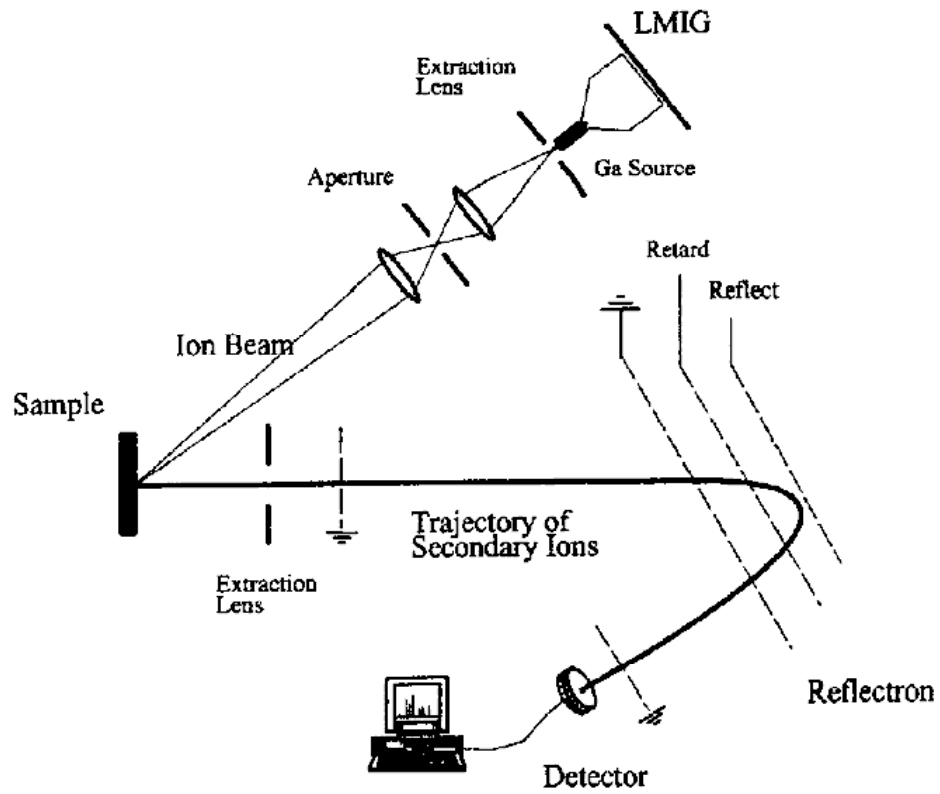


Figure 9. An illustration of the ToF-SIMS (Time of Flight Secondary Ion Mass Spectrometry) surface analysis method (Fisher et al. 1999).

4. Experimental

4.1 Materials

4.1.1 Starches

Two modified potato-based starches were used in our study (Ciba Specialty Chemicals Inc., Raisio, Finland). These starches were modified with a specific focus on stability even at high solids contents in the starch solutions.

A native potato starch was initially modified through oxidation with hypochlorite, and the content of carboxylic groups in the oxidized starch was about 1% ($DS_{\text{-COOH}} = 0.031$). The viscosity of this starch A (Raisamyl 01020) was 20 mPas (Brookfield 100 rpm, 60 °C) at a concentration of 10%. Cationization was done by introducing quaternary ammonium groups followed by oxidation of the starch. The degree of substitution ($DS_{\text{-NH}_4}$) was 0.018. The viscosity of cationic starch B (Raisamyl 24520) was 100 mPas (60 °C) at a concentration of 10%. Four parts of OBA (Optiblanc NF, 3V, Bergamo, Italy) were used in the starch solution. The starch properties are summarized in *Table II*.

Table II. Starch properties.

Property	Solids Content (%)	Starch A	Starch B
Viscosity, Brookfield 100 rpm at 60 °C (mPas)	8	27	35
	12	48	65
	15	60	95
	18	70	140
	21	65	207
	24	80	338
	27	125	–
	30	158	–
Average molecular weight, M_w (g/mol)		27,000	$\sim 50,000$ ¹⁾
Degree of polymerization, DP		150	300
Degree of substitution, DS		0.031 ²⁾	0.018 ³⁾
¹⁾ Not measurable with the columns used in Size Exclusion Chromatography (SEC) ²⁾ Degree of substitution of carboxyl groups ($DS_{\text{-COOH}}$) ³⁾ Degree of substitution of quaternary ammonium groups ($DS_{\text{-NH}_4}$)			

4.1.2 Furnishes and Base Papers

A woodfree furnish was used in making the base paper for the study on the effect of basis weight and press to dryer draw (*Paper V*). The furnish properties are summarized in *Table III*.

Table III. Furnish properties (Paper V).

Properties		
Freeness (CSF)	ml	505
Filler content	%	23.3
Filler type		CaCO ₃
Length weighted fiber length	mm	1.28
Softwood/hardwood content	%	30/70
Birch	%	70
Pine	%	21
Spruce	%	9

Woodfree base papers without surface sizing and basis weights of 82, 71 and 89 g/m² were used for the study. The properties of the base paper are presented in *Table IV*. The scope of measurements differs in these studies due to their different in the objectives and individual topics.

Table IV. Base paper properties.

Properties		Values		
Basis weight	g/m ²	82	71	89
Ash content	%	14.7	10.0	–
Internal sizing	%	0.8	0.8	–
Density	kg/m ³	736.5	738	844
Air permeability, Bendtsen	ml/min	775	709	–
Oil absorption, Cobb-Unger (10 sec)	g/m ²	47.7	34.3	–
Surface strength, IGT (MD)	m/s	1.32	–	–
Internal strength, Scott Bond	J/m ²	147	305	–
Bending stiffness (MD)	MNm	0.48	0.63	0.64
Bending stiffness (CD)	MNm	0.15	–	0.25
Opacity	%	93.8	–	–
ISO-brightness	%	93.9	–	–
Elastic modulus, Young (MD)	N/mm ²	–	–	7079
Elastic modulus, Young (CD)	N/mm ²	–	–	3206
References		(Paper I and III)	(Paper II)	(Paper IV)
"–" = not measured				

4.2 Methods

4.2.1 Paper Analysis Methods

Paper properties were measured based on the standards reported in *Table V*

Table V. Measurement methods and standards.

Methods	Standard
Basis weight	SCAN-P 6:75
Density	SCAN-P 7:96
Ash content	SCAN P 5:63
Oil absorption, Cobb-Unger (10 sec)	SCAN-P 37:77
Air permeability, Bendtsen	SCAN-P 60:87
Bending stiffness ¹⁾	SCAN-P 64:90
Bending stiffness, Taber ³⁾	TAPPI 489 om-99
Bending stiffness ⁴⁾	SCAN-P 64
Opacity	SCAN-P 8:93
ISO-Brightness	SCAN-P 3:93
Internal strength, Scott Bond	TAPPI T833 om-96
Surface strength, IGT	SCAN-P 63:90
Starch amount	TAPPI 419 om-91 ³⁾
Elastic modulus, Young ²⁾	SCAN-P 38:80
¹⁾ Papers I and II ²⁾ Paper III ³⁾ Paper V ⁴⁾ Paper IV	

The *rheological characterizations* of the starch solutions were performed at starch solution temperatures of 20°C, 30°C, 40°C and 50°C for each solids concentration (i.e. 8%, 12%, 15%, 18%, 21%, 24%, 27% and 30%). Flow in the low shear rate region (1–1500 s⁻¹) was studied with a rheometer based on Couette viscometric flow, where the inner cylinder is a stator and the outer cylinder rotates (Bohlin VOR rheometer, Bohlin Inc., Lund, Sweden). A yield stress, τ_b , describing the stress needed to obtain flow was calculated for the starch solutions according to the Bingham plastic flow model. An intermediate shear region (10³–10⁵ s⁻¹) was studied for the starch solutions with a rheometer based on Searle flow geometry, where the inner cylinder rotates and the outer cylinder is a stator (Hercules, HiShear rheometer, Kaltec Scientific Inc., Detroit, MI, USA). An air pressure region corresponding to a high shear region of 10⁵ s⁻¹ to 10⁶ s⁻¹ was used in the air pressure-driven capillary viscometer (ECV, Gradek Oy, Kauniainen, Finland), where the controlled shear stress measurements are based on Hagen-Poiseuille viscometric flow. Stainless steel capillaries were used with a length of 100 mm and a diameter of 0.55 mm. The data were adjusted for entrance effects according to Hagenbach-Couette and end-wall effects according to the Rabinowitz-Weissenberg equation (Grön and Eklund 1998).

The *total starch amount applied* (Papers I, II and III) was measured from paper samples using lithium chloride analysis (Mendham *et al.* 2000), where a weighed portion of the sample is burned in a muffle furnace. The residue is dissolved with acids and the individual element concentration is then determined with ICP-AES (Inductively Coupled Plasma Atomic Emission Spectroscopy).

Pore size distribution (Coulter) was determined by immersing the specimen in oil with low surface tension, thus causing the pores of the specimen to be filled. The wetted specimen was then placed in a sample holder. Compressed air with controllable pressure and measurable air flow was then applied to the other side of the specimen, increasing the flow in small steps. After repeating this sequence with a dry sample, the distribution of pores of different diameters was calculated using the relationship between the air pressure required to force the oil out of different diameter holes (Pore diameter = Constant * Surface tension / Air pressure).

At starch solids contents from 8% to 18% (*Paper I*), the results are presented for both starches at starch amounts of 1.8 and 2.5 g/m² total applied starch. The specific starch amounts are obtained by creating a linear trend line from the measured paper properties as a function of starch amount. Paper properties at given starch amount levels were then obtained by assigning the values 1.8 and 2.5 to the trend line equations. The results at starch solids contents 21% and 24% are presented with starch amounts of 3.2–3.3 with starch A and with starch amounts of 2.4–2.5 g/m² with starch B. Results at a solids content of 27% are presented with a starch amount of 3.2 with starch A, and at a solids content of 30% with starch A at an applied amount of 3.9 g/m².

4.2.2 Papermaking Conditions

The base paper (for the study reported in *Paper V*) was produced on a pilot paper machine (Metso Paper, Inc.) to basis weights of 68, 74 and 78 g/m² (bone dry) with three press to dryer draw levels (1%, 2% and 3%). The running speed in the paper machine trial was 1200 m/min.



Figure 10. Two photo images of the pilot paper machine used in the study (Source: Metso Paper, Inc.)

The drying of the base paper rolls was done at Keskuslaboratorio (KCL) in Helsinki, Finland. For surface sizing with high solids starch solutions, 9 rolls were made altogether. In addition, one roll was produced at 77 g/m² basis weight and with 3% press draw level to

be surface sized with a 10% starch solution as a reference. The furnish used in base paper making is explained in *Table III*.

4.2.3 Surface Sizing and Calendering

The trials were run as a two-sided simultaneous MSP application (OptiSizer, Metso Paper Inc.) at a speed of 1200 m/min and a linear load of 25 kN/m. In papers I and II the roll cover material used was polyurethane with a hardness of 36 P&J and the roll diameter was 950 mm. In Paper V the hardness of the cover was 32 P&J in the bottom position and 40 P&J in the top position, and the roll diameter was 1415 mm.

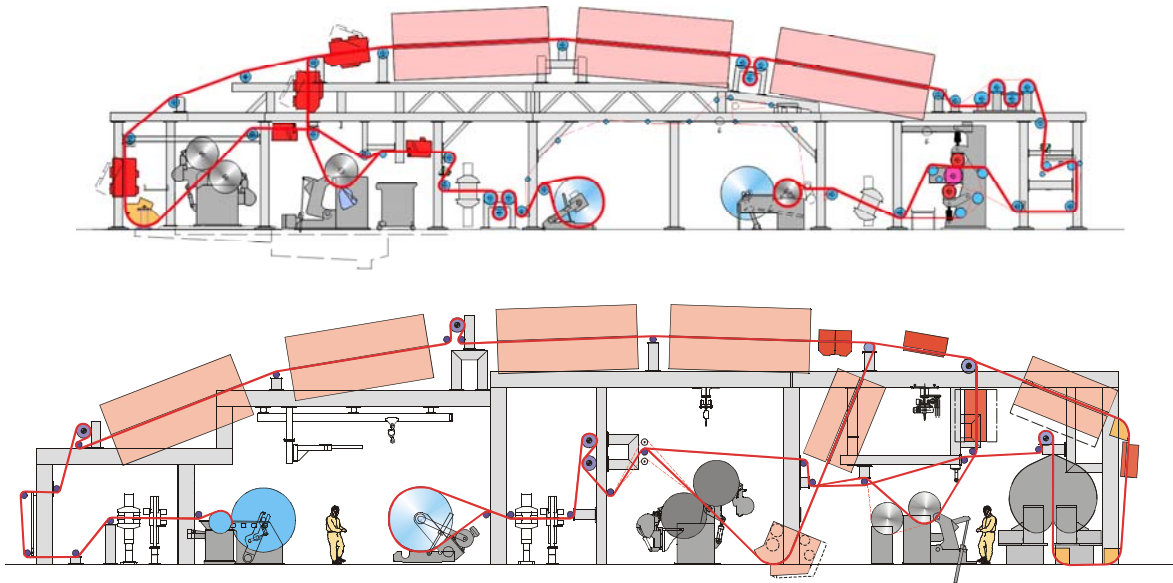


Figure 11. Pilot coaters used in the study: CTC Pilot OptiSizer, top (Papers I, II and III) and Metso Paper Järvenpää Pilot OptiSizer, bottom (Paper V).

Film metering was performed with both 10 mm grooved rods and 10 to 35 mm smooth rods. The grooved rod profiles selected were 0.25/23, 0.20/20 and 0.35/30 (Metso Paper, Inc.) to produce the different film thicknesses needed to obtain a constant dry starch amount of approximately 1 g/m²/side (*Paper I*) or 1.5–2 g/m²/side (*Paper II*) with different starch solids contents. The rod type was selected based on wet film amount measurements according to Grön *et al.* (1998). Here, the wet film amount premetered on the roll was determined by a "scraping-off" method. A device was used to remove starch solution from the roll surface on a specific width (0.050 m), time (seconds) and machine speed (m/s). The removed starch solution was gravimetrically determined, and an amount of premetered surface sizing starch was obtained at a given speed. *Figure 12* illustrates the scraping off sequence in determining the applied starch amount.

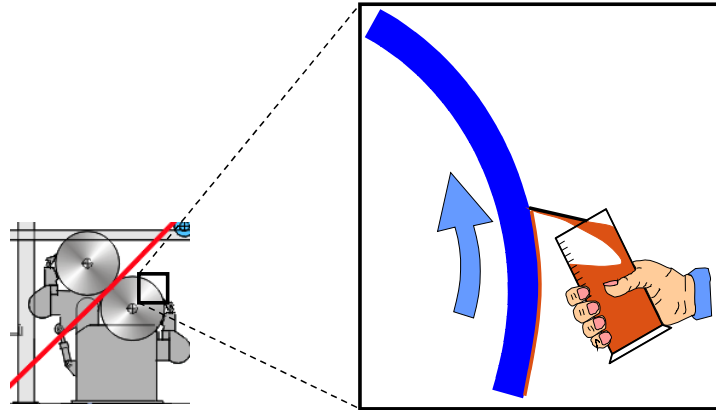


Figure 12. Arrangement for determining the premeted starch solution amount on the MSP roll.

The confidence of the method is dependent mainly on the accuracy of timing the scraping with a stop watch and the completeness of the scraping off the premeted film. Here, due to the hydrodynamical nature of the scrape off, approximately 5% of "remaining film" is left on the roll after the blade.

The trial was performed using a series of rod loads to obtain a set of film thicknesses. For example, solids content solutions of 15%–18% were applied using 20 mm smooth rods for low viscosity starch A and 15 mm smooth rods for high viscosity starch B to achieve the targeted dry starch amount. Further, solids content solutions of 21%–30% were applied using 10 mm smooth rods.

At solids contents from 8% to 18% (*Paper I*), the remaining film on the bottom roll was measured at each trial point in order to determine the transfer ratio in the film transfer process. In measuring the remaining film, however, the scraping time was increased to 20 s (instead of 10 s used in measuring the applied film) due to the almost negligible remaining film amount.

A single-nip soft calender was used at a machine speed of 1200 m/min, a steel roll temperature of 60 °C, and a linear load of 45 kN/m. The top side of the paper was run against the steel roll. The hardness of the polymer roll was 90 ShD and diameter 420 mm.

4.2.4 Preparation of Sheets through Starch Impregnation with Different Starch Amounts

Surface Sizing of Sheets

The surface sizing of the sheets was performed by applying a thin layer of 1% starch solution with a paint roller. Starch was applied to one side of the sheet and the sheet was then immediately placed on a forming fabric-supported vacuum table to impregnate the

starch into the sheet. After 5-second impregnation the vacuum table was brought under an impingement hood for 30 seconds of drying while still maintaining the vacuum. The temperature, impingement air velocity, and moisture content of the impingement air were set to 150°C, 30 m/s and 50%, respectively. Two different vacuum levels were used in the study. First a 3 kPa vacuum level was used allowing the sheet to shrink during the trial. Then, a higher vacuum level (12 kPa) was used to restrict drying shrinkage. Here, the restriction of shrinkage was assisted by fastening the edges of the sheet to the fabric using aluminum tape.

Each starch application was performed on both sides of the sheet. The different total starch amounts were then obtained through sequences of multiple application and drying stages. Iodine stained cross sections of the paper samples were observed to ensure the penetration of the starch at each application sequence. As the application and drying sequences proceeded, the pores of the sheet were eventually filled with starch and no more starch could be impregnated into the paper. This level would then represent the maximum reachable starch content in the sheets and the sheets were considered saturated. *Figure 13* illustrates the surface sizing and drying arrangement used.

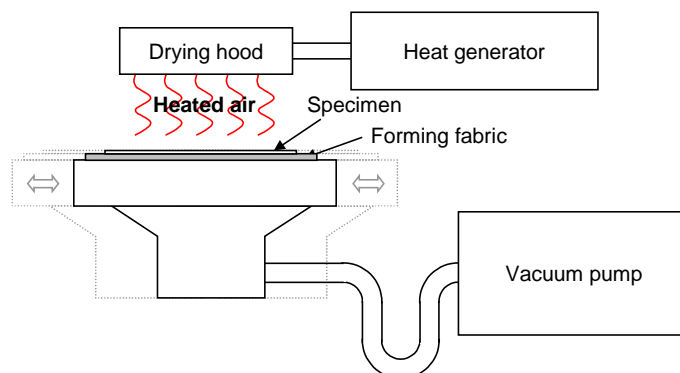


Figure 13. Schematic picture of the surface sizing and drying arrangement used in the study.

The applied starch amount was measured from the starch impregnated samples. In the case of paper samples prepared with water as a reference, paper samples were weighed right after the application of water to control the amount of water. Here, the same amount of water was targeted as in the 1% starch solution treatments. It was then possible to isolate the net effect of starch on the results.

A fairly broad range of different starch contents was selected for the study. The reason for this lies in the starch distributions achieved with different surface sizing techniques and starch solids contents (e.g. Bergh and Åkesson 1988 and Tehomaa *et al.* 1992), which sometimes result in starch concentrating intensively on the surface layer of the sheet. The applied starch amount of 2 g/m²/side will give an average starch content of 5% in the sheet with 80 g/m² standard copy paper. With high solids surface sizing the majority of starch

may even remain in the outermost 10% layer of the sheet on either side. The starch content of the surface layer then equals approximately 25%. This roughly determined the upper limit of the range of interest in terms of the starch content used in this work. This principle is illustrated in *Figure 14*.

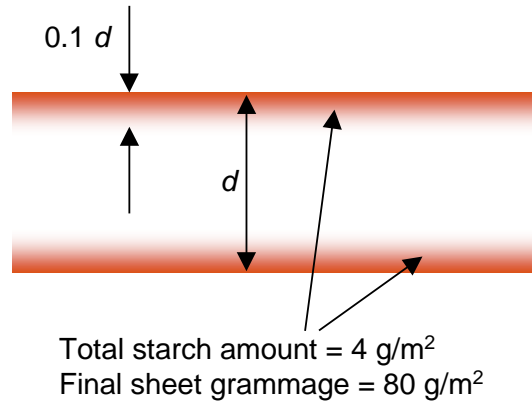


Figure 14. The effect of a schematic starch distribution in a commercial paper sheet on the starch content range studied.

The starch amounts obtained in the study, keeping in mind the targeted maximum starch content described above, are presented in *Figure 15*. One can observe that the starch content reached in the sheets varied from roughly 5% to more than 30% of starch. This gave a sufficient starch amount range for the study to consider the results representative of the highest starch contents in the top layer of a surface sized sheet of paper.

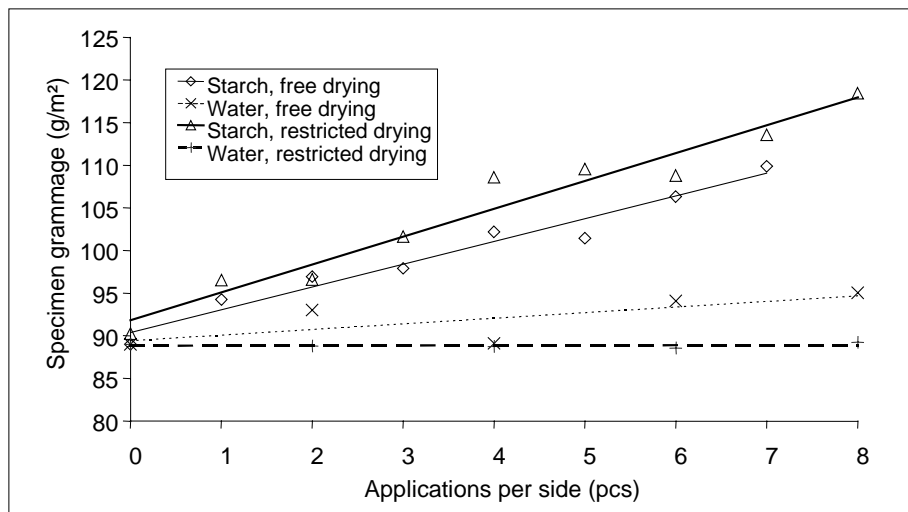


Figure 15. Basis weight of the sheet at different trial points of free and restricted drying with water and starch. The basis weight of the base sheet was 89 g/m².

In *Figure 15*, one can observe a slight difference between free and restricted drying both starch treated and water treated specimens. With water treated specimens, the difference can be explained through increased shrinkage of the specimens. In order to evaluate drying

shrinkage during the procedure, parallel specimens were prepared with a millimeter grid photocopied on the sheets. The shrinkage of the sheets could then be measured through changes in the millimeter pattern.

The results obtained with the method described here are presented in part 7 on page 61.

4.2.5 Starch Penetration Analysis

If a quantitative starch distribution analysis method providing reliable and repeatable information on starch penetration were available, more fundamental knowledge could be obtained of the parameters affecting the penetration of starch. Surface sizing and base paper parameters, and their effect on starch penetration – and on the desired paper properties obtained through starch – could then be investigated in much greater detail. Therefore, the aim of this part was to further develop the iodine staining starch penetration evaluation method in order to obtain quantitative starch penetration information.

Two main challenges were encountered in acquiring the aforementioned quantitative starch penetration (or starch distribution) curves:

- Defining a standardized procedure for preparing and photographing the iodine stained cross-sections. This way image acquisition would not be dependent on personal factors.
- Automated image analysis of the cross-sectional images.

The final aim was to develop a method for producing quantitative and comparable starch penetration curves and also a parameter for characterizing the *z*-directional penetration of starch, i.e. a dimensionless penetration number. This parameter could then be used in interpreting starch penetration-related paper properties. This information could, in turn, be used in evaluating and optimizing the papermaking parameters that influence starch penetration in the surface sizing process.

The results obtained with the method described are presented in part 6 on page 54.

Sample Preparation

Surface sized paper samples were cut in the machine direction with a surgical blade fastened to the side of a smooth-based metal block. Cutting was performed on a hard plastic plate. The surface of the cross-section was thus as smooth and planar as possible to give a clear and focused image of the whole cross-section under a microscope. A smooth surface was also necessary for uniform absorption of the I-KI solution into the cross-sectional surface. The blade was replaced after cutting 50 strips. The cross-sectional surface of the strip was then dipped in a 1–2 ml dose of 0.1 M iodine potassium iodine (I-KI) solution, which was pipetted into a separate glass bowl from a light-protected container immediately before dipping. The I-KI solution was replaced after each dipping to ensure its

purity and to keep light from weakening the dyeing reaction. The strip moistening time was approximately 1 second. After dipping excess I-KI solution was removed from the specimen by pressing a blotting board on the top and bottom surfaces of the strip without touching the cross-sectional surface itself. The strip was then set under a microscope to photograph the iodine-stained cross-sectional surface. The cross-section of the moistened sample was photographed under a microscope using a Nikon Eclipse ME600 light microscope (Nikon Corporation, Kawasaki, Japan), a PCO 12-bit CCD camera (PCO Computer Optics GmbH, Kelheim, Germany), and a variable Fostec DCR II planar light source (Schott Fostec, Auburn, NY, USA). The field of view under the microscope was 0.85 x 0.68 mm, and the size of the RGB image acquired of the cross-section was 1280 x 1024 pixels. The resolution of the image produced was therefore 0.664 $\mu\text{m}/\text{pixel}$. DF (Dark Field) illumination from above was used to light the specimen under the microscope. After manually focusing the image, specimens creating deep shadows (i.e. the edges of the cross-section not clearly visible) due to excessive cockling of the strip were discarded at this stage. Here, shadows at the edges of the cross-sectional image could distort the subsequent grayscale image analysis.

When changing the parameters of the cross-sectional imaging, e.g. a change in the exposure time t_{exp} , a reference target – a plastic slip of standardized lightness – was required for the determination of changes in the quantity of light reaching the CCD sensor, i.e. for the calibration of the imaging parameters to ensure the comparability of the images. The lightness of the reference target was $L^* = 34$, determined by spectrophotometry. The value of the global threshold, $T_{t_{exp}}$, used in the segmentation of the image was determined as follows:

$$(3) \quad T_{t_{exp}} = \langle GR \rangle_{t_{exp}} + T_{Bias}$$

where $\langle GR \rangle_{t_{exp}}$ was the mean of the grayscale histogram in an image of the reference target with exposure time t_{exp} , and where T_{Bias} was the global threshold that was used to select the darkness of pixels classified as starch. The grayscale threshold determined for the reference target using the illumination time t_{exp} was always employed for segmenting cross-sectional images acquired using the same exposure time.

Image Analysis of the Cross-Sectional Images and Acquisition of Penetration Curves

At the first stage of the image analysis, the location of the cross-section in the original 1280 x 1024 image was roughly determined using the contrast between the background and the strip itself. This was performed by segmenting the grayscale image into a two-level (binary) image $\mathbf{B}(i,j)$ of the grayscale cross-section. Thus, pixels labeled 1 correspond to the strip and pixels labeled 0 correspond to the background. The first estimate for the location of the strip in the image was obtained by calculating a projection from the binary image on the y axis. A rectangle within the sample to be analyzed was then chosen as the

Region of Interest, ROI (*Figure 16*). At the subsequent stages of image processing only this ROI was analyzed. This way the following image analysis required less computing power than analyzing the whole original 1280 x 1024 image.

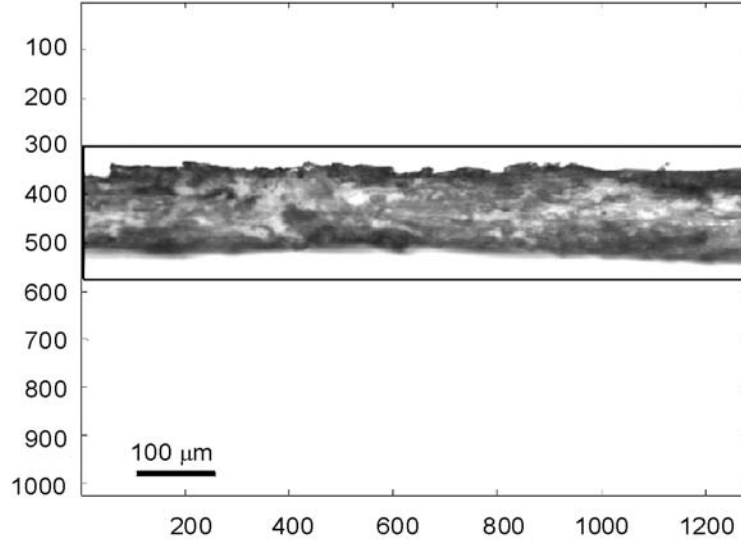


Figure 16. Identification of the position of the cross-section on the original microscopic digital image. The Region of Interest (ROI) – where the following image analysis is performed – is presented as a rectangle around the cross section.

Then, the binary image $\mathbf{B}(i,j)$ was analyzed column by column in order to identify the edges (i.e. the top and bottom surface curves) of the cross-sectional image. If there were bright undyed areas in the cross-sectional image, it was possible that the edges of the cross-sectional image could not be identified correctly in some columns of the matrix $\mathbf{B}(i,j)$. The vectors of edge points z_{top} and z_{bottom} were therefore filtered with a median filter. Vectors containing edge pixel values z_{top} or z_{bottom} can be presented as follows:

$$\begin{aligned}
 & z = z_{top} \quad \text{or} \quad z = z_{bottom} \\
 & G1(x_i) = med(z(x_{i-L1}), \dots, z(x_i), \dots, z(x_{i+L1})) \\
 & G2(x_i) = med(z(x_{i-L2}), \dots, z(x_i), \dots, z(x_{i+L2})) \\
 & G_{top}(x_i) = \max(G1(x_i), G2(x_i)) \\
 & G_{bottom}(x_i) = \min(G1(x_i), G2(x_i))
 \end{aligned}
 \tag{4}$$

where $G1(x_i)$ and $G2(x_i)$ are median filtered vectors, $L1 > n * L2$, $n \geq 5$ and $G_{top}(x_i)$ and $G_{bottom}(x_i)$ are the filtered vectors containing values of edge pixels at the top and bottom edge of the cross-sectional image. As seen in *Figure 17*, the filtration of vectors affects more the outward objects than the inward ones. Fibers and fines pointing outward from the surface (i.e. fibers torn off from the surface during the cutting of the cross-sectional surface) could thus be filtered from the cross-sectional image. The determined edge does, however, follow the surface to the bottom of any pores, as *Figure 17* (top) illustrates.

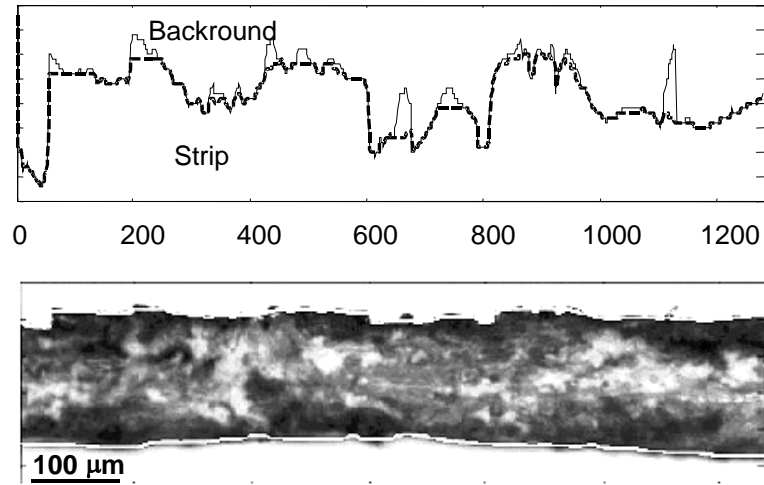


Figure 17. The edge detection method is illustrated using the top edge of the strip (top). The vector containing the values of edge pixels $z_{top}(x_i)$ is presented as a solid line and the median filtered one $G_{top}(x_i)$ as a dashed line (i.e. the determined top side edge curve of the strip). The bottom figure illustrates the completed top and bottom edge detection fitted on an image of the cross-section.

At the next stage of image processing, only the area between the detected top and bottom edges of the cross-sectional image was analyzed. Here, the area between the detected edges of the cross-sectional grayscale image was segmented using the global threshold T_{exp} (Eq. 3). T_{Bias} was the standard grayscale threshold, which was used to determine the darkness of pixels that were classified as starch. In our study, the threshold value T_{Bias} was determined by making a similar cross-sectional image of a base paper sample not containing surface sizing starch. T_{Bias} was set at a level at which less than 0.8% of the pixels in the base paper – based on the wet end starch content of the paper – were under the global threshold T_{exp} . The purpose of this approach was to calibrate the analysis of the dyeing reaction based on wet end starch in the specimens. In this study the threshold grayscale value T_{Bias} selected based on this condition was set at 16.

In order to determine the z-directional distribution of starch-containing pixels, cross-section thickness variations had to be removed during image analysis. Here, the thickness of the whole cross-section (i.e. all 1280 columns) was equalized by normalizing the length of the individual columns to a constant length of $w = 200$ pixels. This procedure is illustrated in Figure 18. A cross-sectional image with binary starch location information within a cross-section of constant thickness was then available for acquiring a z-directional distribution curve of pixels classified to contain I-KI-stained starch in the original cross-sectional image.

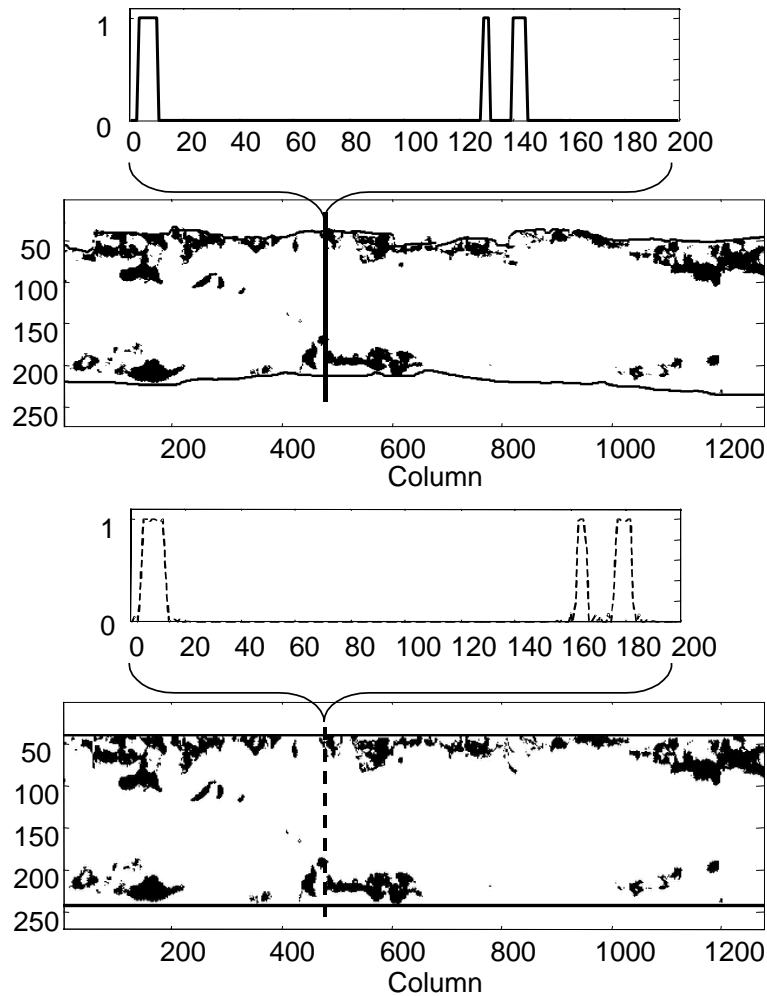


Figure 18. Original binary image with an illustration of a single sequence (top), and a thickness-normalized binary image with an illustration of a resampled sequence (bottom). The equalized thickness, w , of the resampled sequence is 200 normalized units.

As mentioned, the machine-direction length of a single cross-section was only 0.85 mm. On the other hand, several process parameters and paper structure variations – such as flocculation – may affect starch penetration behavior on the order of several millimeters. Therefore, in order to gain reliable information of overall starch penetration and its effect on paper properties on the macro scale, starch penetration information needs to be averaged from a larger amount of data. Examples of starch penetration curves averaged from 1, 3, 16 and 40 cross-sectional images of 1280 normalized columns are shown in Figure 19. Increasing the number of measurements n will give a more reliable estimate of the distribution than any of the measurements taken alone. The standard deviation of the mean, σ_x / \sqrt{n} , decreases slowly as n increases. It can be observed that the shape of the starch penetration curve obtained does not change significantly when 16 or more individual starch distributions are averaged. Sixteen cross-sectional images were consequently averaged to obtain the penetration curve for each specimen. Therefore, a total cross-

sectional sample length of 13.6 mm in the machine direction was included in the determination of the starch penetration analysis.

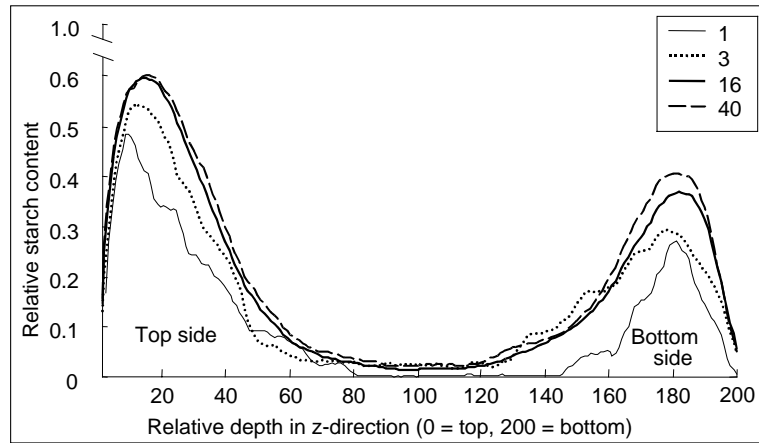


Figure 19. Starch penetration curves averaged from 1, 3, 16 and 40 cross-sectional images. These curves were obtained by averaging the corresponding number of cross-sections, each consisting of 1280 sequences. The relative starch content (between 0 and 1) on the y-axis describes the occurrence of pixels categorized to contain starch in the z-directional thickness of the sheet.

Definition of a Dimensionless Penetration Number, Q_{tot} and the Simulated Starch Content Distribution, $SSC(z)$

Once a usable method for determining a quantitative penetration curve is available, one might suggest that it would also be useful to describe a single dimensionless number to represent the relative penetration depth of starch. Such a number could then be used for the quantitative comparison of paper samples with different starch penetration levels. Further, a penetration number can be quantitatively used in comparing the penetration of starch in different paper samples (e.g. produced under different process conditions) to determine the function of any paper making variable whose contribution to surface sizing starch penetration behavior is of interest. Here, the thickness of paper was divided into four layers equal in thickness, and the integrals (areas covered by the penetration curve) of these sections were defined as A_{0-50} , A_{50-100} , $A_{100-150}$ and $A_{150-200}$. The suggested penetration numbers Q_{top} and Q_{bottom} were defined at both the top and bottom sides separately as the ratio of the area covered by the penetration curve at the inner quarter of the sheet's thickness and the area covered by the penetration curve at the half thickness of the specimen. The mean penetration number Q_{tot} was then calculated as the weighed average of the penetration numbers obtained from the two sides as Q_{tot} . This definition of the penetration number Q is illustrated in Figure 20 and in Eq. 5.

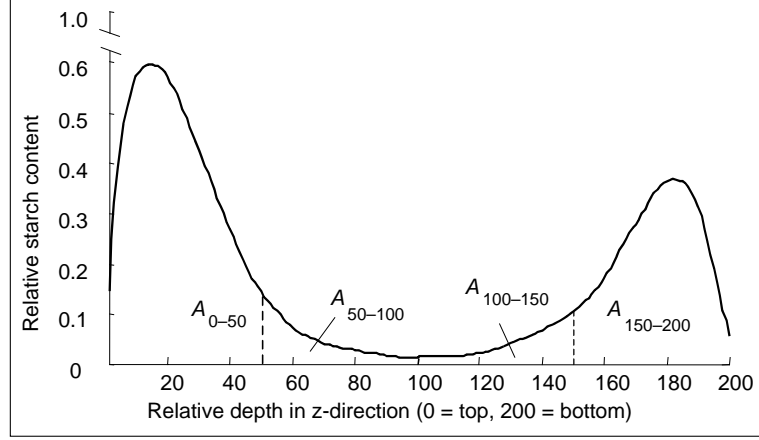


Figure 20. An illustration of the cross-sectional areas A_{0-50} , A_{50-100} , $A_{100-150}$ and $A_{150-200}$ covered by the obtained starch penetration curve. These cross-sectional areas are then used in the determination of the penetration number Q . The relative starch content (between 0 and 1) on the y-axis describes the occurrence of pixels categorized to contain starch in the z-directional thickness of the sheet.

$$\begin{aligned}
 Q_{top} &= \frac{A_{50-100}}{A_{0-50} + A_{50-100}} \\
 Q_{bottom} &= \frac{A_{100-150}}{A_{100-150} + A_{150-200}} \\
 Q_{tot} &= \frac{Q_{top}(A_{0-50} + A_{50-100}) + Q_{bottom}(A_{100-150} + A_{150-200})}{A_{0-50} + A_{50-100} + A_{100-150} + A_{150-200}}
 \end{aligned}
 \tag{5}$$

The characteristics Q_{top} , Q_{bottom} and Q_{tot} are standardized within [0,1]. When starch penetration decreases, Q approaches zero. If starch is distributed evenly in the z-direction, the value of Q_{tot} is 0.5. If $Q_{tot} > 0.5$, there is more starch in the inner parts of the cross-section sample than on its surfaces.

Starch penetration curves obtained with the method described here cannot, in principal, be directly interpreted as starch content distributions, similarly to filler distribution analysis, since pixels of the cross-sections were only evaluated “to contain” or “not to contain” starch based on the threshold analysis described above without any scalar information of starch at individual pixels. However, when penetration curves for different specimens are compared, penetration curves processed to represent starch amount distributions in the z-direction using the separately measured starch amount can be of interest. Here, the quantitative starch penetration curves were used to illustrate the assumed starch content distribution by normalizing the integrals of the individual starch penetration curves (i.e. the covered area under the penetration curve) to correspond to the actual starch content in the specimens. If we define the starch penetration curve P as a function of thickness z as $P(z)$, the separately measured starch amount as ρ_{starch} , and the starch amount normalized Simulated Starch Content (i.e. SSC) as a function of thickness as $SSC(z)$, and the equalized thickness as w , we can define

$$(6) \quad SSC(z) = \frac{\rho_{starch}}{w} \frac{P(z)}{\int P(z)}$$

Now we can plot the starch penetration curve as a simulated starch content curve $SSC(z)$ giving an assumption of the starch amount distribution across the sheet thickness using units of weight per unit area (e.g. g/m^2).

Sample Preparation for ToF-SIMS Analysis Followed by Image Analysis

In our study, the ToF-SIMS method was employed as the method of comparison for the I-KI dyeing method of cross-sections. ToF-SIMS was used to identify the lithium ions of LiCl_2 added to starch during the surface sizing process. Here, LiCl_2 dissolved in the starch solution was expected to penetrate into the paper structure along with starch. The distribution and amount of the LiCl_2 was then meant to be traced from the prepared cross-sectional images.

Paper samples were embedded in epoxy resin and cross-sectioned. ToF-SIMS analyses were used to obtain ion distribution maps for the lithium ion in the cross-sections. The instrument used for the ToF-SIMS analysis was a PHI TRIFT II (ULVAC-PHI, Chigasaki, Japan). ToF-SIMS images were acquired in the positive ion mode at 25 kV accelerating voltages using a Ga liquid ion metal gun over a mass range of 2–2000 amu. The analyzed area was $200\mu\text{m} \times 200 \mu\text{m}$. Specimens (roughly $2 \times 10 \text{ mm}$) were cut in the machine direction. After cutting the specimens were put in a flat embedding mold made of silicone rubber (Agar G369). The specimens were embedded in transparent cold mounting epoxy resin (Struers Epofix kit). An Epofix kit has two components, Epofix resin and Epofix hardener, which were mixed immediately before use (25 parts of resin and 3 parts of hardener by weight). Then the epoxy resin was allowed to cure at room temperature for about 8 hours. After the curing of the epoxy resin, the specimens were cross-sectioned in the machine direction with a Leica RM 2165 microtome (Leica Microsystems, Wetzlar, Germany). Cross-sections were made using a glass knife in order to obtain a smooth surface. The ToF-SIMS analysis of paper was made directly from the resulting epoxy block. *Figure 21* presents an example of an overall ion image of the cross-section as well as the corresponding Li^- image of a paper sample with a starch solids content of 18% and a total starch amount of 1.8 g/m^2 .

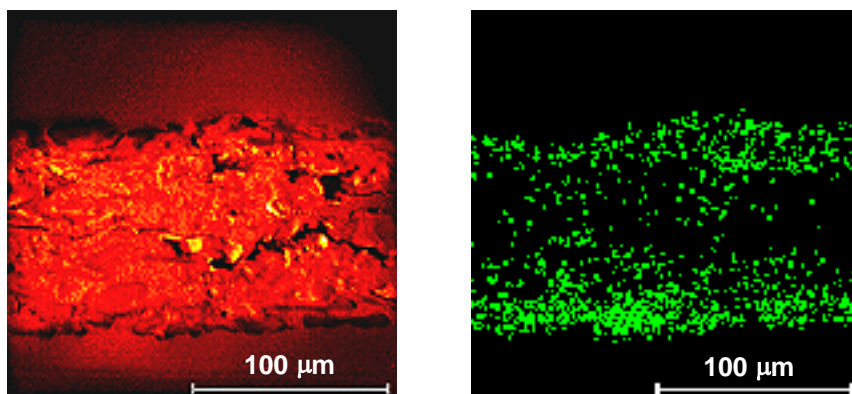


Figure 21. The total ion image of the cross-section (left) and the corresponding Li^- image (right). Bright dots in the image on the right indicate lithium ions.

The Li^- cross-sectional images were analyzed column by column similarly to the cross-sections treated with the I-KI dyeing method in order to determine the distribution of the Li^- ions across the z -direction. Edge detection began with detecting the furthest top and bottom Li^- pixels in each column of the Li^- image (Figure 22, top). This group of pixels was classified in all columns i as edge pixels only when the distance w between the topmost and the lowest Li^- pixels in column i was $w(I) > W_{min}$ pixels, the value of W_{min} being based on the thickness of the strip. In the study, the requirement for the minimum width of the cross-section was $W_{min} = 80$ pixels ($\approx 63 \mu\text{m}$). A continuous edge curve was then obtained using linear interpolation, after which all elements i of edge point vectors $z_{top}(i)$ and $z_{bottom}(i)$ had numerical values. Then the edge point vectors were filtered with a median filter, similarly to the procedure with I-KI images (Figure 22, middle). Further, the columns were normalized to a standard length of $w = 200$ (Figure 22, bottom). Finally, the cross-section Li^- distribution was obtained by averaging the resampled sequences of all columns. The length of a single Li^- image of the cross-section was $200 \mu\text{m}$. In total, ToF-SIMS images of 25 cross-sections were used in order to determine the Li^- distribution.

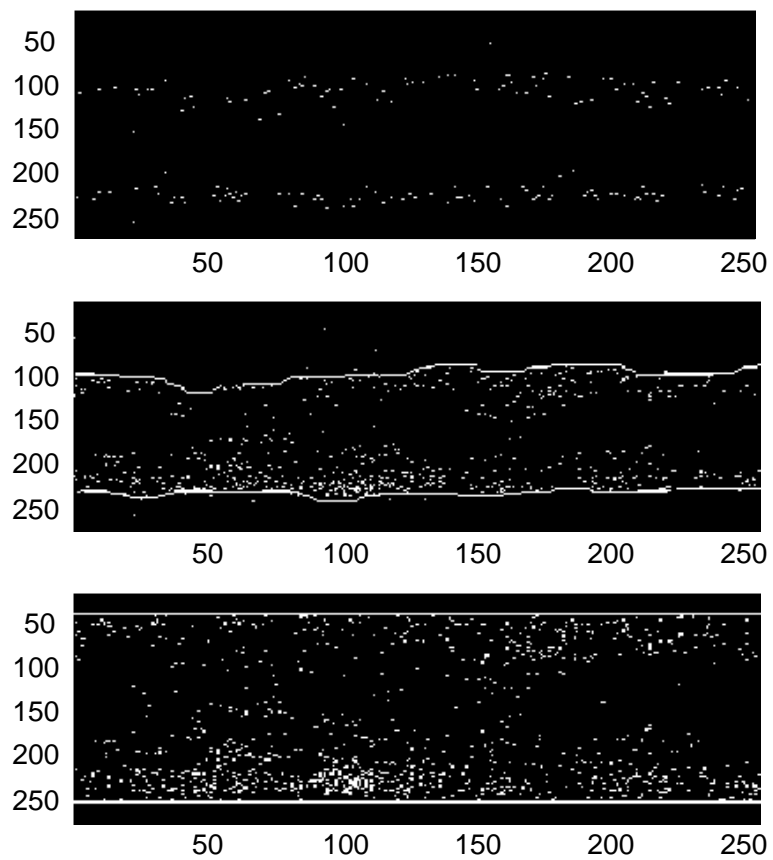


Figure 22. The furthest Li^+ pixels at the low end and top end of each column of a Li^+ image of the cross-section (top), median-filtered edge detection of the Li^+ image, (middle), and the thickness-normalized Li^+ image (bottom).

5. Surface Sizing with Starch Solutions at High Solids Contents Up to 30%

The influence of increasing the solids content of starch solutions in the surface sizing process is investigated. This discussion is supported by the work reported in *Papers I and II*.

5.1 Results

5.1.1 Rheological Properties of Starch Solutions

Viscosity at Different Shear Rates

The flow properties of the two starch solutions were determined in a shear rate region from 10^0 to 10^6 s^{-1} with solids concentrations from 8% to 18% (*Paper I*) at a temperature of 40°C (*Figure 23* and *Figure 24*). The reason for presenting the rheometer results at 40°C was the fact that it was difficult to maintain higher temperatures in the capillary during measurement. It was found that the main viscosity difference was due to initial modification differences, where the higher molecular weight of the cationic starch B gave a more pronounced shear-thinning flow compared to starch A.

When the solids content of starch B was increased above 12%, its viscosity exceeded that of starch A in the same shear rate region. This means that the metering conditions for a smooth rod need to be changed (i.e. higher rod pressure, smaller rod, etc.) to maintain the same size amount. It is also evident that the flow of the low viscosity starch A at low solids content levels becomes unstable at high shear rates ($> 500,000 \text{ s}^{-1}$), especially for the 8% solution (*Figure 23, left*). This increase in viscosity could be an effect of unstable liquid flow in the capillary (i.e. non-laminar flow). Here, the Reynolds number with 8% starch solution exceeded 2000 at high shear rates ($> 500,000 \text{ s}^{-1}$).

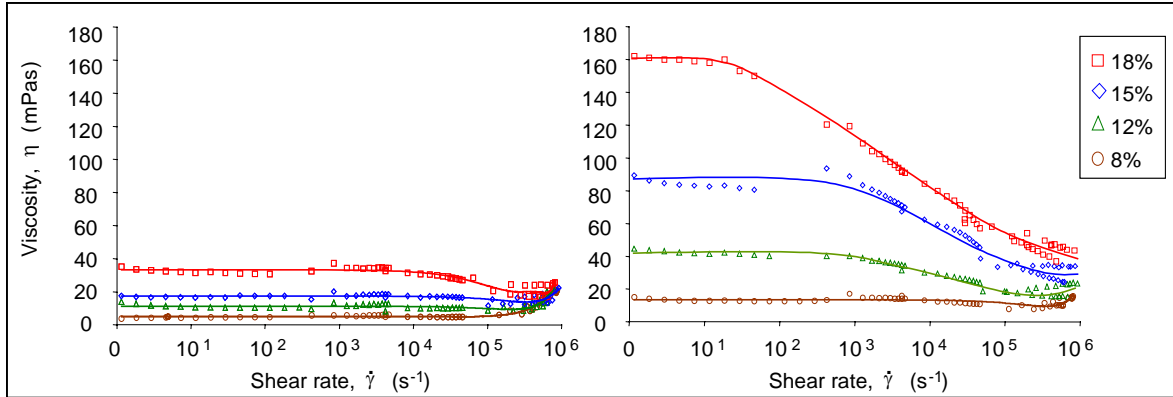


Figure 23. Effect of the solids content ($\phi_c = 8, 12, 15$ and 18%) of the starch solutions on viscosity (η) at shear rates from 10^0 s^{-1} to 10^6 s^{-1} ($40 \text{ }^\circ\text{C}$) with low viscosity starch A (left) and high viscosity starch B (right).

In the shear rate region of 10^5 – 10^6 s^{-1} , the viscosity differences between the two starch types are smaller at all solids content levels than the initial viscosity difference. One could suggest, that – as film forming mechanisms using smooth rods can be seen as hydrodynamic phenomena with high shear viscosity as a major contributing factor (Grön and Rantanen 2000) – similar film amounts should be reached with both starches under comparable conditions despite the large initial viscosity difference. Flow stability during the measurements – even at the highest shear rates – appears to have a stable shear thinning effect throughout the whole shear rate region. One can also observe that there is a drop in viscosity in the shear rate region 10^4 s^{-1} – 10^5 s^{-1} with the low viscosity starch A. This may be related to differences in the measurement methods used at the shear rates of 10^3 and 10^5 s^{-1} rather than an actual change in the rheological properties of the starch solution within the shear rate region mentioned. This possibility was brought up also by Roper and Attal (1993). The different high shear viscosity behavior at a shear rate of $500,000 \text{ s}^{-1}$ is further illustrated in Figure 25.

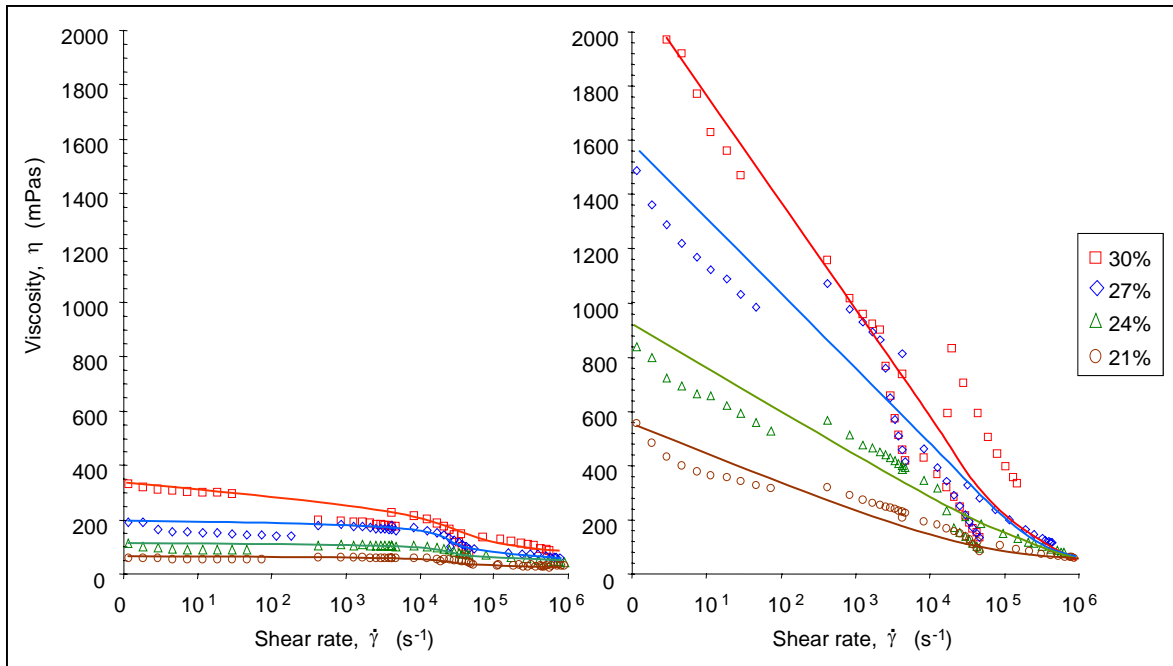


Figure 24. Effect of the solids content ($\phi_c = 21, 24, 27$ and 30%) of the starch solutions on viscosity (η) at shear rates from 10^0 s^{-1} to 10^6 s^{-1} ($40 \text{ }^\circ\text{C}$) with low viscosity starch A (left) and high viscosity starch B (right).

The differences in rheometric behavior of the two starches may be explained due their differences in molecular weight, degree of substitution and degree of polymerization (see Table II on page 17). As reported, the higher molecular weight of the starch B gave a more pronounced shear-thinning flow, whereas the low-viscosity starch A did not show the same shear-thinning effect but rather gave a Newtonian flow. One can suggest, that higher molecular weight may induce shear thinning behavior through orienting the polymers along the flow as the shear rate is increased, resulting in a clear shear thinning behavior. With low molecular weight starch, however, the shorter polymers orienting along the flow as shear rate is increased would effect the viscosity level less, resulting in a more Newtonian behavior.

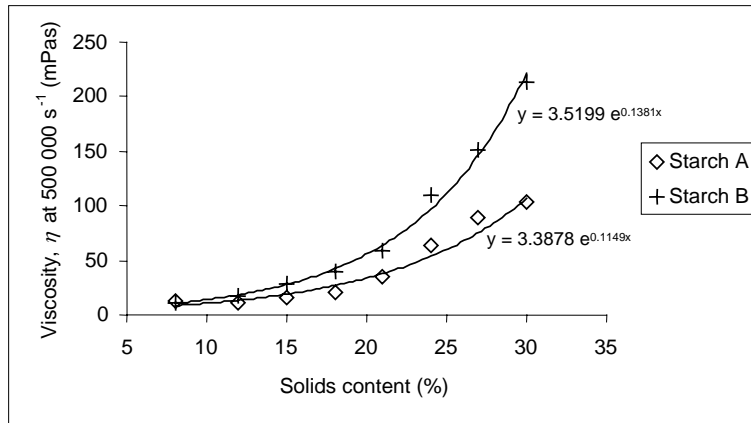


Figure 25. Effect of the solids content of the starch solutions ($\phi_c = 8, 12, 15, 18, 21, 24, 27$ and 30%) on viscosity (η) at a shear rate of $500,000 \text{ s}^{-1}$ and a temperature of 40°C with low viscosity starch A and high viscosity starch B.

The Effect of Solids Content on Yields Stress

It was expected that the starch molecules would create a weak network that would develop initial yield stress prior to breaking. Yield stress, τ_β , describing the stress needed to obtain flow was calculated for the starch solutions according to the Bingham plastic flow model. Figure 26 represents an example of the Bingham flow model in determining the yield stress, τ_β with starch B at solids content 27% .

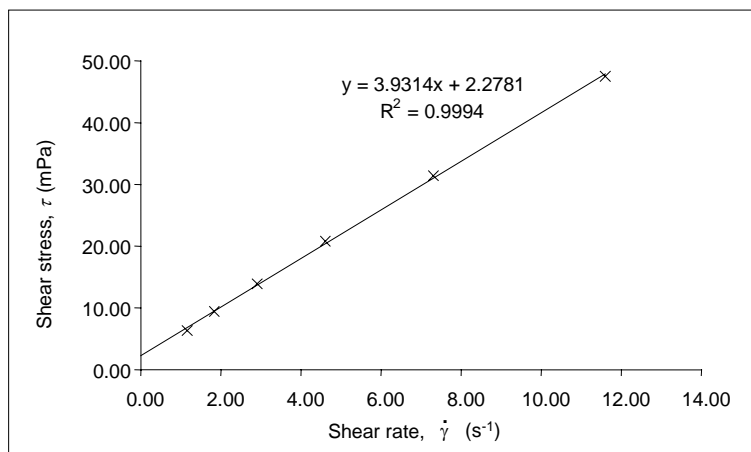


Figure 26. An example of the Bingham flow model used in determining the yield stress, τ_β with starch A at 27% solids content.

Yield stress was found to be low for both starch solutions, even up to 18% solids content. For starch B, low yield stress was also measured, which was very surprising since the viscosity level was quite high (Figure 27, left). Based on the results, excellent film forming and coverage were also found within the whole solids content range, which correlates with the weak starch molecule network (i.e. low yield stress values).

When relating starch properties to process conditions, it was expected that yield stress might explain differences in the web release force for different starch solutions. Here, higher yield stress means that more force is needed to obtain flow in the starch which, in turn, would affect the cohesion of the starch resulting in longer web release distances. If so, yield stress needs to be minimized to avoid uneven web release at such solids contents and viscosity levels. No web release problem was detected in this study even up to 30% solids contents with low viscosity starch A, and up to 21% solids contents with high viscosity starch B. This observation could be supported by the low yield stress values. However, with starch solids contents of 21%–30%, higher yield stress values were measured especially with high viscosity starch B (*Figure 27, right*).

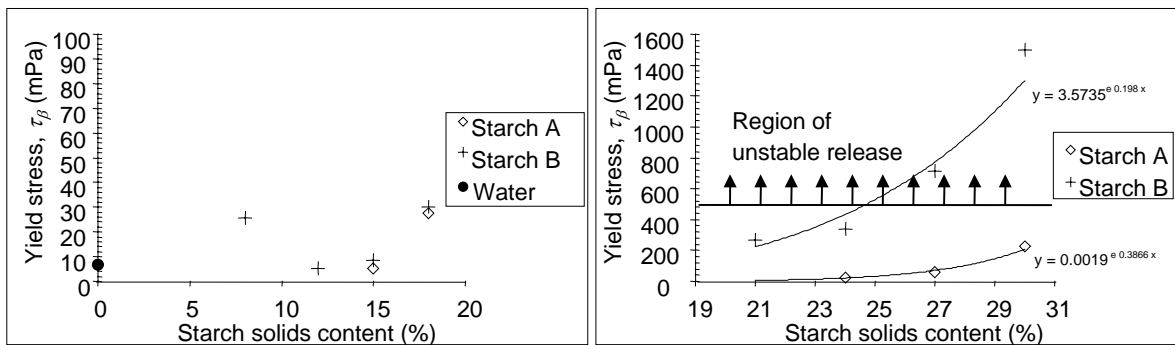


Figure 27. Effect of the solids contents ($\phi_c = 8, 12, 15, 18\%$, left, and $21, 24, 27$ and 30% , right) of the starch solutions on yield stress (τ_β) at temperature of 40°C with low viscosity starch A and high viscosity starch B.

It was observed during the trial that an increased web release force was required when using high viscosity starch B at a solids content of 24%. Here, the release distance of the web on the bottom roll increased up to 200 mm. With starch solution solids contents of 27% and 30% of the high viscosity starch B, the web was not able to be released from the bottom roll. Starch A, however, would release up to 30% solids content. When comparing web release behavior with the different solids contents and starch types, one can suggest a correlation with the required level of yield stress in the starch. Here, a yield stress level below 400 mPa provided sufficient polymer mobility for stable web release in the MSP roll nip (*Figure 27*).

5.1.2 Influence of Starch Solution Solids Content on Film Application, Starch Penetration and the Properties of Paper

Starch Amount and Transfer Ratio

The wet film amount measurement results are presented in *Figure 28*. Using these measurements it was possible to determine the required pressure level and rod type to obtain a similar starch amount on either side of the sheet in the actual trial. As expected,

the wet film amount measurements indicate a strong dependence between the wet film and rod pressure. The measured premetered film amount follow well the power trendline equations with an average R^2 value of 0.926.

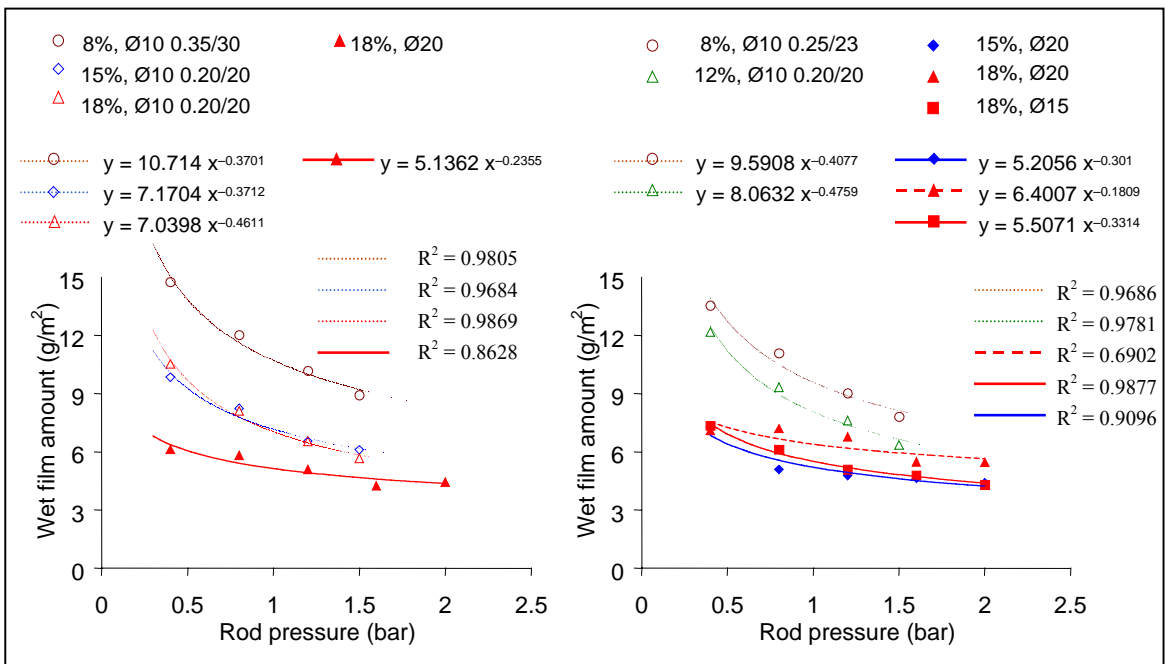


Figure 28. Measured wet film amounts with low viscosity starch A (left) and high viscosity starch B (right). 10 mm grooved rods ($\varnothing 10$ mm) are presented with open symbols, while smooth rods ($\varnothing 15$ and $\varnothing 20$ mm) are plotted with filled symbols. The codes of the grooved rods represent the groove profile shapes used.

The transfer ratio during the trial presented in Figure 29 was determined by measuring the remaining film on the bottom roll during the trial. The higher viscosity starch gives higher transfer to the sheet than the low viscosity starch. However, it should be noted that the transfer ratio was always above 95%, which involves some variation in the measured values. When observing the transfer ratio values, one should note that the remaining films were extremely thin and that the film may not have been scraped off completely during measurement.

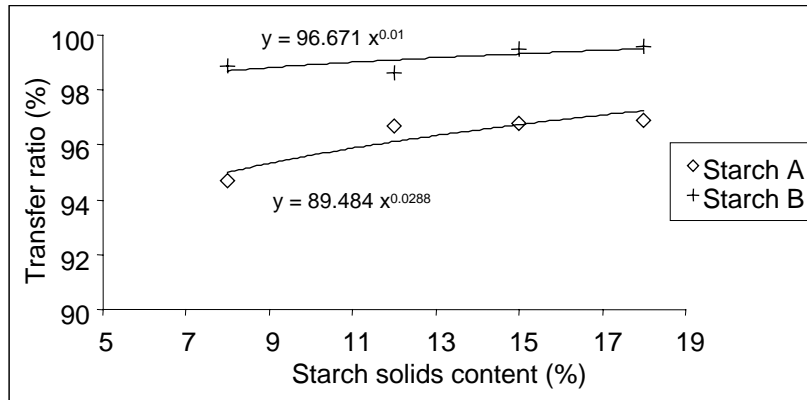


Figure 29. Transfer ratio determined by measuring the remaining film amount in the film transfer process. The individual values plotted represent averages measured from a set of 4–5 test points at each solids content with low viscosity starch A and high viscosity starch B.

Starch Penetration

Increasing the solids content of the starch solution from 8% to 18% reduces starch penetration and leaves more starch on the paper surface. The dry starch amount applied on the paper surfaces illustrated in *Figure 30* was approximately 2.0 g/m², where both starches penetrated through the paper at 8% and remained on the surface at 18%. This has also been reported in a study by Bergh (1984), where he found that a starch solution applied with a flooded nip size press at 15% solids content penetrated far less than at 4% despite the same viscosity of the solutions. He explained this result as more rapid closing of the pores with the higher solids content. In our study, the solids content of the starches also dominated their penetration behavior, but the high viscosity level of starch B seemed to slightly enhance the concentration of starch on the paper surface. This can be seen when observing the starch penetration behavior differences between the two starch types at starch solids contents of 12% and 15%. With the starch solids content levels mentioned, lower viscosity starch A seems to penetrate into the fiber network more than higher viscosity starch B. When observing these starch penetration differences one must also recognize the fact that when the dry starch amount is kept constant, the liquid volume added to the paper structure depends directly on the starch solids content used. For example, when the starch solids content is increased from 8% to 18%, the liquid volume added to the sheet is decreased by 56%, filling the pores mainly at the surface of the sheet. However, some of the penetration differences, especially between the two different starches at comparable solids contents and film amounts, may be explained by the effect of solids content on the viscous flow of the starch solution into the porous network of the sheet.

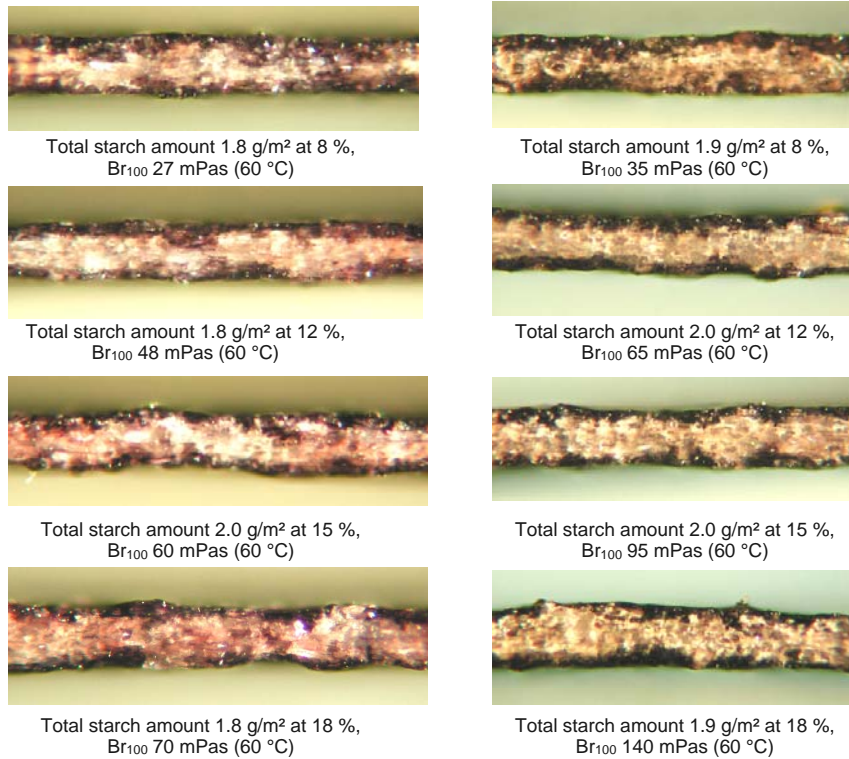


Figure 30. Cross-sections of surface sized paper with approximately 2.0 g/m² of total starch applied at different solids contents (8%, 12%, 15% and 18%) with low viscosity starch A (left column) and high viscosity starch B (right column). The iodine stained starch can be seen as darker areas in the pictures.

The observation of the greatest penetration difference in the medium solids content range is also supported by *Figure 31* where the starch penetration is evaluated using the cross-section iodine staining penetration evaluation method (the complete results of this method are explained in detail in part 6 on page 54). Here, the dimensionless starch penetration number Q_{tot} shows different penetration behavior in the two starches when the starch solids content is increased from 8% to 18%. In *Figure 31* one can observe that starch penetration with the higher viscosity starch decreases more significantly – compared to the lower viscosity starch – when the starch solids content is increased from 8% to 15%. The penetration of the high viscosity starch also does not decrease further when the starch solids content is increased above 15%. At the same time the penetration of the low viscosity starch keeps decreasing with starch solids content levels up to 18%.

As mentioned in part 6, the confidence interval around the penetration number (in terms of the standard deviation of penetration numbers Q in parallel specimens) is $\pm 5\%$. This observation can thus be considered statistically reliable.

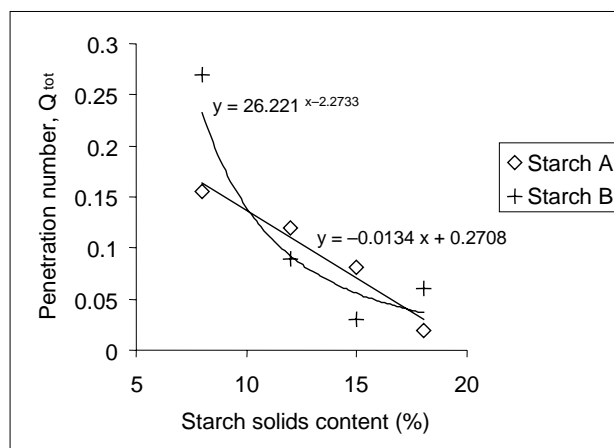


Figure 31. Penetration number Q_{tot} with different starch solids contents with starches A and B. The starch amount was 1.8–2.0 g/m².

When the solids content of the starch solution is increased from 8% to a level of 21%–30%, less starch penetrates the sheet and more starch remains on the paper surface. At this level the penetration of starch is almost negligible at all of the starch solids content levels studied. Figure 32 presents cross-sections of paper samples with starch amounts of 3.2 and 3.9 g/m² at solids contents of 21% and 30%. It can also be observed, however, that starch seems to have locally penetrated into the larger pores of the sheet also at the highest starch solids levels.



Applied amount 3.2 g/m² at starch solution solids 21 %, Br₁₀₀ viscosity 80 mPas (60°C)



Applied amount 3.9 g/m² at starch solution solids 30 %, Br₁₀₀ viscosity 158 mPas (60°C)

Figure 32. Cross-sections of surface sized paper with 3.2 and 3.9 g/m² of total starch amount at 21% and 30% solids content of low viscosity starch. The iodine stained starch can be seen as darker areas in the pictures.

Paper Properties

Increased solids contents increase the surface strength of paper since starch remains on the surface. The effect of the solids content is more evident with higher viscosity starch B, which can be seen in Figure 33. Here, the higher molecular weight of starch B, with potentially more binding power, gives increasing surface strength levels also at lower starch amounts.

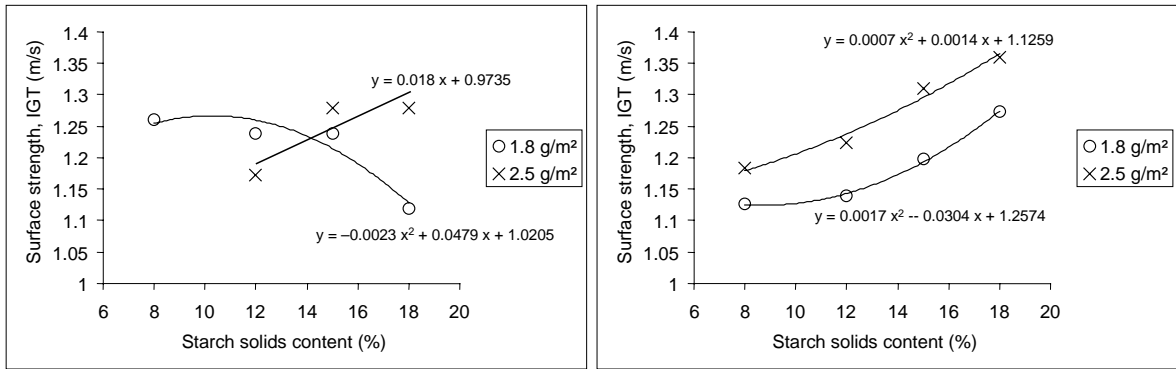


Figure 33. Effect of solids content on surface strength (IGT) with low viscosity starch A (left) and high viscosity starch B (right).

There is no major change in surface strength as the solids content is changed from 21% to 30%. As the starch is already concentrated on the paper surface at a solids content of 18% (Paper I), no significant increase can be seen in Figure 34.

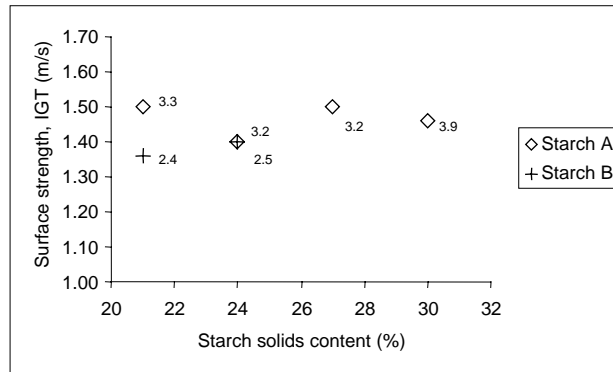


Figure 34. Effect of solids content on surface strength (IGT) with two different amounts of starch A and one of starch B. The starch amounts are presented next to the observations.

The porosity of paper decreases by almost 50% in terms of Bendtsen air permeability at higher starch solids contents (Figure 35). With both starches, air permeability was reduced from 800–600 ml/min to 400 ml/min at 18% solids content. The most evident reduction in air permeability was seen for high viscosity starch B. One can also observe, that starch amount (i.e. 1.8 g/m² and 2.5 g/m²) seems not to have an effect to Bendtsen air permeability. This may be explained if we assume the starch layer not forming a continuous film on the paper surface. Then, one can suggest, that merely varying the amount of this non-continuous layer of starch may not necessarily have a significant effect on the airflow through the paper structure, which is used in determining the air permeability of the sheet.

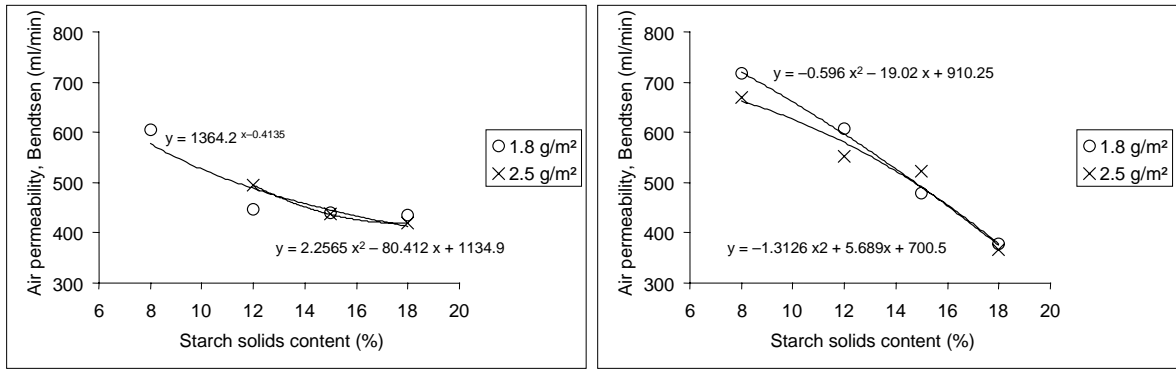


Figure 35. Effect of solids content on air permeability (Bendtsen) with low viscosity starch A (left) and high viscosity starch B (right).

When increasing the starch solids content above 20%, the air permeability of the paper decreases by 60%–80% compared to the base sheet (Figure 36). With both starches air permeability was reduced from 700 ml/min to 275–100 ml/min at the highest solids contents. With the high viscosity starch solution, a more complete sealing of the sheet was obtained due to this reduced starch penetration. Another factor contributing to lower air permeability with starch B may be more complete film forming capability with its longer molecular chains.

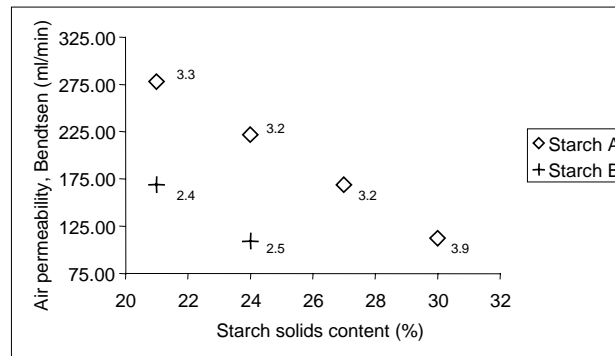


Figure 36. Effect of solids content on air permeability (Bendtsen) with two different amounts of starch A and one of starch B. The starch amounts are presented next to the observations.

The absorption of oil is reduced at increased starch solids contents (Figure 37). The reduced openness of the paper surface with a higher starch concentration on the sheet surface is naturally the explanation for this behavior. Especially high viscosity starch B gave a clear oil absorption reduction from 40 g/m² to 25 g/m² as the starch solids content was increased by 10 percentage points.

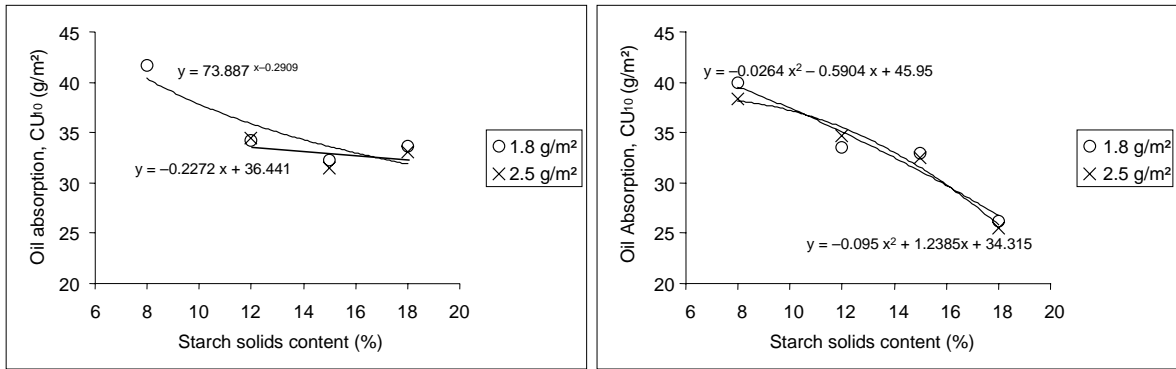


Figure 37. Effect of solids content on oil absorption (Cobb-Unger, CU_{10}) with low viscosity starch A (left) and high viscosity starch B (right).

Oil absorption is further reduced when starch solids are increased above 20% (Figure 38). The reduced openness of the paper surface with a higher starch concentration is naturally the explanation for this result. Especially high viscosity starch B gave a clear oil absorption reduction from 34 g/m^2 for the base sheet to less than 7 g/m^2 as the starch solids content was increased up to 30%. Oil absorption was also decreased to 7 g/m^2 with the lower viscosity starch A.



Figure 38. Effect of solids content on oil absorption (Cobb-Unger, CU_{10}) with two different amounts of starch A and one of starch B. The starch amount values are presented next to the observations.

As expected, internal strength (e.g. Scott Bond) decreases as a result of decreased starch penetration at increased solids content in the starch solution (Figure 39). One can suggest that starch B with its higher viscosity remains more on the surface than starch A, and internal strength can therefore be reduced even more. This effect can be seen for both starches, especially at a solids content of 15%. The amount of the two starches applied also has a very dramatic effect on internal strength at different solids contents. Here, the higher viscous starch shows a larger impact on internal strength at solids contents between 8% and 18% as the applied starch amount increases. This may be explained by a further enhanced starch concentration on the surfaces. Penetration differences of the two starches in terms of penetration analysis are discussed further in Figure 31, on page 43.

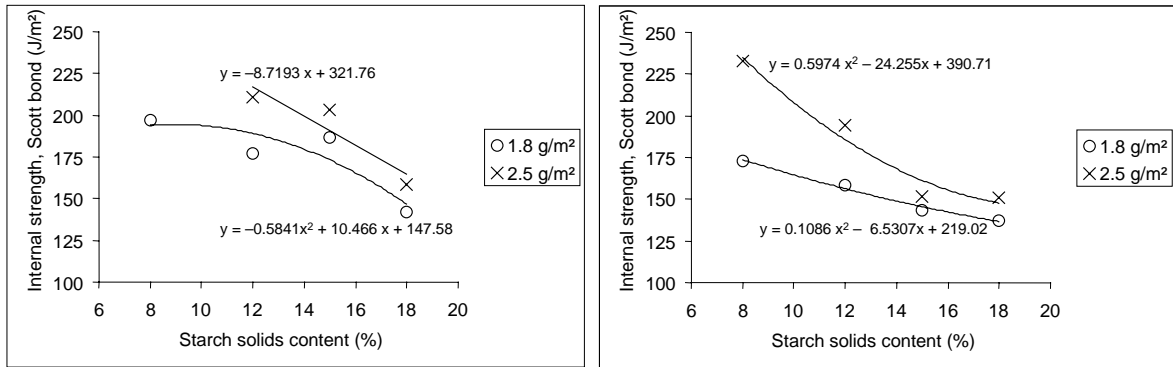


Figure 39. Effect of solids content on internal strength (Scott bond) with low viscosity starch A (left) and high viscosity starch B (right).

With starch solids contents of 20%–30%, it was a bit surprising that – compared to the base sheet – high solids surface sizing increased the internal strength of the sheet (Figure 40). With starch solids contents between 8% and 18%, the internal strength level developed toward base sheet values when using 18% starch solution.

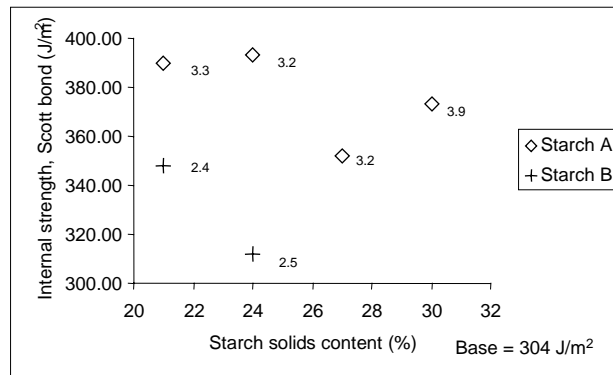


Figure 40. Effect of solids content on internal strength (Scott bond) with two different amounts of starch A and one of starch B. The starch amount values are presented next to the observations.

With the lower viscosity starch one could explain this by the effect of pore size on penetration even at the highest solids content levels. The development of internal strength reported here at increased solids contents is somewhat contradictory to the findings in Paper I, where an almost negligible increase in base sheet internal strength was reported with 18% starch solids for an 82 g/m² base sheet. This result may also be explained through the lower basis weight of the base sheet, which may promote the development of internal strength even at low starch penetrations. Lowering the base sheet basis weight below 80 g/m² is known to increase Scott bond values due to the decreased probability of potential rupture planes during Scott bond measurement (Kajanto 2000). The increased starch amount used at the 30% solids content also most probably has an effect on the increased Scott bond values. This observation also agrees well with the findings of

Küstermann (1990), who reported increased Scott bond values at increased starch solids content levels when he simultaneously increased the amount of starch.

The influence of solids content on paper stiffness can be seen more clearly in the CD direction where stiffness is increased at higher solids contents (*Figure 41*). Again, this increase in stiffness as a function of solids content can be explained by decreased penetration. This observation also agrees with previous studies (Tehomaa *et al.* 1992), where increased sheet stiffness was achieved with SDTA blade application and reduced starch penetration.

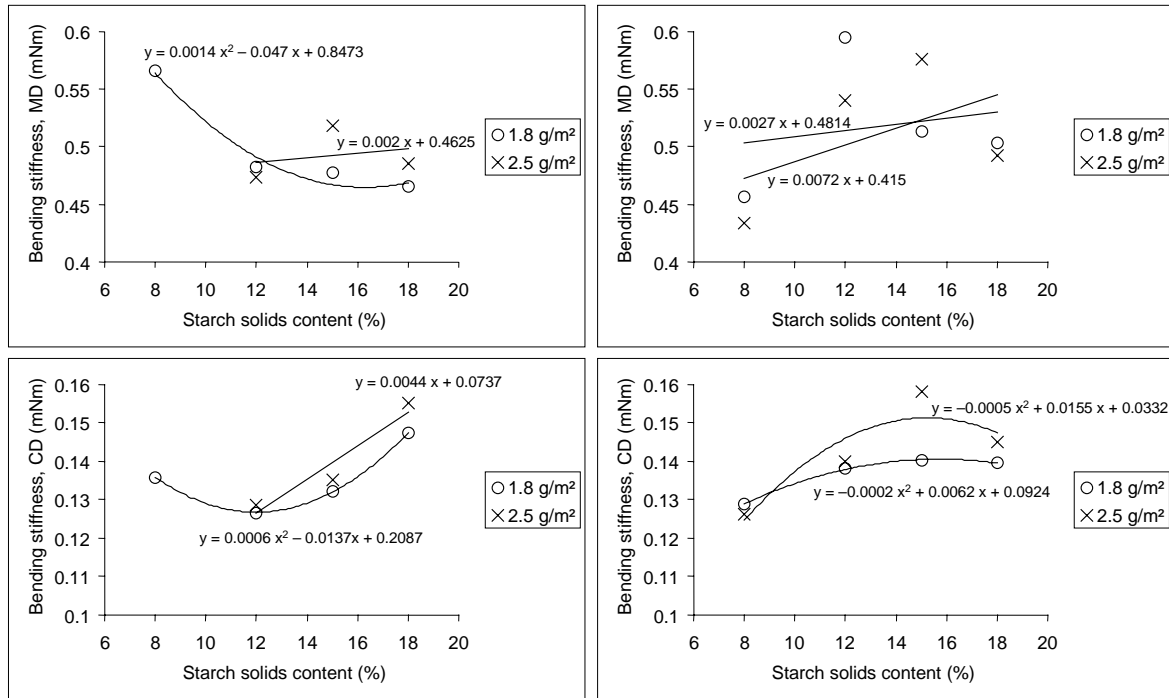


Figure 41. Effect of solids content on MD (top) and CD (bottom) bending stiffness for starch A (left) and starch B (right).

The effect of solids contents on MD bending stiffness is unclear for both starch solutions. Starch concentrating on the sheet surface and its effect on the local z-directional elastic modulus may be different in the MD and CD directions. This approach is discussed in more detail in part 7 on page 61.

In related literature (e.g. Tehomaa *et al.* 1992), increased bending stiffness is reported with increased starch solids, explained by starch being more concentrated on the surface of the sheet. Here, when starch solids are increased above 20%, the influence of solids content on bending stiffness show no significant change as starch solids are increased toward 30% (*Figure 42*). This may be due that when starch is already concentrated on the surface of the sheet at 18% solids content, as reported, increasing the solids content further may not effect the distribution of starch to an extent necessary to be seen in bending stiffness measurement.

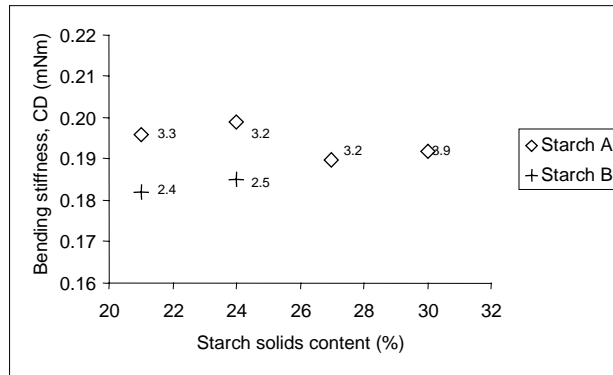


Figure 42. Effect of solids content on cross-directional bending stiffness with two different amounts of starch A and one of starch B. The starch amount values are presented next to the observations.

The penetration of starch also affects the optical properties of paper. As seen in Figure 43, ISO brightness increases as the starch solids content is increased. This can be explained through the fact that the optical brightener attached to the starch molecules is also more concentrated on the paper surface. One can support this observation when the different penetration behaviors of the two starches at solids contents from 12% to 15% are visually compared (Figure 30). Here, the higher viscosity starch B remains more on the sheet surface compared to the lower viscosity starch B, especially at a solids content level of 12%. As seen in Figure 43, the difference in the ISO brightness values between the two starches is the most evident within this solids content region.

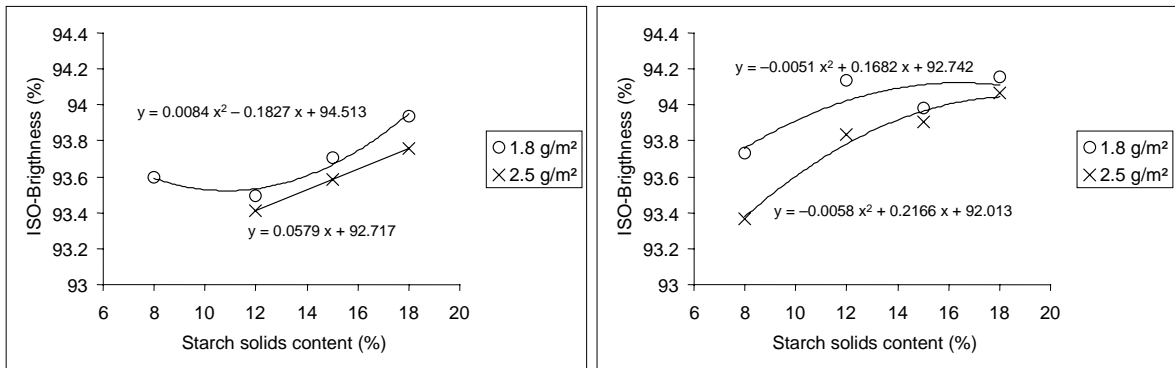


Figure 43. Effect of solids content on ISO brightness with low viscosity starch A (left) and high viscosity starch B (right).

Starch solids content also affects the opacity of paper through the penetration behavior of the starch. Whereas no clear effect of the starch solids content can be seen with the low viscosity starch A, the higher viscosity starch B increases the opacity of paper since starch remains more on the sheet surface. This may be explained through a more uniform starch layer on the sheet surface that weakens the optical contact between the sheet surfaces, leaving more fiber-air interfaces in the inner parts of the sheet. Again, as opacity can be

seen to decrease with increased starch amounts, the effect of starch filling the pores and therefore reducing scatter is supported.

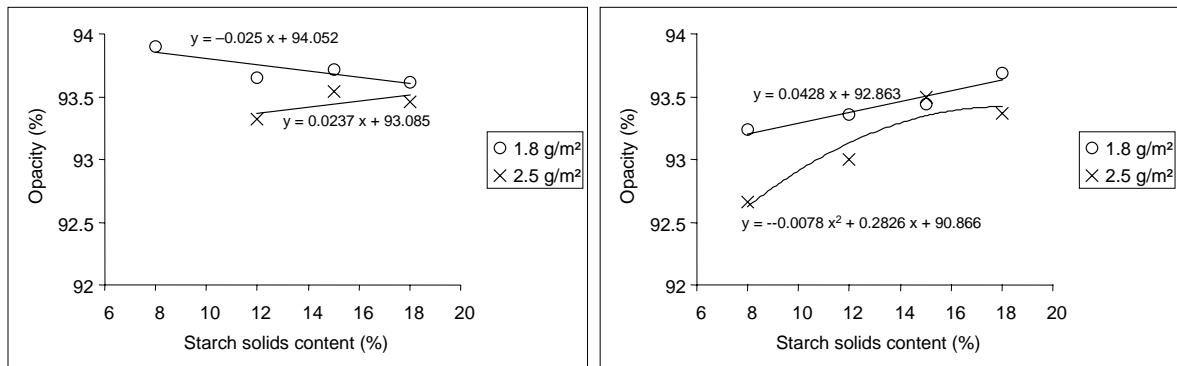


Figure 44 . Effect of solids content on opacity with low viscosity starch A (left) and high viscosity starch B (right).

5.1.3 Effect of Increasing the Solids Content on Drying Capacity and Runnability

When maintaining the starch amount while the starch solids content is increased, it is possible to achieve up to 50% savings in energy consumption and investment costs for the afterdryer section. Both surface sizing and coating capabilities could be achievable on paper machines with online MSP application units. In these cases drying capacity needs to be over-dimensioned for coating to be able to evaporate the water applied during surface sizing. But, surface sizing using high solids contents could eliminate the need for additional drying capacity in comparison to pigment MSP coating. This is explained in Table VI as a difference in the required evaporation capacity.

Table VI. Evaporation capacity required for MSP coating at a solids content of 67% compared to MSP sizing at starch solution solids contents of 8%, 18% and 30%. A transfer ratio of 0.80 was used in the calculations for coating and 0.95 for surface sizing.

	Solids Content (%)	Film Thickness (g/m ²)	Dry Amount Applied / Side (g/m ²)	Water to be Evaporated/Side (g/m ²)
MSP coating	67	18.8	10	4.9
MSP surface sizing	8	19.7	1.5	17.3
MSP high solids surface sizing	18	8.8	1.5	6.8
	30	5.3	1.5	3.5

Table VI indicates that it is possible to utilize the same afterdrying capacity for coating and surface sizing when the size solids content is increased from 8% to 30%. Table VI also presents the basic requirements for high solids surface sizing, where only a very thin starch

solution film is required to achieve the desired dry starch amount. This film requirement also underscores the stability of the starch solution, especially in terms of the CD stability of the applied film.

A considerable reduction in the number of web breaks can also be gained by increasing the surface size solids content and keeping the applied starch amount constant due to higher web dryness after the MSP unit (i.e. more than 85% instead of about 70%). Here, if we calculate the change in web dryness after the size process, we can observe that sheet dryness is increased from 70% to 85% when starch solids content is increased from 8% to 20% keeping the starch amount constant, e.g. at 3 g/m². According to Breght *et al.* (1959), the wet breaking load of the sheet can then increase by up to 200% (i.e. from 600–700 g/cm to 1800 g/cm) as sheet dryness is increased from 70% to 85% since the interdependence of wet strength and sheet dryness can be characterized as exponential. Web breaks at the surface sizing unit are mainly induced by the wetting of the sheet and the increased solids content of the starch solution can be expected to improve paper machine efficiency by up to 2 percentage points. The ability to use smooth rods and softer roll covers (compared to surface sizing) may also allow using the same application and afterdrying concept for both the MSP coating and surface sizing processes.

5.2 Summary

As reported, it is possible to apply starch at remarkably higher solids contents without significantly affecting the dry starch amount. The results presented also show that it is possible to use a wide variety of starch viscosities and molecular weights with increased starch solids contents. Therefore, increasing the starch solids content is not necessarily restricted only to highly degraded starches with their lower binding power potential. Increased starch solids content levels gave a high transfer ratio without restrictions, such as an uneven web release from the roll after the nip. Application is done here from 15% to 30% with smooth rods instead of conventionally used grooved rods.

Based on the results reported here, increased solids contents in the sizing solution decrease its penetration into the sheet. This decreased penetration can be explained through a decreased volume of liquid transferred to the sheet, as well as by the effect of the increased solids content on the viscous flow of the starch solution into the porous network of the sheet. Decreased penetration of starch improves such paper properties as surface strength and bending stiffness. Decreased sheet air permeability and oil absorption can also be achieved. These observations agree with Tehomaa *et al.* (1992), who could retain starch on the surface of paper by using SDTA application compared to MSP technology. However, some reduction in internal strength can also be observed. All these results can be explained by decreased penetration at increased starch solids contents. Air permeability and oil absorption were further decreased compared to solids content levels below 20% when the starch solids content was increased up to 30%.

Greater effort needs to now be placed on optimizing the rheological properties of starch solutions when the solids content is considerably increased. Flow characteristics will have a large impact on metering conditions since metering will be based on hydrodynamic principles (i.e. smooth rods) instead of the current volumetric (i.e. grooved rods) approach. It was also seen that the runnability of the MSP unit was stable with the low viscosity starch up to a starch solids content of 30%. At a high starch viscosity, web release was stable even up to a solids content of 24%. When the solids content of the high viscosity starch was above 24%, decreased polymer mobility increased the tension required to release the web from the MSP roll. Here, when comparing web release behavior using different solids contents and starch types, one can suggest a correlation with the required level of yield stress in the starch. A yield stress level of less than 400 mPa provided sufficient polymer mobility for stable web release in the MSP roll nip.

However, when increasing the starch solids content even up to 30% – despite an overall decrease in penetration – local starch penetration could be seen with low viscosity starch even at the highest starch solids content levels. Pore size distribution results obtained with Coulter oil porosimetry are presented in *Figure 45*.

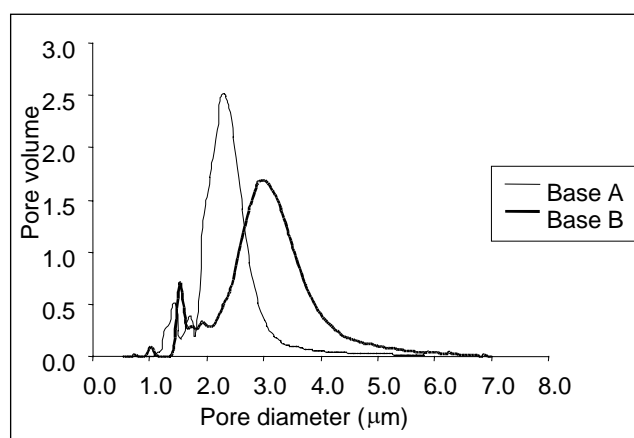


Figure 45. Pore size distributions (Coulter) of the two different base papers used in the study. Base papers A and B were used with starch solids content ranges of 8%–18% and 21%–30%, respectively.

Here, one can suggest that local starch penetration into the larger pores of the sheet may be an explanation for the high internal strength achieved with low viscosity starch at very high solids contents. One can suggest that optimizing the pore size characteristics of the base sheet can be seen as a tool for compensating for the loss of internal strength in surface sizing even at the highest solids content levels. It can be discussed in general whether the internal strength of uncoated fine paper really should be gained through surface sizing. Would it be more beneficial to produce the required internal strength at an earlier stage in the papermaking process by further optimization of the base sheet properties, furnish components, and the internal sizing process? Compared to the current conventional sizing

concepts, increased surface strength could then be produced through a more cost-effective surface sizing operation. This will open opportunities for reducing raw material costs and increasing the productivity of paper machines. An additional new and desirable paper property is the reduced porosity gained through reduced starch penetration, which is possible with a low starch amount at high solids contents in an MSP application.

6. Starch Penetration Analysis through Iodine Staining and Image Analysis of Cross-Sections of the Paper Structure

A novel method for the quantitative determination of starch distribution in cross-sectional images of surface sized paper samples is discussed. The specific aim was to discuss the possibility of formulating a fast and inexpensive method for determining z-directional starch distribution curves from paper cross-sections. The discussion is supported by the work reported in *Paper III*.

6.1 Results

The following figures illustrate the starch penetration curves obtained as examples of utilizing the method developed (*Figure 46*). These curves show differences in starch penetration depending on the surface sizing solids content as starch concentrates on the surface or penetrates more through the sheet based on starch solids content. The results presented here are produced using the specimens whose paper properties are reported in part 5 on page 35. A base paper sample with no surface sizing was also analyzed in a similar manner as the surface sized samples. Here, some I-KI dyeing of the base paper sample through reaction with fibers, fillers and wet end starch can be seen in the starch “penetration” curve of the non-surface sized base paper.

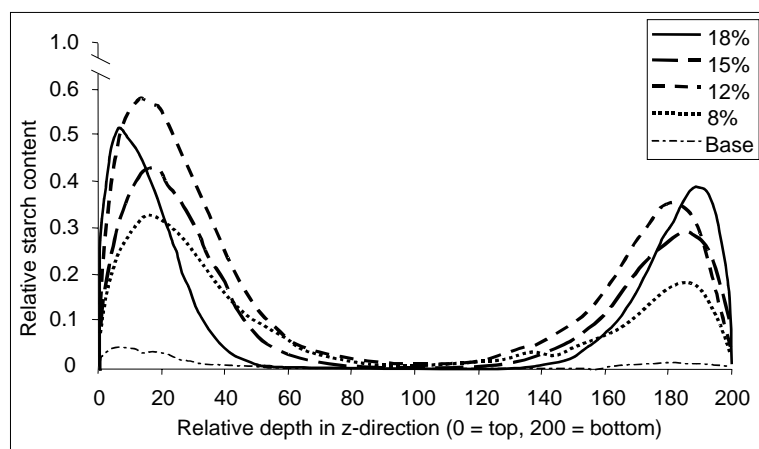


Figure 46. Starch penetration curves with starch amounts of 1.8 g/m^2 , 2.0 g/m^2 , 2.0 g/m^2 and 1.8 g/m^2 and starch solids contents of 18%, 15%, 12% and 8%, respectively. A reference curve obtained from the base paper sample is also presented. The relative starch content (between 0 and 1) on the y-axis describes the occurrence of pixels categorized to contain starch in the z-directional thickness of the sheet.

Using the Simulated Starch Content distribution calculation, *SSC*, starch penetration curves were rearranged by normalizing the integrals of the starch penetration curves based on the starch amount measured from the specimens (*Eq. 6* on page 32). These normalized curves

(Figure 47) show a logical arrangement of the starch penetration curves according to starch solids content.

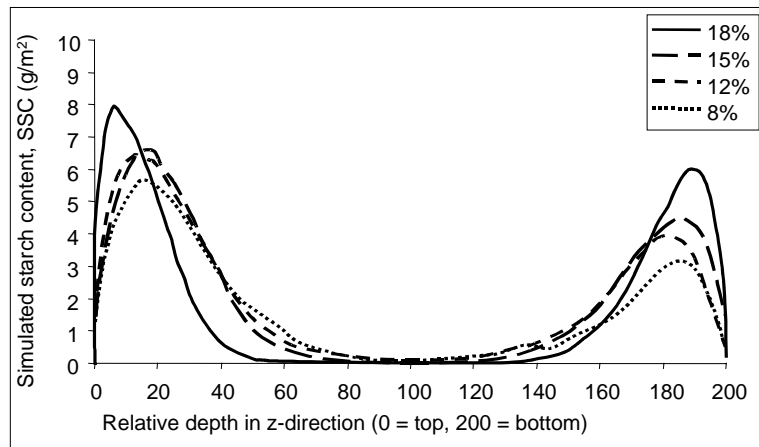


Figure 47. Starch penetration curves normalized to cover an area proportional to the corresponding starch amount for each paper sample (i.e. Simulated Starch Content distributions, SSC) at starch amounts of 1.8 g/m^2 , 2.0 g/m^2 , 2.0 g/m^2 and 1.8 g/m^2 with starch solids contents of 18%, 15%, 12% and 8%, respectively.

The starch amount in paper samples is seldom equal at the top and bottom side of paper. Therefore, a direct comparison of the starch distribution curves at each side or as a function of the entire thickness of paper can be complicated. Here, unless penetration at each side of the paper is of special interest, averaging the curves obtained from the top and bottom sides of paper can be useful. Figure 48 presents examples of such half curves. The top and bottom averaging is obtained from the Simulated Starch Content curves seen in Figure 47.

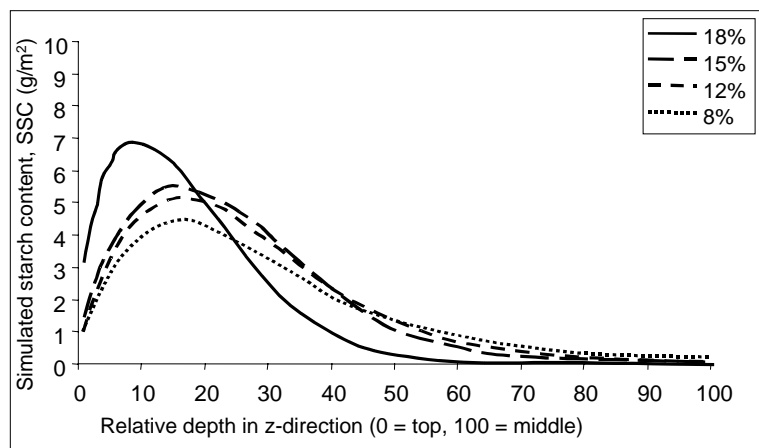


Figure 48. Top and bottom side averaged starch penetration curves with starch amounts of 1.8 g/m^2 , 2.0 g/m^2 , 2.0 g/m^2 and 1.8 g/m^2 and starch solids contents of 18%, 15%, 12% and 8%, respectively. Penetration curves were normalized to cover an area proportional to the corresponding starch amount at each point (i.e. Simulated Starch Content distributions, SSC).

In *Figure 48* one can observe, that starch penetration with solids content of 18% differs significantly from the penetration of starch solutions at 8%–15%. This may be explained through observing the rheometric behavior of this starch illustrated in *Figure 23*. Here, as high shear viscosity does not increase linearly according to the solid content, the viscosity of starch A at 18% is significantly higher compared to the lower solids contents starch solution throughout the whole shear rate region. As liquid penetration to a paper structure can be seen as pressurized capillary penetration, high shear viscosity may then be used to quantitatively characterize the penetration potential of the starch.

Figure 49 illustrates the calculated penetration number Q_{tot} as a function of the starch solution solids used (i.e. 8%, 12%, 15% and 18%). One can observe in *Figure 49* that the penetration number described here gives a relevant view of starch penetration at different solids contents.

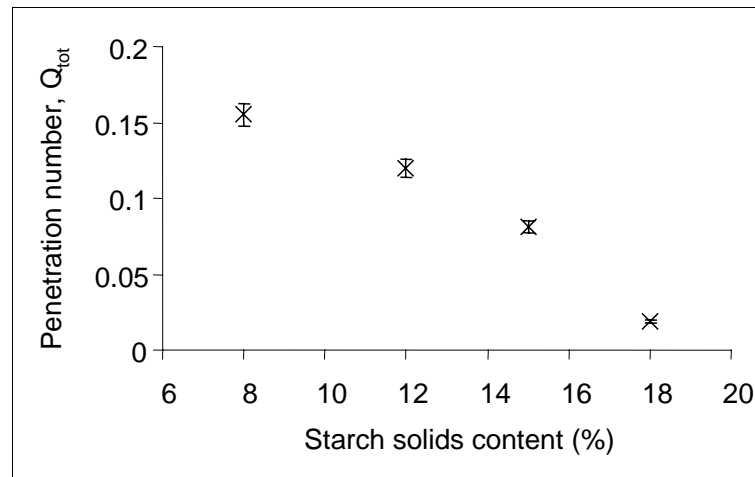


Figure 49. Determined penetration number Q_{tot} as a function of the starch solids content used (i.e. 8%, 12%, 15% and 18%). The total starch amount was 1.8–2 g/m². The confidence intervals represent the estimated 10% confidence.

Similarly, the Scott bond internal strength measurements are compared against the penetration number. When observing *Figure 50*, one can suggest that the penetration number Q_{tot} introduced here can well be used in evaluating the internal strength of the sheet in terms of starch penetration.

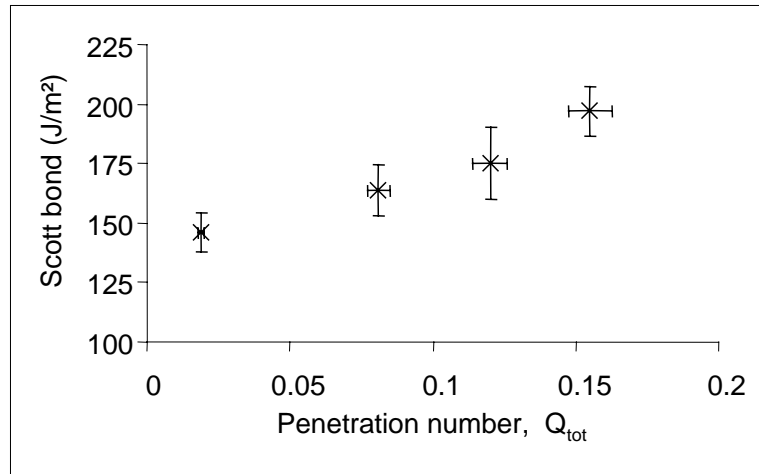


Figure 50. Measured internal strength (Scott bond) as a function of the penetration number. The total starch amount was 1.8–2 g/m². The confidence interval indicate the 2 σ variation of the Scott bond measurements. Regarding the penetration number Q , the confidence intervals represent the estimated 10% confidence.

Figure 51 presents the lithium ion distribution of a paper sample with a starch solids content of 18% and total starch amount of 1.8 g/m². Figure 51 shows that the lithium ions were more evenly distributed across the z-direction of the paper than indicated by the starch penetration information from the analysis of binary images of the I-KI dyed cross-sections (Figure 46 and Figure 47). In other words, the lithium ion content of the paper is greater in the middle of the sheet than expected based on the I-KI distributions.

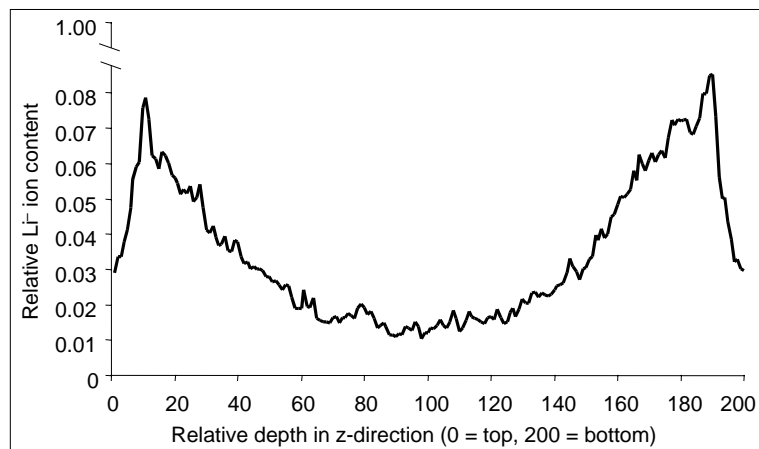


Figure 51. Averaged Li^- distribution determined for a series of cross-sectional images (25 images). The starch solids content at the specimen was 18%, and the total starch content 1.8 g/m². The relative Li^- ion content (between 0 and 1) on the y-axis describes the occurrence of pixels categorized to contain Li^- ions in the z-directional thickness of the sheet.

Figure 51 also suggests that the maximum Li^- concentration is not quite on the surface of the cross-section but at a depth of about 5 μm from the surface of the specimen. This

observation agrees well with the findings on the I-KI starch penetration curves, where the maximum starch penetration was also found to be at a similar depth from the sheet surface.

The accuracy of the method developed can be evaluated by observing starch penetration results from parallel specimens. Four specimens were analyzed in the following figures in order to find out the level of confidence, and further, the repeatability of results with the method developed.

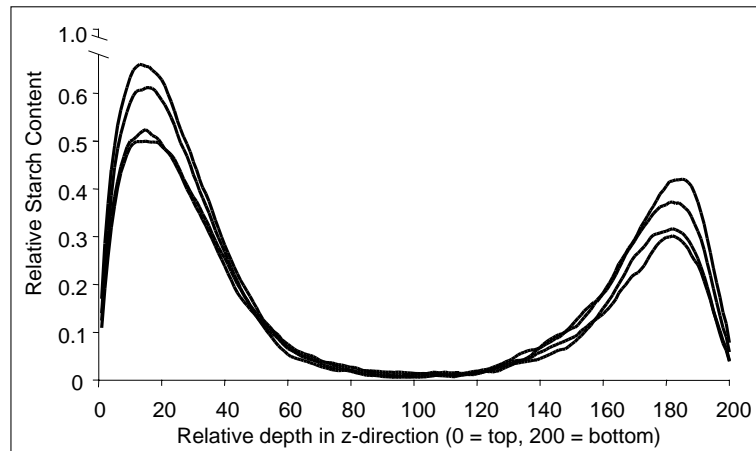


Figure 52. Examples of relative starch content distributions from four parallel specimens, each consisting of averaged information from 16 cross sections. Starch content in the specimen was 2.0 g/m^2 at starch solids content of 12%.

In Figure 52, four parallel relative starch content distributions are compared. One can observe roughly 30% variation in starch content maximum values between the curves. Comparing results based on relative starch content curves alone can therefore be complicated.

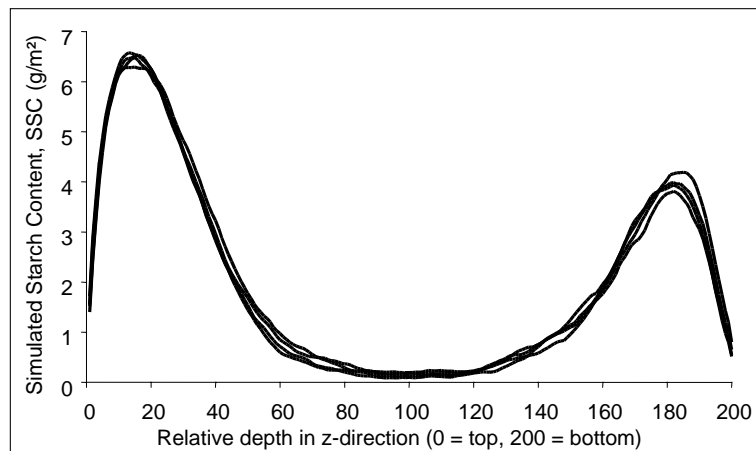


Figure 53. Examples of Simulated Starch Content (SSC) distributions from four parallel specimens, each consisting of averaged information from 16 cross sections. Starch content in the specimen was 2.0 g/m^2 at starch solids content of 12%.

However, if the results with the Simulated Starch Content (SSC) distribution are observed, good repeatability of the results can be seen (*Figure 53*). Looking at the Simulated Starch Content distribution and normalizing the curves based on the measured (or targeted) starch amount using *Eq. 6* is therefore the most useful form of plotting the penetration curves. Further, the penetration numbers Q_{tot} for the specimens compared here give values 0.114, 0.124, 0.104 and 0.131 with an average of 0.118 and standard deviation of 0.012. The method developed for determining the penetration number gives quantitative starch penetration information with coefficient of variation (CV) of 10%.

6.2 Summary

A quantitative method for the evaluation of starch penetration was presented in this study. The dyeing of the specimen in the iodine potassium iodine (i.e. I-KI) solution and the image analysis of the resulting dyed cross-sections were quick to conduct. The dyeing of the specimen, image acquisition of the dyed cross-sectional surface, and image analysis of the cross-sectional image were defined and specified so as to obtain reproducible and comparable information of quantitative starch penetration. Person-dependent factors that may affect the procedure and the results obtained, such as variations in the handling of specimens, were then minimized. The penetration curves produced by the method described in this study give an additional tool for studying the effect of papermaking process parameters on the quantitative z-directional penetration of surface sizing starch. The method introduced for obtaining Simulated Starch Content (SSC) distribution curves also gives a helpful tool for characterizing the effect of various process parameters on the z-distribution of starch in a sheet. An additional feature of the method is the definition of a dimensionless penetration number Q_{tot} that can be quantitatively used in comparing the penetration of starch in different paper samples to determine the function of any papermaking variable whose contribution to surface sizing starch penetration behavior is of interest. Such variables may be starch viscosities and/or solids contents, linear loads of the MSP unit, roll diameters and hardnesses, or such base paper properties as porosity or pore size characteristics. The results presented here showed a good correlation between starch solids content and the internal strength of the sheet, for example. The method described will open new possibilities for describing starch penetration compared to the conventionally used qualitative evaluation of iodine stained cross-sections.

One must note that the penetration curves described here should, in principal, not be directly interpreted as starch amount distributions due to the method used in determining the curves. Here, the method is based on evaluating whether the individual pixels across the cross-section contain starch or not – instead of quantitative information on starch content at that particular location. Nevertheless, the simulated starch content (SSC) distribution curves presented seem to also represent the expected relative starch amount distribution in the z-direction quite well.

The starch penetration curves were also compared against Li^- distributions obtained through ToF-SIMS using LiCl_2 as a marker for starch, which described the distribution of the starch solution in the z-direction. The comparative ToF-SIMS results repeat the observation made with I-KI dyed and image analyzed cross-sections showing a drop in starch content in the 5 μm layer of the topmost surface of the sheet. However, the Li^- distributions show deeper penetration compared to the I-KI curves. This may be explained through the LiCl_2 marker migrating through the fiber network with the water in the starch solution. One can then suggest that the starch molecules (low molecular weight anionic starch A used in these samples) were not able to prevent Li^- ions from washing into the paper structure with water and deeper in the z-direction than the starch itself.

A Simulated starch content (SSC) distribution derived by normalizing the curves using the measured (or targeted) starch amount is the most useful form of plotting the penetration curves. Further, the penetration number gives quantitative starch penetration information that is 90% accurate.

7. Mechanical Properties of Woodfree Paper Sheets at Different Surface Size Starch Amounts

The effect of starch content on woodfree paper and its mechanical properties are discussed. The specific aim was to discuss elasticity properties (elastic modulus) and other mechanical properties, such as bending stiffness, as the starch content of paper is increased. This discussion is supported by the work reported in *Paper IV*.

7.1 Results

The following figures are presented as a function of cumulative water addition, which was applied to the paper during the complete set of multiple application sequences in both 1% starch application and the water treatments performed for reference. The water reference results can thus be evaluated together and compared with the starch application results.

Shrinkage results are presented below. It can be noted that starch promotes strong shrinkage in unrestricted drying, especially in the cross direction. However, some shrinkage can also be observed in the results based on “restricted” drying despite the attachment of the sheets to the fabric during drying. This is most probably due to the relaxation of drying stresses after sheets were released from tape attachment in the drying apparatus used, which resulted in some degree of shrinkage.

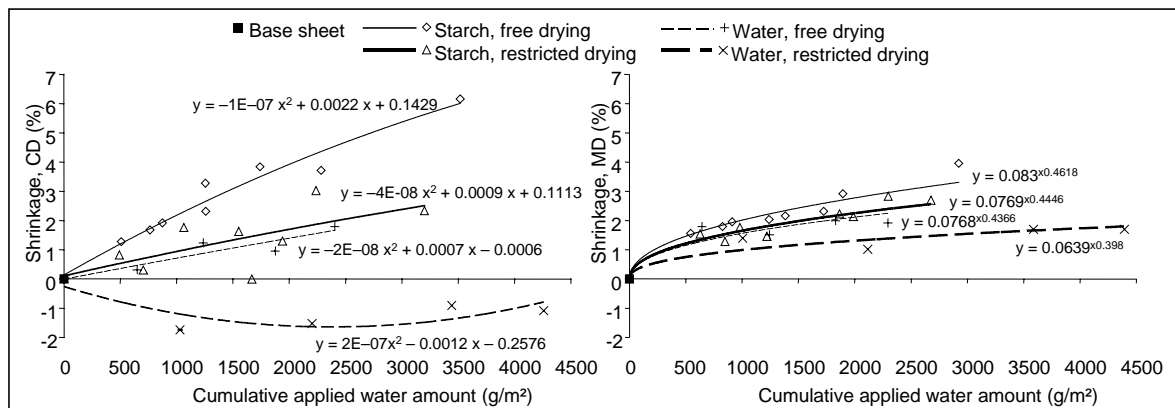


Figure 54. Drying shrinkage in the cross direction (left) and in the machine direction (right) as a function of cumulative water addition. Starch added as 1% starch solution.

Elastic modulus results both in the cross direction and machine direction are presented in *Figure 55*. Elastic modulus values with both starch and water treatments are presented in these figures for both restricted drying and free drying. One can observe in the figures that the modulus of elasticity decreases with less restrained drying, as reported by Setterholm and Kuenzi (1970) and Htun (1980), for example, who reported that the modulus of elasticity decreases significantly when drying shrinkage is allowed. One can suggest that

starch-induced excessive shrinkage leads to a “crimped” sheet structure with very low resistance against tensile stress, and therefore to low elastic modulus values in the specimen, as suggested by Silvy (1971).

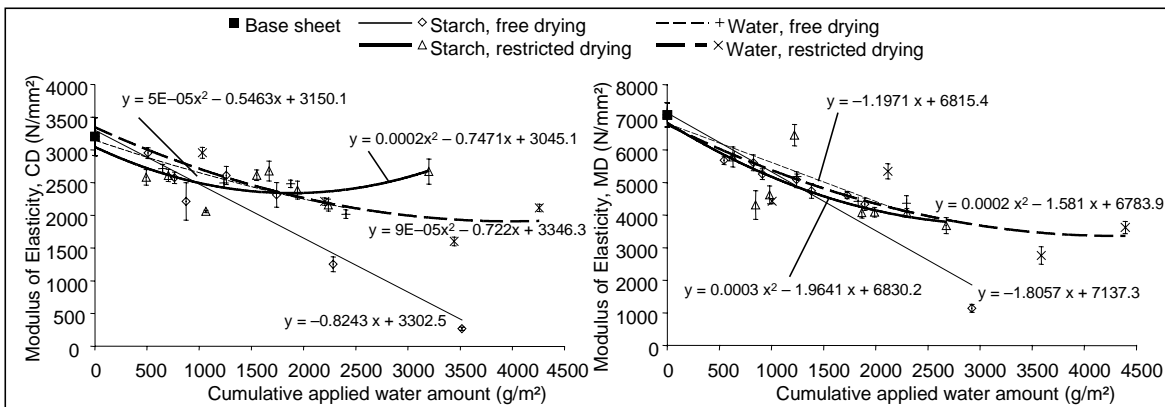


Figure 55. Modulus of elasticity in the cross direction (left) and in the machine direction (right) as a function of cumulative water addition. Starch added as 1% starch solution. The confidence intervals indicate the 2σ variation of the measurements.

Different drying arrangements with starch and water treatments have an effect to the paper thickness, as seen in Figure 56, where the results are presented as a function of applications per side. Here, thickness seems to increase due to drying restriction. This phenomenon is more evident with starch treated samples. The thickness increase may be explained through the known phenomena of thickness increase during wet straining: wet straining has explained to increase thickness of the sheet through fiber "undulations", when some fibers are pulled straight in the network (Retulainen *et al.* 2000). Here, the effect of starch – through the suggested mechanism of increased drying stresses – may be inducing wet straining of the fibers and fiber bonds, resulting in promoting of increase of sheet thickness when starch is present with restricted drying conditions.

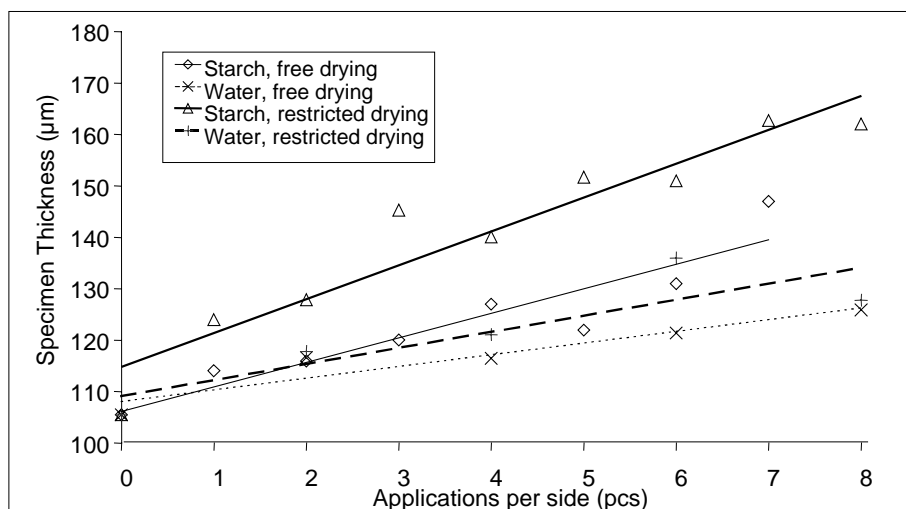


Figure 56. Thickness of the sheet with different trial points of free and restricted drying with water and starch. Average standard deviation of thickness measurement was $\pm 2.4\%$.

Water treatment decreased the elastic modulus of sheets as well, but not as drastically as starch. On the other hand, starch-treated samples developed a higher elastic modulus under restricted drying than water-treated samples, which resulted in a net increase in elastic modulus at higher starch amounts. One should note here that this observation is mainly based on the maximum starch amount reached with the drying-restricted starch treated sample. However, given the confidence interval of the elastic modulus measurement at this point, this observation can be considered valid. This suggests that the prevention of starch-induced shrinkage resulted in a remarkable increase in drying tension – much as suggested by Silvy (1971) – and therefore a higher final elastic modulus. Drying tension has earlier been reported to increase the elastic modulus of fibers and that of the fiber network (e.g. Jenzen 1964, Htun 1980). Drying stress has been shown to increase fiber stiffness through fiber segment activation (Tanaka *et al.* 2001).

Breaking elongation (Figure 57) in the machine and cross direction reflected the elastic modulus behavior as the highest breaking strain values were achieved with starch-treated free-dried samples in both directions. Starch application with restricted drying also produced decreasing breaking elongation as more starch was introduced to the sheet.

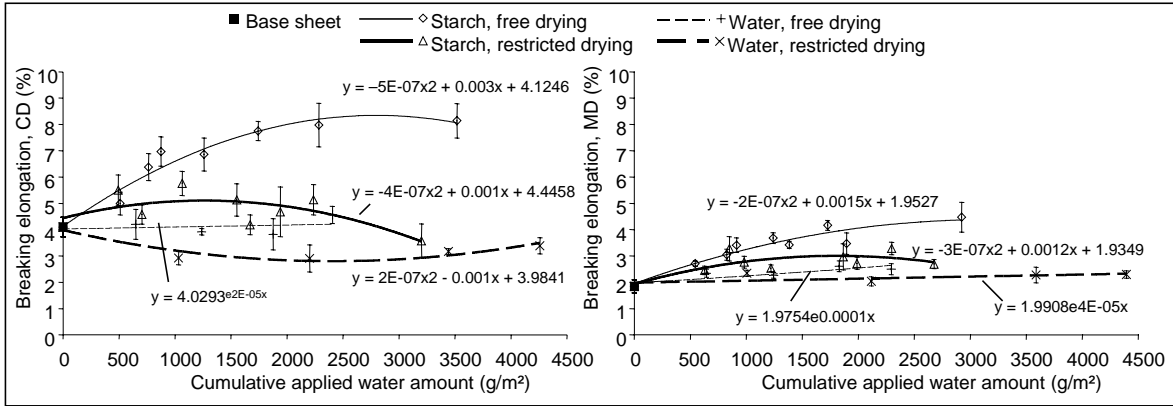


Figure 57. Breaking elongation in the cross direction (left) and machine direction (right) as a function of cumulative water addition. Starch added as 1% starch solution. The confidence intervals indicate the 2σ variation of the measurements.

Shrinkage during drying and elongation at rupture are well correlated as shrinkage resulted in the "crimped" sheet structure noted above, which allowed both a decrease in elastic modulus and an increase in breaking elongation as the crimped structure opened up during loading and elongation continued further before breaking. All of these results on the correlation of elastic properties and elongation at break agree well with previously published results, e.g. Gates and Kenworthy (1963) and Silvy (1971).

The measured bending stiffness values of the specimens are presented in Figure 58. Here, the effect of the cubed sheet thickness ($S_b = E d^3 / 12$) appears to dominate the bending stiffness behavior of paper despite the decreased elastic modulus in restricted drying with added starch. This is due to the increased thickness of the specimens as a result of multiple starch additions. Here, the basis weight of the starch treated specimens is increased from 89 g/m² to approximately 120 g/m² during the application sequences.

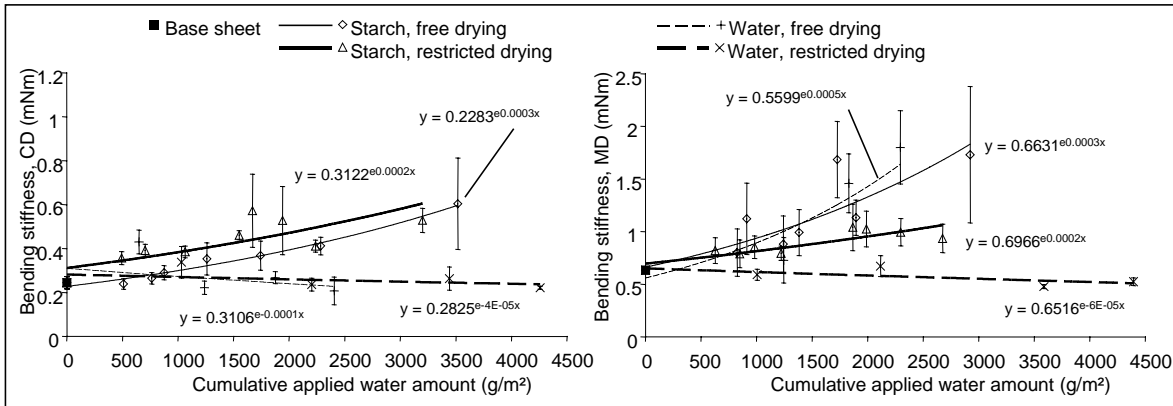


Figure 58. Bending stiffness values in the cross direction (left) and machine direction (right) as a function of cumulative water addition. Starch added as 1% starch solution. The confidence intervals indicate the 2σ variation of the measurements.

Figure 60 presents the net effect of starch as a function of starch content. The figure was produced by substituting corresponding water amounts in elastic modulus trend line equations for both starch and water-treated results (in Figure 55). The calculated values were then adjusted to the same elastic modulus value at the origin (i.e. the elastic modulus of the base paper). The net effect of starch was then reduced to the difference between these values. This procedure is illustrated in Figure 59. The results were subsequently plotted with starch content on the x-axis in Figure 60.

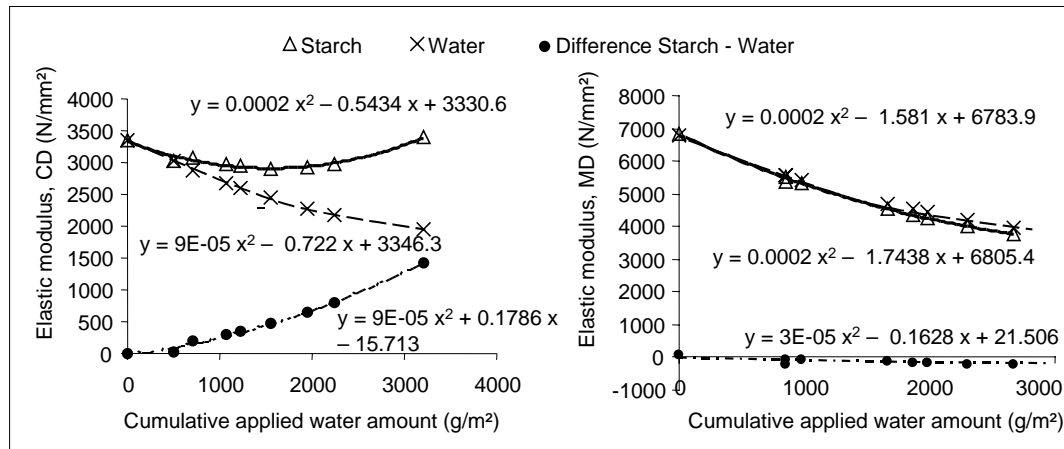


Figure 59. Explanation of deriving the net starch effect with water effect isolated from the trendline equations of the starch application results in CD (left) and MD (right). Difference curve were then drawn after offset adjustments based on the base paper's elastic modulus CD and MD values.

One can observe that in terms of the net effect described here starch increased the cross-directional elastic modulus of sheets. However, machine direction elastic modulus was not positively affected by the presence of starch. The differences in cross and machine direction elastic modulus development may be explained through the shrinkage differences between MD and CD in an oriented sheet, as suggested by e.g. Gates and Kenworthy (1963). Different shrinkage potential would then introduce different drying stress levels in MD and CD – also in the presence of shrinkage inducing starch – resulting in differences in elastic modulus in different directions. In other words, as starch is promoting shrinkage more in CD than in MD direction, the starch content has more effect in elastic modulus in cross direction of the sheet.

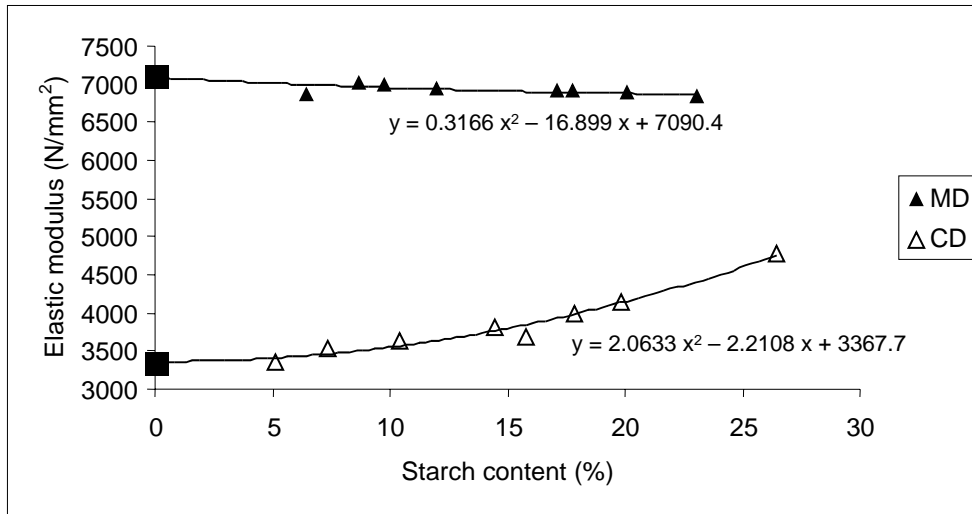


Figure 60. Net elastic modulus effect of starch plotted as a function of starch content in the cross and machine directions.

This observation can be supported by the findings in *Paper I*, where a clear improvement in cross-directional bending stiffness was seen when increasing the starch solids content (and therefore concentrating starch on the sheet surface). On the other hand, it was noticed that the effect of starch remaining on the sheet surface is much less clear with respect to machine direction bending stiffness. This agrees well with the different CD and MD effects of starch on the elastic modulus of paper observed here.

7.2 Summary

Measurement results were reported in this study for different starch amounts in uncoated woodfree base paper sheets. Two different starch application-induced behaviors were suggested on the basis of these results regarding the elastic modulus of the sheet:

- 1) Starch application with low drying restriction (shrinkage allowed) resulted in a decrease in the elastic modulus of the sheet both in the cross and machine directions of the sheet.
- 2) Starch application with highly restricted drying (shrinkage limited) resulted in an increase in the net elastic modulus of the sheet (net effect = results were adjusted using results from parallel specimens with water application), especially in the cross direction where an increase in elastic modulus compared to parallel water additions was noticed. However, an increase in the machine direction elastic modulus of the sheet did not occur compared to water treatment.

The effect of restricted drying together with starch addition increasing the elastic modulus of the sheet suggested that the prevention of starch-induced shrinkage resulted in remarkably increased drying tension in the sheet – and therefore higher final elastic modulus. Drying tension and stress have earlier been reported to increase the elastic

modulus of fibers and the fiber network, as well as fiber stiffness, through fiber segment activation. Therefore, starch may not – at least to the extent that has been believed – directly increase the elastic modulus of the sheet through fiber/fiber or starch/cellulose molecule bonding, i.e. as the general term “binder” suggests. In increasing the elastic modulus – and further the bending stiffness of the sheet – starch may merely promote shrinkage potential instead, which then leads – when shrinkage is not allowed – to increased drying stress. This, in turn, leads to an increase in elastic modulus, as described in related literature. This mechanism is illustrated in *Figure 61*.

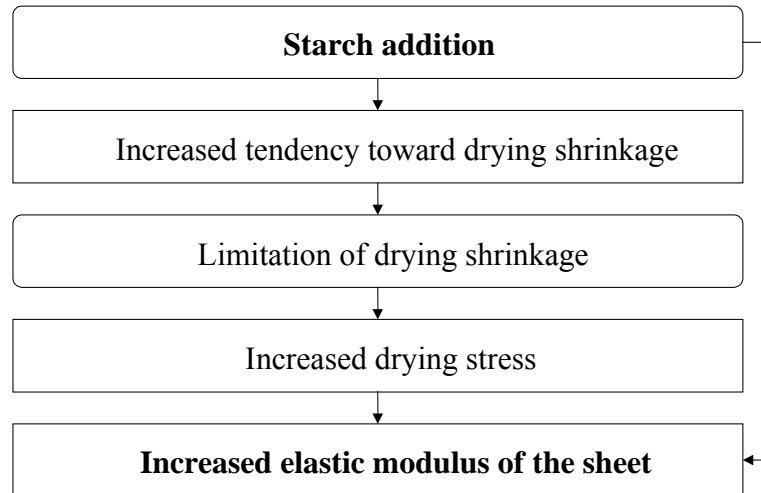


Figure 61. Suggested mechanism for the development of the elastic modulus of a sheet with starch promoting shrinkage potential, which – after drying with limited shrinkage – results in an increase in elastic modulus through increased drying stress.

However, allowing shrinkage may lead to higher thickness of the sheet, which again increases the bending stiffness of the sheet by the third power of thickness. This will compensate for the decrease in elastic modulus associated with the shrinkage of the sheet mentioned earlier. The suggested mechanism is illustrated in *Figure 55*. The actual development of bending stiffness is most probably a combination of both mechanisms, which can also vary in an actual papermaking process in the CD direction as the shrinkage profile of the sheet is seldom flat in the cross direction of the paper machine.

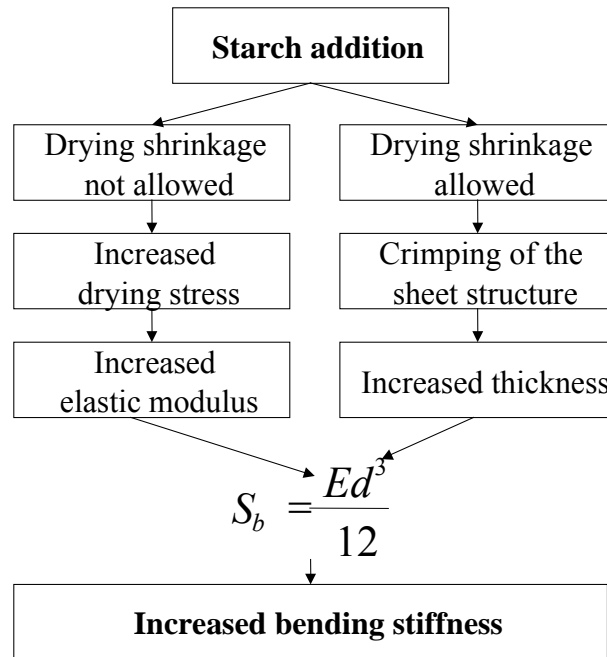


Figure 62. Suggested mechanism for the role of starch in the development of the bending stiffness of a sheet.

Results also suggested that the presence of starch increased the elastic modulus of the sheet only in the cross direction of paper but not in the machine direction. This behavior can also be explained through the shrinkage prevention and drying stress approach described earlier. If we remember that individual fibers experience greater shrinkage in the transverse direction than in the longitudinal direction (e.g. Nanko and Wu 1995), one can state that drying stress (due to prevented drying shrinkage) is potentially greater in the cross direction as fibers are more oriented in the machine direction. In the machine direction, however, where fibers tend to shrink less, drying stress levels do not get as high. Starch-induced elastic modulus development due to the presence of starch is then much less distinct in the machine direction than in the cross direction.

8. Effect of Basis Weight and Press Draw on Woodfree Paper Properties during High Solids Surface Sizing

Increased starch solution solids contents in surface sizing may decrease the penetration of starch. This may lead to problems with the reduced internal strength of the sheet. This paper examines the possibility of increasing the base sheet's internal strength by reducing the press to dryer draw to compensate for this decrease in starch penetration. In this study, base paper was produced on a pilot paper machine producing basis weights of 69 g/m² to 78 g/m² at press to dryer draw levels of 1% to 3%. This base paper was then surface sized using a pilot MSP coater at starch solids contents of 10% and 25%.

This discussion is supported by the work reported in *Paper V*.

8.1 Results

Starch amounts measured from the paper samples are presented in *Table VII*.

Table VII. Measured applied starch amounts for different trial paper basis weights, press draw levels, and solids contents.

Basis (g/m ²)	Starch Amount (g/m ²)			
	25% Starch Solids			10% Starch Solids
	Press draw 1%	Press Draw 2%	Press Draw 3%	Press draw 3%
69	3.51	3.51	3.44	–
72	3.49	3.49	3.50	–
78	3.51	3.57	3.52	2.38

As seen in the table, an almost constant starch amount was achieved with a total dry applied amount of 3.5 g/m² at a 25% solids content. With a 10% starch solids content, however, the same level of dry applied amount was not reached. The difference in starch amounts has to be considered when evaluating the results at different starch solids contents.

When interpreting the results presented in the following figures, one should note that all curves are plotted as a function of base paper basis weight (i.e. basis weight before surface sizing) even when the results relate to surface sized samples. This is to facilitate the parallel evaluation of both surface sized and base paper results.

The effect of press draw and base paper basis weight on starch penetration (*Paper III*) is illustrated by the simulated starch content (SSC) distribution and by the penetration number (Q_{tot}) in *Figure 63*.

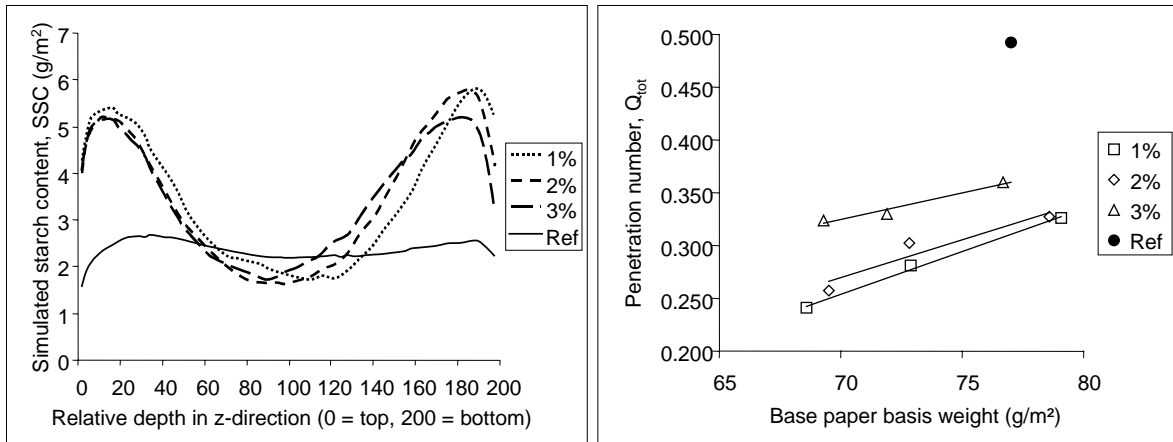


Figure 63 left: Simulated Starch Content (SSC) distribution determined for the highest basis weight paper samples produced at 1%, 2%, and 3% press draw with 25% surface sizing solids and reference papers produced at 3% press draw and 10% starch solids (Ref). Corresponding dimensionless penetration number values Q_{tot} are also presented on the right.

In Figure 63 on the left, one can observe on the basis of the simulated starch content (SSC) distributions that decreasing the press draw from 3% to 1% will decrease the penetration of starch and boost the amount of starch remaining on the sheet surface. This observation can be explained through the decreased openness of the base sheet as the press draw is decreased (Figure 64). Figure 63 left also suggests that differences in starch penetration are more evident on the bottom side of the sheet. Here, surface sizing at a low solids content (10%) resulted in an almost even distribution of starch throughout the z-direction, whereas starch remained more on the sheet surface at a 25% solids content. In Figure 63 right, a dimensionless penetration number Q_{tot} was used to characterize the starch distribution with different base papers surface sized with starch solution solids at 25%. These results are compared against a reference sample with 3% press draw and 10% starch solids. The results indicate further the relationship between press draw and consequent sheet openness – and its effect on starch penetration. Here, decreasing the press draw seems to very consistently decrease starch penetration Q_{tot} by closing the sheet. In addition, one can observe an increase in starch penetration when basis weight is increased. This can be explained through increased total void volume at higher basis weights enhancing the flow of liquid into to the porous fiber network.

The effect of basis weight, press draw and surface sizing on air permeability with different solids contents are illustrated in Figure 64.

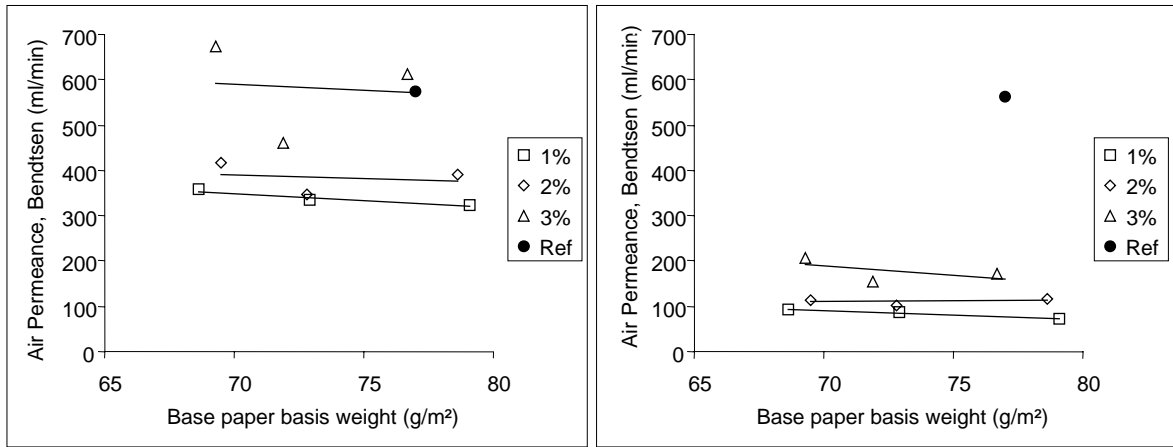


Figure 64. Effect of basis weight and press draw on base paper (left) and surface sized final paper (right) air permeability as a function of original base paper basis weight. Surface sizing was done with 25% starch solids at three press draw levels (1%, 2% and 3%) and 10% as a reference with a press draw of 3%. The CV of the results were 4.8% (base paper) and 8.1% (surface sized paper).

Lowering the press draw considerably reduces the air permeability of the base sheet. This effect is also seen with a surface sized sheet. Surface sizing with high solids starch further reduces air permeability. This reduction in air permeability was achieved both by reducing the press draw (Juppi and Kaihovirta 2002) and increasing the solids content (*Papers I and II*).

As reported earlier (Juppi and Kaihovirta 2002), reducing the press draw increases the internal strength of the base sheet, based on the Huygen measurement (*Figure 65*, left). It can also be observed that lowering the press draw has the strongest positive effect on internal strength at lower basis weights.

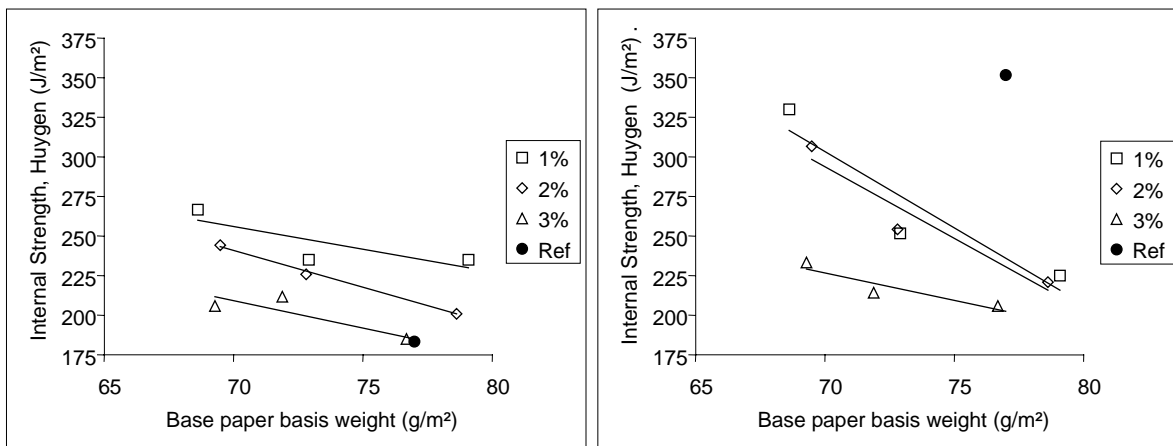


Figure 65. Effect of basis weight and press draw on the internal strength (Huygen) of base paper (left) and surface sized final paper (right) as a function of original base paper basis weight. Surface sizing was done with 25% starch solids at three press draw levels (1%, 2%

and 3%) and 10% as a reference with a press draw of 3%. The CV of the results were 5.3% (base paper) and 4.5% (surface sized paper).

One can observe that when comparing the penetration of starch and the development of internal strength at the individual trial points, the increase in internal strength seems to be highest at the press draw levels of 1% to 2%. This can be observed especially at the lowest basis weights, despite the lowest starch penetration presented in *Figure 63*. It can also be seen that with high solids surface sized paper – in contrast to the base sheet – lowering press draw under 2% does not seem to further enhance the internal strength of paper. This may, again, be explained through the observations in *Figure 63*, where penetration decreases further when the press draw is decreased below 2%. Decreasing starch penetration at a press draw below 2% will then counteract the increasing effect of the low press draw in terms of Huygen internal strength.

Although internal strength also increases based on Z-tensile measurement when press draw is decreased down to 1%–2%, it behaves somewhat differently than the Huygen internal strength (*Figure 66*).

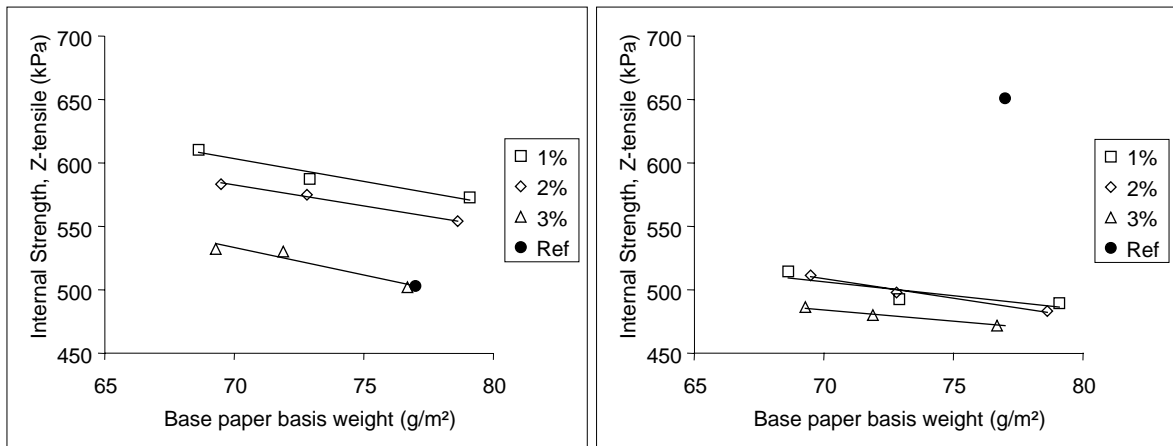


Figure 66. Effect of basis weight and press draw on the internal strength (Z-tensile) of base paper (left) and surface sized final paper (right) as a function of original base paper basis weight. Surface sizing was done with 25% starch solids at three press draw levels (1%, 2% and 3%) and 10% as a reference with a press draw of 3%. The CV of the results were 1.7% (base paper) and 1.5% (surface sized paper).

Here, high solids surface sizing and calendering are actually lowering the absolute measured Z-tensile strength compared to the base sheet. Also differently from the Huygen results, lowering the basis weight does not considerably enhance the Z-tensile values at a 1%–2% press draw compared to a 3% press draw. Here, the increase in Z-tensile between different press draw levels remains fairly constant as basis weight is decreased. A reduced difference in internal strength compared to base sheet press draws of 1% and 2% can also be observed in Z-tensile strength. The explanation of the lowest press draw decreasing the starch penetration can be repeated in this context. Here, the Z-tensile increase in the base

sheet as the press draw is reduced from 2% to 1% is offset by decreasing starch penetration as seen in *Figure 66*. As the high-solids surface sizing reduces Z-tensile strength, the reference values for surface sizing with 10% starch solids are not reached.

The different behavior of Huygen and Z-tensile results (i.e. Huygen increasing and Z-tensile decreasing as high solids starch is applied to the sheet) may be explained through the different principles of the two measurements. Whereas Z-tensile is measuring the *force* per unit area (i.e. z-directional tensile stress) required to delaminate the specimen, Huygen is measuring the delaminating *energy*, which is similar to the more commonly used Scott Bond measurement. At 25% solids content, the surface sizing starch is concentrated on the surface of the sheet, leading to a very steep z-directional starch gradient. Steep gradients in any mechanical construction can cause a local stress peak in the structure under load. This development may explain the actual decrease in Z-tensile strength despite the addition of starch binder into the fiber network. The Huygen measurement, which is based on the absorbed rupture energy of the sheet, may not be similarly affected by the structural gradients of the fiber network and its binder content.

The effect of the base sheet properties and the starch solids content on bending stiffness is presented in *Figure 67*. As expected, bending stiffness increases with higher basis weights. Increasing the press draw also has a positive effect on bending stiffness.

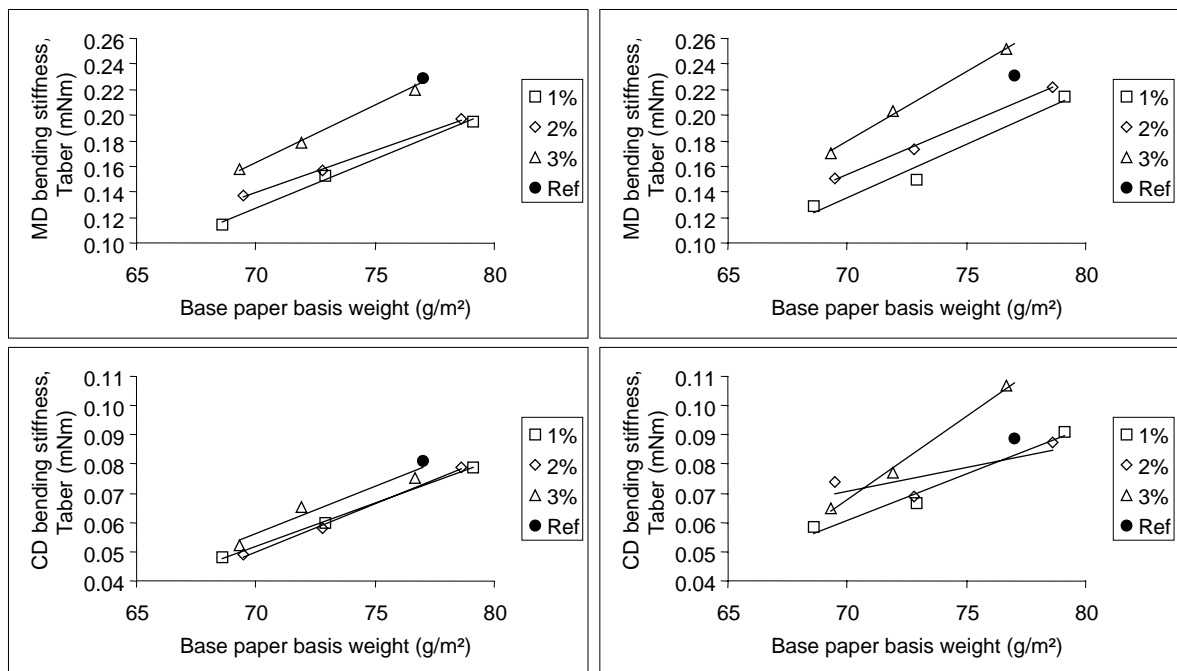


Figure 67. Effect of basis weight and press draw on the bending stiffness (Taber) of base paper (left) and surface sized final paper (right) in the MD (top) and CD (bottom) directions as a function of original base paper basis weight. Surface sizing was done with 25% starch solids at three press draw levels (1%, 2% and 3%) and 10% as a reference

with a press draw of 3%. The CV of the results were 10.9% (base paper) and 33.1% (surface sized paper).

The large coefficient of variation of the measurements of the surface sized specimens is explained through the curling tendency of the specimens. Then, the measurement gave greatly different values in the top and bottom side measurements.

The tendency toward reduced bending stiffness with lower press draws can be partly explained through the elastic modulus behavior of the base sheet (*Figure 68*).

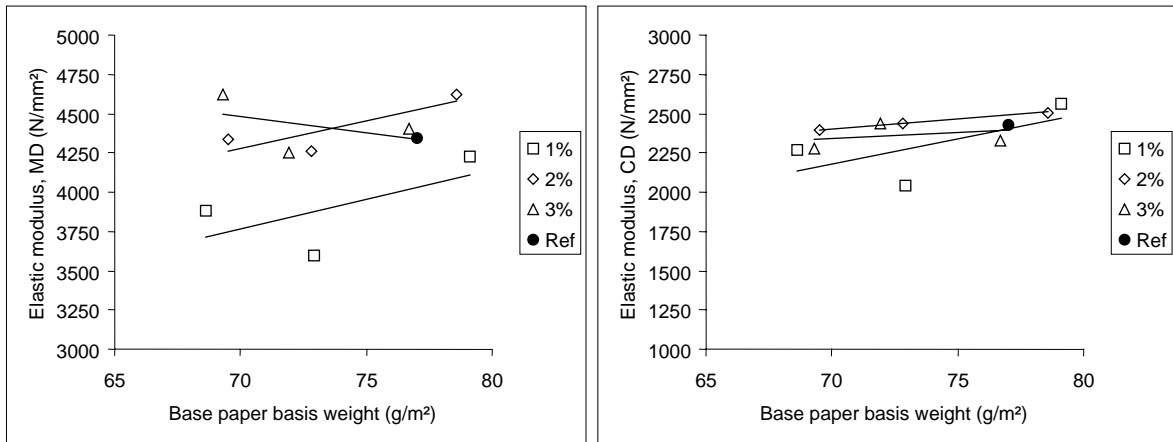


Figure 68. Effect of basis weight and press draw on the elastic modulus of base paper in the machine direction (left) and cross direction (right) as a function of original base paper basis weight. The paper was produced at three press draw levels (1%, 2% and 3%) for high solids surface sizing. The reference data point indicates the base paper that was to be surface sized with low solids (10%) starch solution. The CV of the results was 4.6%.

As seen from the results, elastic modulus is more strongly affected by press draw in the machine direction than in the cross direction. When using a higher draw (3%) directly after the press section with a sheet dryness of approximately 45%–50%, one could suggest that the individual fibers in the fiber network are straightened out in the machine direction. With a low press draw of 1%, the fiber network is taken to the dryer section and dried into a more curly structure. This would then lead to a decreased elastic modulus of the fiber network due to less straight fibers, which contributes to the elasticity of the whole fiber network. The observation that elastic modulus depends on press draw, especially in the MD direction (*Figure 68*, left), can support this assumption. The behavior of bending stiffness at different press draw levels can therefore be partly explained.

The effect of increased draw on elastic modulus through the straightening out of fibers may be supported when the press draw effect on the surface roughness of the base sheet is observed. As seen in the *Figure 69*, press draw reduction increased surface roughness (Bendtsen).

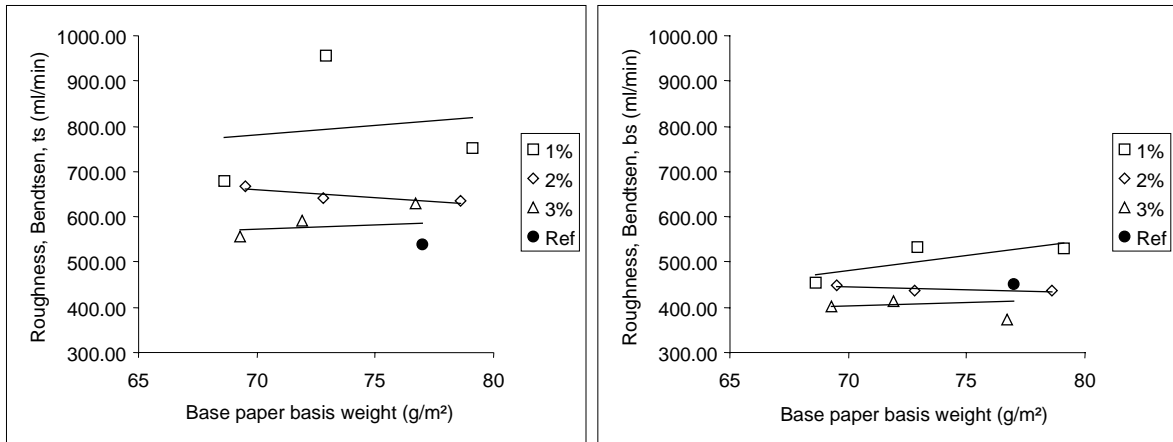


Figure 69. Effect of basis weight and press draw on the top side and bottom side surface roughness (Bendtsen) of base paper as a function of original base paper basis weight. The paper was produced at three press draw levels (1%, 2% and 3%) for high-solids surface sizing. The reference data point indicates the base paper that was to be surface sized with low solids (10%) starch solution. The CV of the results was 11.0%.

One can suggest that if surface roughening reflects the fibers being dried into a more curly structure, a reduced press draw level, say 1%, will result in higher roughness values. Moreover, when considering the effect of roughness on starch pickup in surface sizing (e.g. Dill 1974), optimizing the press draw can be a point of interest also in terms of the surface sizing process.

8.2 Summary

The effect of high solids surface sizing reported here agrees with earlier studies (*Papers I and II*). Additionally, the effect of press draw on base paper properties agrees with findings by Juppi and Kaihoviirta (2002). According to the results of this study, the Huygen internal strength of high solids surface sized paper can be increased by reducing the press draw down to 2%. This will partly compensate for the loss of internal strength caused by starch remaining on the paper surface from high solids sizing (e.g., above 25%). Decreasing the draw below 2% does not necessarily have a further effect on high solids surface sized paper. This was explained through the decrease in starch penetration when a low press draw was used; decreasing the press draw decreased the porosity of the sheet. In this study decreasing the press draw consistently decreased starch penetration due to the more closed base sheet, which had an influence on the internal strength of the surface sized sheet. This mechanism counteracts an increase in the internal strength of the base sheet when a lower press draw level is used. It was further noted that when the press draw is too low, the elastic modulus of the fiber network decreases. The latter effect would have a negative influence on the bending stiffness of the sheet (Kajanto 2000). Here, a difference between two different internal strength measuring methods was noticed when high-solids surface sizing was used. While the Huygen internal strength increased through surface sizing compared to the base sheet, Z-tensile strength decreased despite the addition of binder to

the sheet. This can be explained by a steep Z-directional gradient in the sheet caused by the starch remaining on the sheet surface. This gradient may then create local stress peak areas in the sheet structure under a z-directional load and result in lower rupture resistance. The penetration of starch is negatively affected when the press draw of the base sheet is reduced. This will then counteract the effect of the increasing internal strength of the base sheet when a lower press draw is used. The increase in internal strength due to decreased press draw is most significant at low basis weights. This was due to the negligible starch penetration's minimal negative impact on internal strength at low basis weights.

The results presented here can be utilized to optimize the press draw when high solids surface sizing is used. The aim could be to minimize the press draw below 2% when internal strength or air permeability are critical. However, maximizing the press draw can also be targeted when the bending stiffness of the sheet is critical.

9. Concluding Remarks

The objective of the study was to increase the solids content of surface sizing starch solutions up to 30% while maintaining a constant starch amount. The resulting effects on the properties of paper, as well as consequent requirements for the starch solution and base paper – and effects on the final paper structure – were characterized in this research.

Results from the pilot MSP trials show that it is possible to apply starch at solids contents of up to 30% with a wide variety of starch viscosities and molecular weights. Increasing the starch solids content, and thereby increasing the starch stability requirements, does not necessarily restrict one to highly degraded starches and their lower binding power.

Such rheological properties as yield stress can be used in characterizing the runnability features of starch in terms of web release properties also at very high starch solids contents. Moreover, in terms of high solids surface sizing starch runnability, the essential requirement for application is maintaining a constant starch amount. This would then lead to a need to correspondingly reduce the film thickness by using fine grooved rods, for example, or even smooth rods. High solids starch surface sizing with a thin and uniform film would then result in smooth release of the sheet from the rolls through the low cohesion of the remaining starch film after the nip.

In the MSP trial results paper properties show a decrease in the penetration of starch as the starch solution solids content is increased. This would then lead to increased surface strength and cross-directional bending stiffness. Air permeability, oil absorption and internal strength also decreased as expected. In terms of uncompromised final paper properties in all respects, base paper can be optimized in a way that will compensate for the loss of internal strength in the sheet when low penetration high solids surface sizing is used. Based on pilot paper machine and subsequent high solids surface sizing pilot MSP trials, this means decreasing the press to dryer draw down to 2%. In MSP trials at starch solids of up to 30%, increasing the number of larger pores in the base sheet proved favorable in preserving the internal strength of the final paper through local starch penetration into the sheet.

A novel method for characterizing the starch penetration quantitatively from iodine stained cross-sections was introduced in this study. This method was defined through standardized practices for sample handling and the microscopic imaging of cross-sections, followed by automated image analysis procedures. The resulting starch penetration curves and a new dimensionless penetration number, Q , correlate well with paper properties and the starch solution solids content, which was expected to reflect the penetration of starch into the sheet.

An explanation for the observed increase in cross-directional bending stiffness (and not as much in the machine direction) when starch is concentrated on the surface of the sheet was determined by measuring the elastic modulus of sheets with different starch contents. In increasing the elastic modulus or bending stiffness of the sheet starch merely promotes shrinkage potential, which then leads – when shrinkage is not allowed – to increased drying stress that, in turn, leads to an increase in elastic modulus and further to increased bending stiffness when starch is concentrated on the surfaces of paper using high solids surface sizing. In the machine direction, however, starch-induced shrinkage, and therefore drying stresses, does not get so high. This leaves the starch-induced effect on the elastic modulus of paper, and consequently on bending stiffness, less dominant in the machine direction when starch is concentrated to the sheet surface.

Literature

Allem, R. and Uesaka, T., Characterization of Paper Microstructure: A New Tool for Assessing the Effects of Base Sheet Structure on Paper Properties, Proc. Microscopy as a Tool in Pulp and Paper Research and Development Symposium, Stockholm, Sweden pp. 21 (1999).

Allem, R., Characterization of Paper Coatings by Scanning Electron Microscopy and Image Analysis, J. Pulp and Paper Science, 24(10), pp. 329 (1998).

Bailey, D.F. and Bown, R., The Use of Pigments At The Size Press – A European View, Proc. TAPPI Papermakers Conference, TAPPI Press, Atlanta, GA, USA, pp.199 (1990).

Bailey, J. H. E. and Reeve, D. W., Spatial Distribution of Trace Elements in Black Spruce by Imaging Microprobe Secondary Ion Mass Spectrometry. Journal of Pulp and Paper Science (20) pp. 83 (1994).

Barratte, C., Dalphond, J.E., Manglin, P.J. and Valade, J.L., An Automatic Determination of Threshold for the Image Analysis of Prints, Proc. Advances in Printing Science and Technology, IARIGAI 23rd Research Conference, pp. 451 (1997).

Bergh, N.-O. and Åkesson, R., Upgrading of Supercalendered Papers for Offset Printing, Proc. TAPPI Coating Conference, TAPPI Press, Atlanta, GA, USA, pp. 73 (1988).

Bergh, N.-O., Starches, In Surface Application of Paper Chemicals, Blackie Academic and Professional, London, England, pp. 69 (1997).

Bergh, N.-O., Surface Treatment on Paper with Starch from the Viewpoint of Production Increase, Proc. XXI EUCEPA International Conference, Volumen 2, Conferencias nos 23 a 43, Torremolinos, Spain, pp. 547 (1984).

Brecht, W. and Erfurt, H., Wet-Web Strength of Mechanical and Chemical Pulps of Different Form Composition, TAPPI, 42(12), pp. 959 (1959).

Brinen, J. S. and Kulick, R. J., SIMS Imaging of Paper Surfaces. Part 4. The Detection of Desizing Agents on Hard-to-Size Paper Surfaces. International Journal of Mass Spectrometry and Ion processes pp. 177 (1995).

Brogly, D.A. and Harvey, R.D., Influence of Fluidity of Hydroxyethyl Corn Starch on Metering Rod Size-Press Application and Resultant Paper Properties, Proc. TAPPI Coating Conference, TAPPI Press, Atlanta, GA, USA, pp. 145(1993).

Brown, G. H., Cationic Starch Improves Strength of Groundwood Papers, Paper Trade Journal, pp. 35. February (1969).

Bruun, S.-E., Starch, in Papermaking Science and Technology, Volume 11: Pigment Coating and Surface Sizing of Paper, TAPPI Press, Atlanta, GA, USA, pp. 246 (2000).

Chinga, G. and Helle, T., Structure Characterisation of Pigment Coating Layer on Paper by Scanning Electron Microscopy and Image Analysis, Nordic Pulp and Paper Research Journal, 17(3), 307 (2002).

Deters, L.E., Cationic Corn Starch vs. Cationic Potato Starch – a Practical Study, Proc. TAPPI Papermakers Conference, TAPPI Press, Atlanta, GA, USA pp. 93 (1990).

Dickson, A., Quantitative Analysis of Paper Cross Sections, Appita J., 53(4), pp. 292 (1999).

Dill, D., Control and Understanding of Size Press Pickup, Tappi J., 57(1), 97 (1974).

Felder, H., Sizing of Woodfree Papers with a Pre-Metering Size Press, Proc. TAPPI Coating Conference, TAPPI Press, Atlanta, GA, USA, pp. 267 (1991).

Fineman, I. and Hoč, M., Surface Properties, Especially Linting, of Surface Sized Fine Papers, Tappi J., 61(5), pp. 43 (1978).

Fisher, G. L., Hooper, A. Opila, R. L. Jung, D. R. Allara D. L. and Winograd, N., The Interaction Between Vapor-Deposited Al Atoms and Methylester-Terminated Self-Assembled Monolayers Studied by ToF-SIMS, XPS and IRS, J. Elec. Spec. Rel. Phenom. pp. 139 (1999).

Gates, E.R. and Kenworthy, I.C. Effects of Drying Shrinkage and Fibre Orientation on Some Physical Properties of Paper, Paper Technology, 4(5) pp. 485 (1963).

Glittenberg, D., How to Get More Without Paying for It, Pulp & Paper Asia, 3(2), 6 (2000).

Glittenberg, D and Becker, A, Thermisch modifizierte Stärken – erweiterte Möglichkeiten beim Oberflächenleimen und Streichen, Proc. PTS Starch Symposium, PTS Papiertechnische Akademie, München, Germany, pp 18–5 (2002).

Grön, J. and Ahlroos, J., Influence of Base Paper Filler Content and Pre-calendering on Metered Film Press Coating – Part I: A Coating Process Study. Proc, TAPPI Coating / Papermakers Conference, TAPPI Press, Atlanta, GA, USA, pp. 899 (1998).

Grön, J. and Rantanen, R., Surface Sizing and Film Coating, in Papermaking Science and Technology, Volume 11: Pigment Coating and Surface Sizing of Paper, TAPPI Press, Atlanta, GA, USA, pp. 457 (2000).

Grön, J., Nikula, E. and Sunde, H., Runnability Aspects in High Speed Film Transfer Coating, *Tappi J.*, 81(2), 157 (1998).

Hansson, J. A. and Klass, C. P. High Speed Surface Sizing, *Tappi J.*, 67(1), 64 (1984).

Hoyland, R., Howarth, P., Whitaker, C. and Pycraft, C. Mechanisms of the Size Press Treatment of Paper. *Paper Technology and Industry*, 18(8), pp. 246 (1977).

Htun, M., The Influence of Drying Strategies on the Mechanical Properties of Paper, Department of Paper Technology, The Royal Institute of Technology, Stochlholm, Sweden, pp. 31 (1980).

Jentzen, C.A., The Effect of Stress Applied During Drying on Some of the Properties of Individual Pulp Fibers. pp. *Tappi* 47(7) pp. 412 (1964).

Juppi, K. and Kaihovirta, J., Paper Quality Control in a Dryer Section, Proc. 7th International Conference on New Available Technologies, SPCI – The Swedish Association of Pulp and Paper Engineers, Stockholm, Sweden, pp. 55 (2002).

Kajanto, I., Structural mechanics of paper and board. In *Papermaking Science and Technology*, Volume 16: Paper Physics, TAPPI Press, Atlanta, GA, USA, pp. 323 (2000).

Kartovaara, I.. Gradienttikalanterointi: Gradienttien syntymisen ja kalanterointituloksen arvostelun perusteet. Licenciate Thesis, Helsinki University of Technology, pp. 139 (1989).

Kimpimäki, T., and Rennes, S., New Surface Sizing Concept Significantly Reduces Porosity, Liquid Penetration and Surface Roughness, *Paperi ja Puu – Paper and Timber* 82(2), pp. 525 (2000).

Klass, C. P., Surface Sizing II: Size Press Technology, Proc. TAPPI Sizing Short Course, TAPPI Press, Atlanta, GA, USA, pp. 12 (1997).

Klass, C. P., Trends and Developments in Size Press Technology, Proc. TAPPI Papermakers Conference, TAPPI Press, Atlanta, GA, USA, pp. 177 (1990).

Kulick, J. and Brinen, J. S., Probing Paper Surfaces with ToF SIMS: A New Problem Solving Tool, *Tappi J.*, 81(2), pp. 152 (1998).

Küstermann, M., Pilot Plant Results with a 'Speedsizer', Proc. TAPPI Papermakers Conference, TAPPI Press, Atlanta, GA, USA, pp. 193 (1990).

Laleg, M., Ono, H., Barbe, M.C., Pikulik, I.I. and Seth, R.S., The Effect of Starch on the Properties of Groundwood Furnishes and Paper, Proc. TAPPI papermakers conference, TAPPI Press, Atlanta, GA, USA pp. 383 (1990).

Lekhnitskii, S.G., Chapter IX. Theory of Bending of Anisotropic Plates (thin plates). In *Anisotropic Plates*, Gordon and Breach, Science Publishers, New York, USA, pp. 533 (1968).

Lipponen, J., Grön, J., Bruun, S-E and Laine, T. Surface Sizing with Starch Solutions at High Solids Contents. Proc. TAPPI Metered Size Press Forum, TAPPI Press, Atlanta, GA, USA, pp. 129 (2002).

Marton, J. Fines and Wet End Chemistry, *Tappi* 57(12), pp. 90 (1974).

McQueary, R.T. and Thomas, W., Unique Surface Starches Improve Paper Properties, Proc. TAPPI Papermakers Conference, TAPPI Press, Atlanta, GA, USA, pp. 185 (1991).

McQueary, R.T., Wet end Waxy Amphoteric Starch Impacts Drainage, Retention and Strength, Proc. TAPPI Papermakers Conference, TAPPI Press, Atlanta, GA, USA pp. 137 (1990).

Meaker, D.W., Machine Factors Influencing Sizing (and Vice-Versa), *Tappi J.*, 67 (4), pp.102 (1984).

Mendham, J., Denney, R., Barnes, J. and Thomas, M., *Vogel's Textbook of Quantitative Chemical Analysis*, Prentice Hall, New York, NY, USA, pp. 806 (2000).

Nanko, H. and Wu, J. Mechanisms of Paper During Drying, Proc. International Paper Physics Conference, TAPPI Press, Atlanta, GA, USA, pp 103 (1995).

Odell, M. and Kinnunen, J.S., Multilayering – Method or Madness, Proc. XI Valmet Paper Machine Days, Jyväskylä, Finland, pp. 52 (1998).

Oja, M., Fredrick, C., Nuffel, J. and Lambrechts P., Effects of Starch on Metered Size Press and Paper Properties, Proc. TAPPI Coating Conference, TAPPI Press, Atlanta, GA, USA, pp. 275 (1991).

Peterson, A and Williams, L. C., Determining Paper-Coating Thickness with Electron Microscopy and Image Analysis, *Tappi J.*, 74(10), pp. 122 (1992).

Preston, J.S., Elton, N.J., Husband, J.C., Legrix, A., Heard, P. J. and Allen, G. C., SIMS analysis of printed paper surfaces to determine distribution of ink components after printing, Tappi International Printing & Graphic Arts Conference, TAPPI Press, GA, USA, pp. 101 (2000).

Rantanen, R. and Westergård, S., Valmet's Latest Development in Surface Treatment, Proc. The World Pulp and Paper Week: New Available Techniques and Current Trends, SPCI – The Swedish Association of Pulp and Paper Engineers, Sweden, pp. 698 (1987).

- Remmer, J. and Eklund, D.E., Absorption of Starch During Surface Sizing with Different Methods, Proc. TAPPI Coating Conference, TAPPI Press, Atlanta, GA, USA, pp. 285 (1991).
- Retulainen, E., Niskanen, K. and Nilsen, N. Fibers and Bonds. In Papermaking Science and Technology, Volume 16: Paper Physics, TAPPI Press, Atlanta, GA, USA, pp. 323 (2000).
- Roper, J. A. and Attal, J. F., Evaluations of Coating High-Speed Runnability Using Pilot Coater Data, Rheological Measurements and Computer modeling, Tappi J., 76(5) (1993).
- Ryder, D.J., Practical Experiences with a SymSizer, Proc. PITA Coating Conference, PITA Coating Working Group, pp. 49 (1997).
- Setterholm, V. and Kuenzi, E., Fiber orientation and Degree of Restraint During Drying – Effect on Tensile Anisotropy of Paper Handsheets. Tappi 53(10) pp. 1915 (1970).
- Silvy, J. Effect of Drying on Web Characteristics. Paper Technology, 12(6) pp. 445 (1971).
- Sirois, R. F., The Latest Generation of Surface Sizing Starches, Paper Technology 33(11) pp. 31 (1992).
- Sollinger, H.-P., Speedsizer, Proc. TAPPI Coating Conference, TAPPI Press, Atlanta, GA, USA, pp. 145 (1988).
- Tanaka, A., Hiltunen, E., Kettunen, H. and Niskanen, K., Fracture Properties in Filled Papers, 12th Fundamental Research Symposium, The Pulp and Paper Fundamental Research Society, Lancashire, United Kingdom, pp. 1403 (2001).
- Tehomaa, J., Palokangas, E., Mäkimattila, J. and Tuomisto, M., High Speed Surface Sizing of Fine Papers: A Comparison of Different Techniques, Proc. TAPPI Papermakers Conference, TAPPI Press, Atlanta, GA, USA, pp. 353 (1992).
- Wight, E.W., Operation and Application of the Blade Metering Size Press, Proc. Tappi Coating Conference, TAPPI Press, Atlanta, GA, USA, pp. 123 (1988).
- Williams, G. J. and Drummond, J.G., Preparation of Large Sections for the Microscopical Study of Paper Structure, Proc. Tappi Papermakers Conference, TAPPI Press, GA, USA, pp. 517 (1994).
- Zimmerman, P. A., Hercules, D. M and Loos, W.O., Direct quantitation of Alkylketene Dimers Using Time-of-Flight Secondary Ion Mass Spectrometry. Anal. Chem. (67), pp. 2901 (1995).
- Zsoldos B. and Sebess I., Die Bestimmung des Stärkegehaltes von mit modifiziert Stärke behandelten Papieren. Zellstoff und Papieren (10) pp. 299 (1975).